Ministry of Higher Education
and Scientific research
Babylon University
College of Engineering

COMBINED FREE-FORCED CONVECTION OVER INCLINED SURFACE

A Thesis Submitted
To
The Department of Mechanical Engineering
College of Engineering
Babylon University
In Partial Fulfillment of The Requirements of The Degree
of Master of Science In Mechanical Engineering

BY

FUAD ABDUL-AMEER KHALAF

AL-RAJHI

(B.Sc., 1999)

2006 A.D. **1427 A.H.**

بِسمِ اللهِ الرَّحمنِ الرَّحِيمِ

حَتَّى إِذا أَخَذَتِ آلأَرضُ زُخرُفَهَا وَآزَّيَنَت وَظَنَّ أَهلُهَا أَنَّهُم قَدِرُونَ عَلَيها أَتَهَا أَمرُنَا لَيلاً أَو نَهَاراً فَجَعَلنهَا حَصِيداً كَأَن لَّم تَغنَ بِالأَمسِ كَذَلِكَ نُفَصِّلُ الأيٰتِ لِقَومٍ يَتَفَكَّرُونَ

صَدَقَ الله ألعليُ العظيم

ألاية 24 سورَة يونس

CERTIFICATION

We certify that this thesis entitled (Combined Free-Forced Convection over Inclined Surface) prepared by (Fuad Al-Rajhi) under our supervision at the Department of Mechanical Engineering, Babylon University, as a partial fulfillment of the requirements for the degree of Master of Science in ***Mechanical Engineering (Power Engineering)***.

Signature:
Name: Asst. Prof.
Dr. Tahseen A. H. Al-Hattab
(Supervisor)
Date: / / 2006

According to the recommendation presented by the supervisor of this thesis, I nominate this thesis to be forwarded to discussion.

Signature:
Name: Asst. Prof. Chairman of the Mechanical Engineering Department.
Dr. Adil. A. Al-Moosawy
Date: / / 2006

CERTIFICATE

We certify, as an examining committee, that we have read this thesis and examined the student Fuad Abdul-Ameer Al-Rajhi in its contents and that in our opinion it meets the standard as a thesis for the degree of Master of Science in ***Mechanical Engineering (Power Engineering)***.

Signature:
Name: Asst. Prof.
Dr. Tahseen A. H. Al-Hattab
(Supervisor)
Date: / / 2006

Signature:
Name: Asst. Prof.
Dr. Majid. H. Majeed
(Member)
Date: / / 2006

Signature:
Name: Asst. Prof.
Dr. Qaiser Muslim Al-Assady
(Member)
Date: / / 2006

Signature:
Name: Asst. Prof.
Dr. Adil. A. Al-Moosawy
(Chairman)
Date: / / 2006

Approved by the Council of the College of Engineering in it session in / /2006

Signature:
Name: Prof.
Dr. Abd Al-Wahid K. Rajih
Dean of Engineering College.
Date: / / 2006

الإهداء

إلى
الحق الجديد والعالم الذي علمه لا يبيد
إلى
مهدي الأمم وجامع الكلم
إلى
حجة المعبود وكلمة المحمود
إلى
القائم المنتظر والعدل المشتهر
إلى
شمس الظلام وبدر التمام
إلى
المولى صاحب الزمان الأمام المهدي

(عجل الله فرجه)

ACKNOWLEDGEMENT

By the grace of God, as this thesis has been completed, I gratefully wish to express my sincere thanks and gratitude to Dr. Tahseen A. Al-Hattab for his supervision, sincere efforts, helpful criticism and encouragements given through the preparation of this thesis.

Special appreciation and thanks to Dr. Adil , Head of the Mechanical Engineering Department and all the Staff of this Department for their kind help during the study period.

Finally, great thanks to all who have helped me to have the possibility to do this work.

ABSTRACT

Combined free forced convection over inclined surface problem has many applications in mechanical components, electronics devices cooled by fans and heat exchangers placed in a low velocity environment, an analytical solution such as integral method and similarity solution method are generally using to solve this problem.

The aim of this work is to analyze the study state laminar tow dimensional uniform flow over inclined heated flat plate for both constant wall temperature and constant heat flux and investigate the effect of buoyancy force and inclination angle on Nusselt number and hydrodynamic properties with combined free-forced convection.

An analytical and a numerical solution used to study local heat transfer by mixed convection for steady state free stream with Prandtl number range from 0 up to 100 over homogeneous inclined heated surface. The integral method is used to solve the constant wall temperature cases while the similarity solution used to solve the constant heat flux cases with the assistance of the (MathCAD) computer package.

Results show the variation of boundary layer thickness, Nusselt number and shear stress with the buoyancy force, inclination angle and the physical properties of the fluid represented by Prandtl number, where the Nusselt number increases for the same Reynolds number about range from $0.3*Re_x^{1/2}$ up to $6*Re_x^{1/2}$ and Stanton number increases about range from $0.3/Re_x^{1/2}$ up to $6/Re_x^{1/2}$ with the increases of the Richardson number in range from 0 up to 10 and the inclination angle from 0º up to 90º, while the boundary layer thickness decreases with the increases of the buoyancy force and the inclination angle.

CONTENTS

Chapter Four*: *Results and Discussion

Chapter Five*: *Conclusions and Recommendations

Appendices

NOMENCLATURE

The following symbols are used generally throughout the text.

Others are defined when used.

SYMBOLS	……	UNITES
B	Wedge angle factor	-
C	Arbitrary constant	-
f	Function of similarity variable (η).	-
Gr_x	Local Grashof number: Ratio of buoyancy force to the viscous force, $Gr_x = g.\beta.\Delta T.x^3/\nu^2$	-
g	Acceleration due to gravity.	m/s^2
h	Local heat-transfer coefficient.	$W/m^2.K$
k	Thermal conductivity of the plat.	W/m.K
L	Characteristic length of the plate	m
m	Exponent of Variable defined as $m = \frac{B}{2 - B}$	-
n	Constant – exponent of Variable	-
Nu_x	Local nusselt number $Nu_x = h.x/k$	-
P	Pressure	N/m^2
Pr	Prandtl number: Ratio of momentum diffusivity (υ) to heat diffusivity (α), $Pr = \nu/\alpha$	-
q	Specific Local heat transfer rate.	W/m^2
Re_x	Local Reynolds number: Ratio of inertia force to the viscous force, $Re_x = U_\infty.x/\nu$	-
Ri_x	Local Richardson number: Ratio of buoyancy force to the change of momentum flow. $Ri_x = g.\beta.\Delta T.x/U_\infty^2$	-
Ra	Rayleigh number: Ratio of natural convective to change of momentum flux. $Ra = Gr * Pr$	-
St	Stanton number: Ratio of actual to adventives heat flux. $St = Nu/Re * Pr$	-
T	Temperature	K

U_∞	Free stream velocity in x-direction	m/s
u	Velocity in x-direction	m/s
v	Velocity in y-direction	m/s
x	Coordinate along the inclined surface	m
y	Coordinate perpendicular to the inclined surface	m
x^*	Dimensionless coordinate along the inclined surface $x^* = \frac{x}{L}$	-
y^*	Dimensionless coordinate perpendicular to the inclined surface. $y^* = \frac{y}{L}$	-
u^*	Dimensionless velocity in x-direction $u^* = \frac{u \cdot L}{\nu}$	-
v^*	Dimensionless velocity in y-direction $v^* = \frac{v \cdot L}{\nu}$	-
U^*_∞	Dimensionless free stream velocity in x-direction $U_\infty{}^* = \frac{U_\infty \cdot L}{\nu}$	-

Greek Symbols

α	Thermal diffusivity	m^2/s
β	Coefficient of thermal expansion	K^{-1}
δ	Hydrodynamic boundary-layer thickness	m
δ_t	Thermal boundary-layer thickness	m
θ	Dimensionless temperature $\theta = \frac{T - T_\infty}{T_w - T_\infty}$	-
μ	Viscosity of the convective fluid	Kg/m.s

ν	Kinematics viscosity of the convective fluid	m^2/s
ρ	Density of convective fluid	Kg/m^3
ψ	Stream Function	-
Φ	Inclination Angle	Dgree
η	Similarity Variable	-
τ	Sheer Stress	N/m^2
Superscript		
*	Dimensionless condition	-
'	Derivative with respect to η	-
Subscript		
∞	Condition at infinity	-
w	Condition at the wall	-
o	Forced flow condition	-
mix	Mixed flow condition	-

CHAPTER ONE

INTRODUCTION

1.1 General:

The mixed convection flow occurs in several industrial and engineering technical applications which include electronics devices cooled by fans, heat exchangers placed in a low velocity environment, and solar central receivers exposed in wind currents. In the study of fluid over heated or cooled surface, it is customary to neglect the effect of the buoyancy force when the flow is horizontal. However, for vertical or inclined surface, the buoyancy force modifies the flow field and the heat transfer rate. Therefore, it is not possible to neglect the effect of buoyancy force for vertical or inclined heated or cooled surface. [1].

1.2 Introduction:

Convection is defined as the transport of both mass and energy by potential gradient and gross fluid motion can be induced by either forced or natural convection. Convection uses the motion of fluids to transfer heat in a typical convective heat transfer, a hot surface heats the surrounding fluid, which is then carried away by fluid movement, such as wind. The warm fluid is replaced by cooler fluid, which can draw more heat away from the surface. Since the heated fluid constantly replaced by cooler fluid, the rate of heat transfer enhanced. [2] and [3].

Forced convection refers to fluid motion which induced some external process such as a fluid machine. The boundary layer is initially laminar but at some distance from the leading edge small disturbances appear, they are amplified and after a transition region they developed into a completely turbulent flow region. Therefore, assumed that at some distance (***critical distance*** x_c) from the leading edge, the turbulent flow occurs, this location is determined by the Reynolds number, if $Re < 5*10^5$ the flow is laminar, where the transient region form laminar to turbulent

is about $10^5 < Re < 10^7$, and assumed turbulence if Re is much higher than 10^7 as shown in Fig. (1-1). [3], [5], [7] and [8].

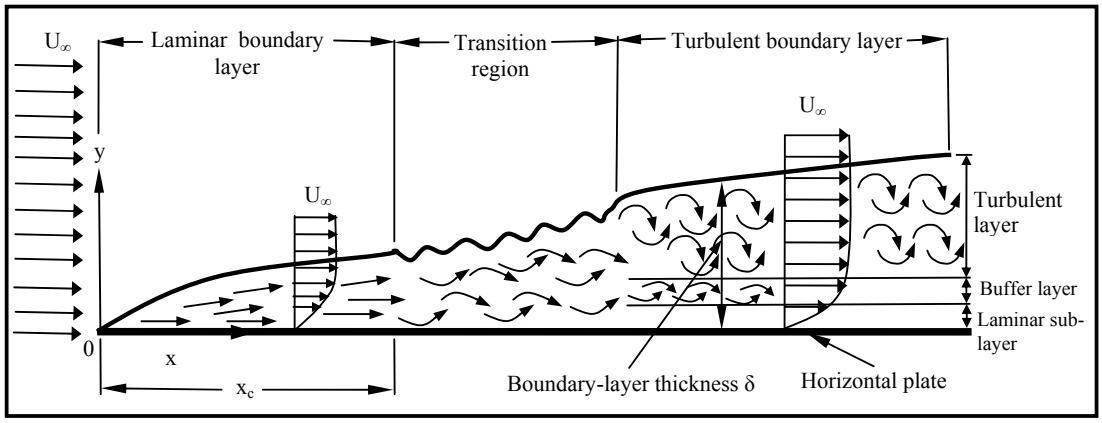

Fig. (1-1). Flow regime for the forced flow. Ref. [5].

The flow in the boundary layer is said to be laminar where fluid particles move along the streamlines in an orderly manner. Where turbulent flow is characterized by the irregular movement of particles of the fluid. There is no definite frequency as in the wave motion. The particles travel in irregular paths with no observable pattern and no definite layers.[7] and [9].

There is another number which is important in forced convection, as in the case of free convection one has to consider the Prandtl number. The significance of the Prandtl number is that it represents the ratio between energy transport by diffusion in the velocity layer and the thermal layer. For gases the Prandtl number is close to 1, for liquid metals Pr << 1, for viscous oils the opposite is true, Pr >> 1. [6].

This ratio usually assumed the value $\delta/\delta_t << 1$ for liquid metals, $\delta/\delta_t \approx 1$ for gases, and $\delta/\delta_t >> 1$ for viscous oils. Thus, for liquid metals, the limit $\delta/\delta_t \rightarrow 0$ of $\delta/\delta_t << 1$ suggests that the momentum boundary layer be ignored relative to the thermal boundary layer. For gases, begin slightly less than unity, δ/δ_t is very closely approximated when thickness of both layers are assumed identical. For viscous oils, the limit $\delta/\delta_t \rightarrow \infty$

of $\delta/\delta_t >> 1$ suggests that the development of the momentum boundary layer, being much faster than that of the thermal boundary layer be ignored and the momentum be assumed fully developed relative to the thermal layer. For various fluids, the thickness ratio of momentum and thermal layers and their limits are sketched in Fig. (1-2). [6] and [8].

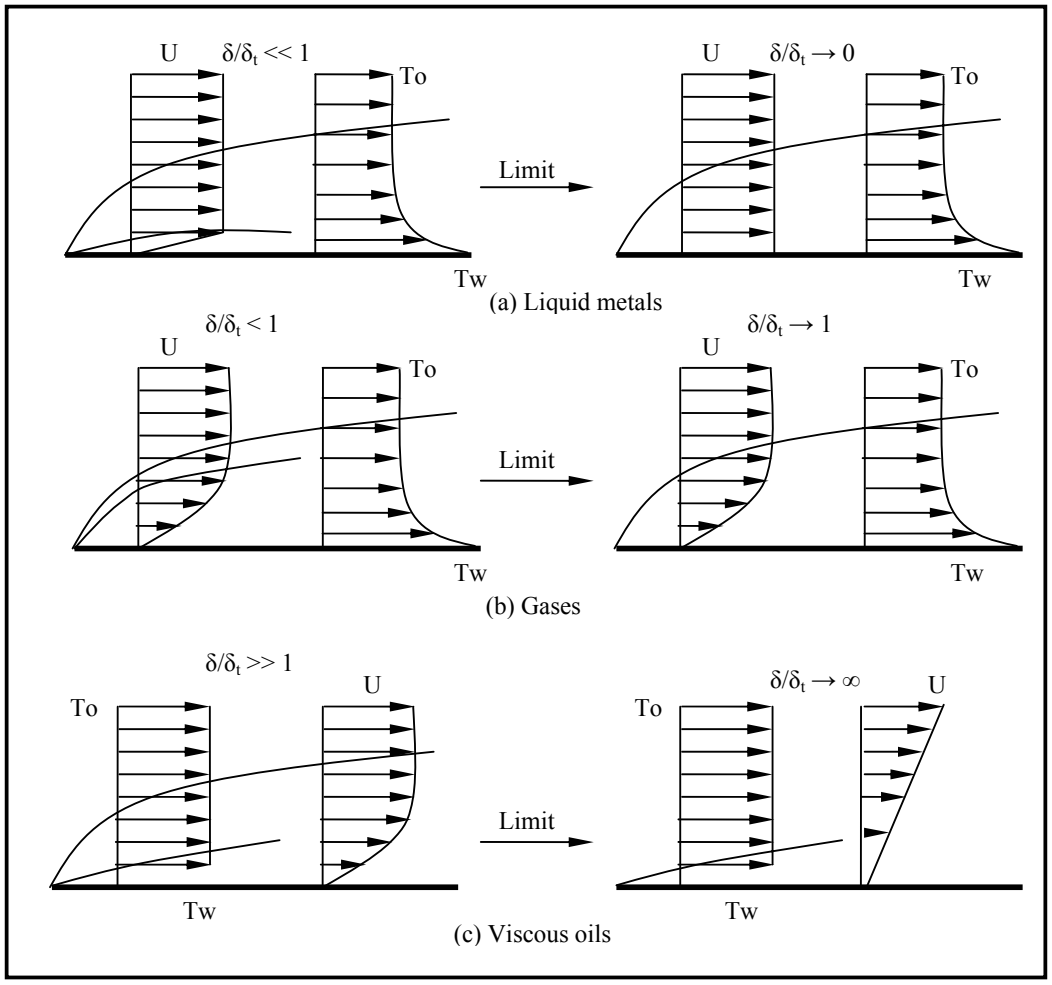

Fig. (1-2). thickness ratio of momentum and thermal boundary layer for various fluids. Ref. [6].

Natural convection refers to a case where the fluid movement is created by the warm fluid itself. The density of fluid decrease as it is heated thus, hot fluids are lighter than cool fluids. Warm fluid surrounding a hot object rises and replaced by cooler fluid, the result is a circulation of air above the warm surface, as shown in Fig. (1-3). [3].

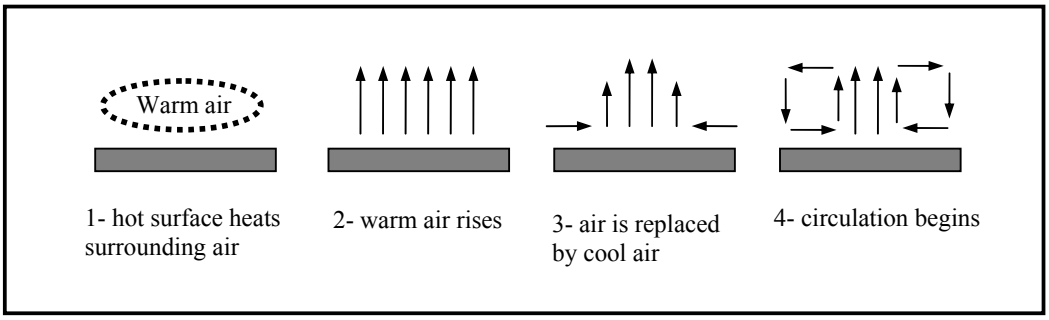

***Fig. (1-3). Natural convection. Ref.* [3].**

Natural convection on a vertical flat plate occurs when a plates is in contact with a fluid of different temperature from the surface. Density differences provide the body force required to move the fluid. The boundary layer is initially laminar and it is developed into a completely turbulent flow. Therefore, assumed that at some distance (***critical distance*** x_c) from the leading edge the turbulent flow occurs. This location is determined by the Rayleigh number, if Ra < 10^9 the flow is laminar, and if Ra >10^9 the flow is turbulent as shown in Fig. (1-4). [5], [7] and [8].

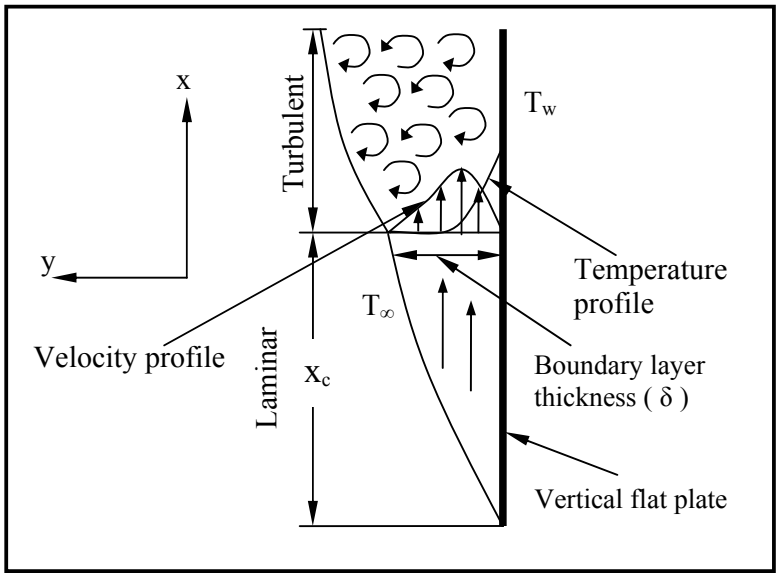

***Fig. (1-4). Temperature boundary layers and Flow regimes for the Natural Convection flow. Ref.* [5].**

Buoyancy is defined as the tendency of a body to float or rise when submerged in a fluid. The effect of buoyancy on heat transfer in a forced flow is strongly influenced by the direction of the buoyancy force relative to that of the flow. Three special cases that have been studied extensively correspond to buoyancy-induced and forced motion having the same direction (assisting flow), opposite direction (apposing flow), and perpendicular direction (transverse flow). Upward and downward forced motions over a heated vertical plate are examples of assisting and apposing flows, respectively, as shown in Figs. (1-5, a and b). Examples of transverse flow include horizontal motion over a heated cylinder, sphere, or horizontal plate. As shown in Fig. (1-5, c). [3], [10] and [11].

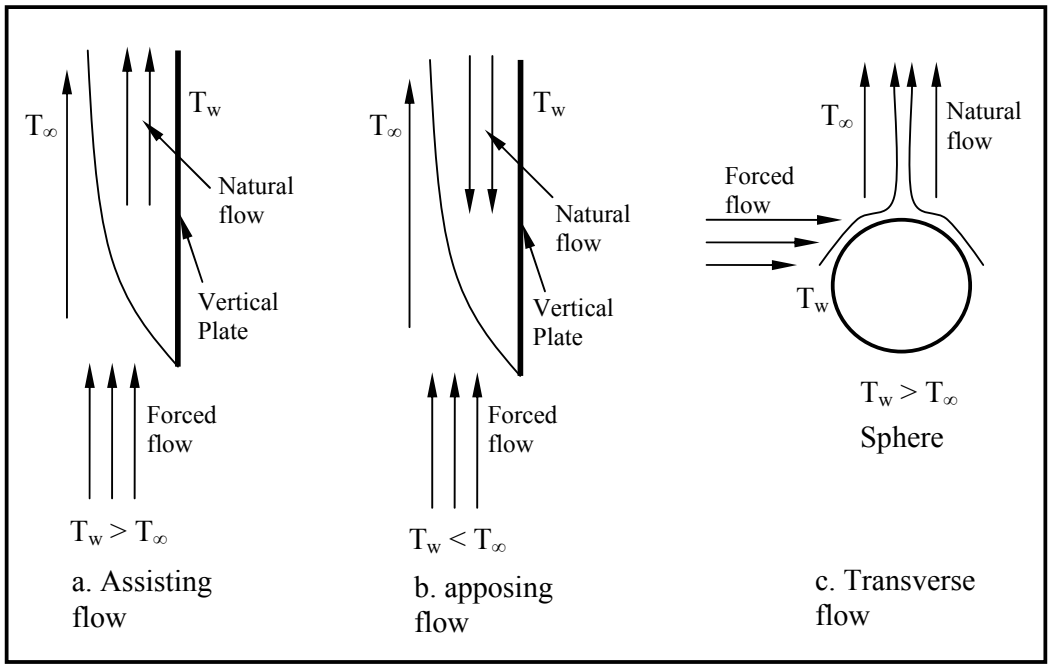

Fig. (1-5). Buoyancy force flow direction relative to the forced flow.

Mixed convection primarily occurs with laminar and transitional flows for the forced flow and moderate to large (Gr) i.e. (turbulent flow for the free convection), and the onset of mixed convection depends on

the relative magnitudes of (Gr) and (Re), which termed Richardson number $Ri_x = \frac{Gr_x}{\mathrm{Re}_x^{\,2}}$ and called as buoyancy force term,[3].

The buoyancy force term will be negligible if (Ri <<1) and forced convection will dominate. Correspondingly, if (Ri >>1), the buoyancy force effects will dominate and the flow will essentially be free convection, as shown in Fig. (1-6). [3], [6], [10] and [12].

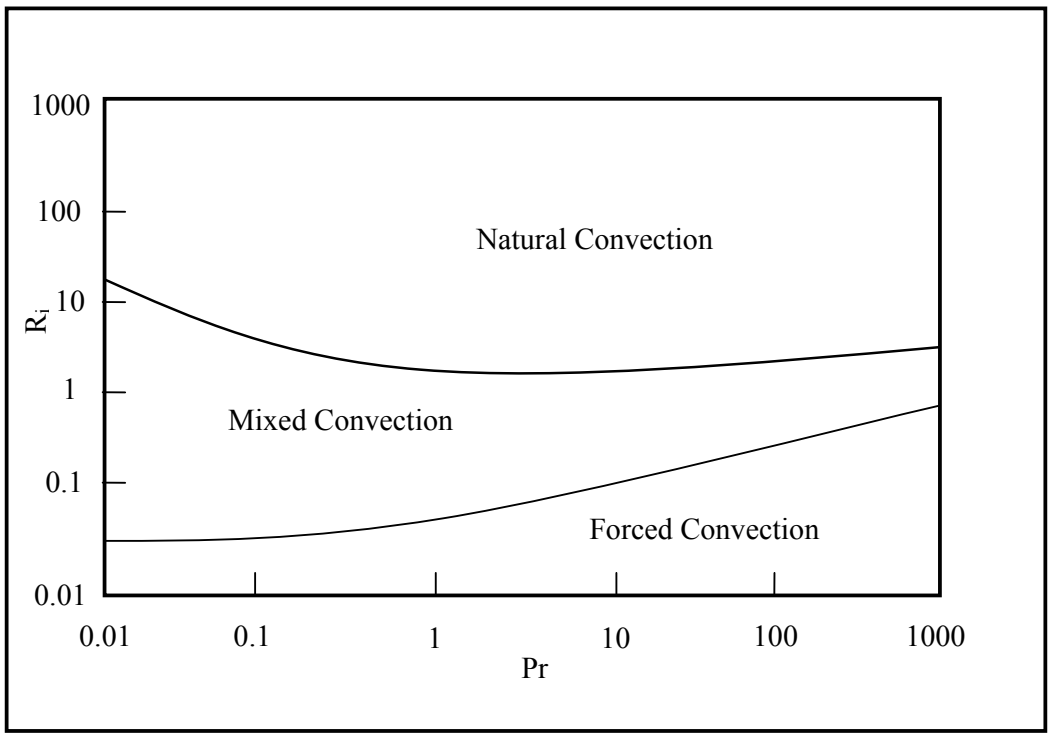

Fig. (1-6). Heat transfer regimes in adding laminar Mixed Convection from a vertical isothermal surface for constant heat flux case. Ref. [12].

Resulting buoyancy force aids the convection motion, expect the Nusselt number to be greater than the force-convection value at that Reynolds number. And when ($T_w < T_\infty$), the buoyancy force would oppose the flow and Nusselt number would decrease, [3]. In the present work convective flows that originate in part or exclusively from buoyancy force considered, and introduced the dimensionless parameter needed to

characterize such flows, to be able to discern when free convection effects on forced convection are important and to quantify the associated heat transfer rates.

1.3 Layout of the thesis:

The present thesis divided in to five chapters.

The first chapter include the introduction of the types of the convection heat transfer.

The second chapter is devoted to the literature survey for relevant work which studied the mixed convection over horizontal, vertical and inclined surfaces.

Third chapter includes mathematical modeling of the governing momentum and energy equations by integral method and similarity solution method for both constant wall temperature and constant heat flux with mixed convection.

The fourth chapter include results and their discussions. While chapter five present conclusions drawn from this work with the suggestions for the farther works.

1.4 Scope of the present work

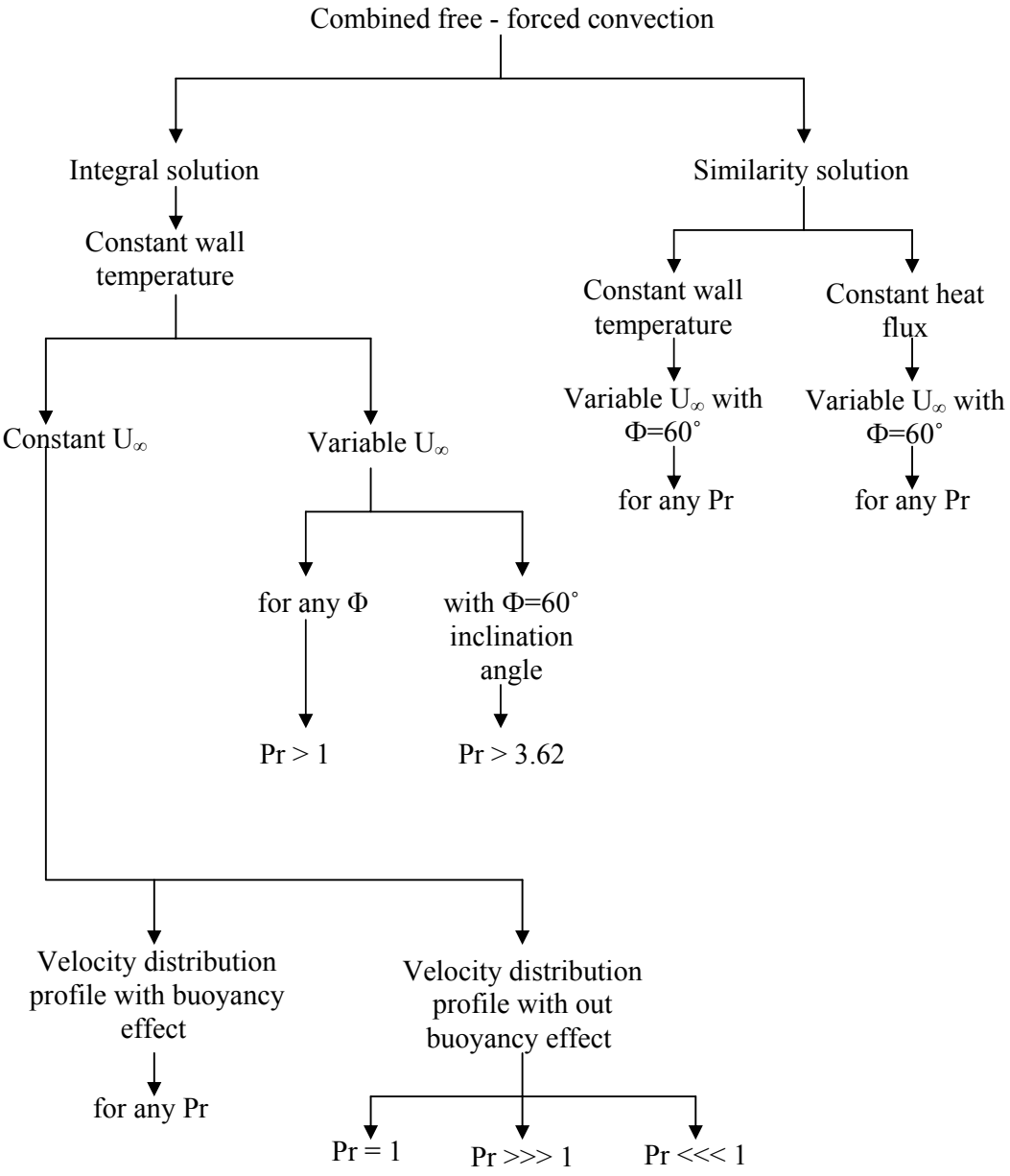

Chapter Two

Literature Review

2.1 Horizontal flat plate:

Schneider and Wasel [13], studied the break down of the boundary-layer approximation for steady state mixed convection above horizontal heated flat plate with constant wall temperature and constant heat flux for the Prandtl number rang from 0.5 up to 10. Boundary-layer equations modified to account for the hydrostatic pressure variation across the boundary layer are solved numerically by a finite difference scheme. Concluded As a critical distance from the leading adage is approached, the derivation of the wall shear stress becomes infinite, while the wall shear stress it self remaining finite and non-zero, thus the boundary-layer approximation breaks down before the classical separation criterion of vanishing wall shear stress is satisfied.

Tasawwur and Noor Afzal [14], studied analytically the steady state mixed convection boundary-layer above horizontal heated flat plate in a uniform stream for the Prandtl number of 0.72. For constant heat flux and constant wall temperature cases is investigated using computer extension of the perturbation series, the direct expansion is transformed by Euler transform and other techniques. The results shows for the buoyancy adding or apposing the main flow for uniform wall temperature, the maximum error is 5.983% for skin friction and 1.072% for heat transfer. For uniform heat flux, the maximum error is 6.9% for skin friction and 1.9% for wall temperature.

Appukuttan A. *et al*. [15], are studied experimentally the effect of buoyancy caused by heat generation from a microelectromechanical system (MEMS)-based thermal shear stress sensor. For study state laminar flow in horizontal channel with Prandtl number of 0.71 and 1, operating power of the shear stress sensor is taken the range $4*10^{-4}$ to $1.6*10^{-3}$, temperature difference between the shear stress sensor and free stream temperature is taken to be in the range 50-450K and the operating

Gr_s for the (MEMS) shear stress sensor range from 0.05 up to 0.5, with Re_x = 500 and Grashof range of 10^4 to 10^6. as shown in Fig. (2-1)

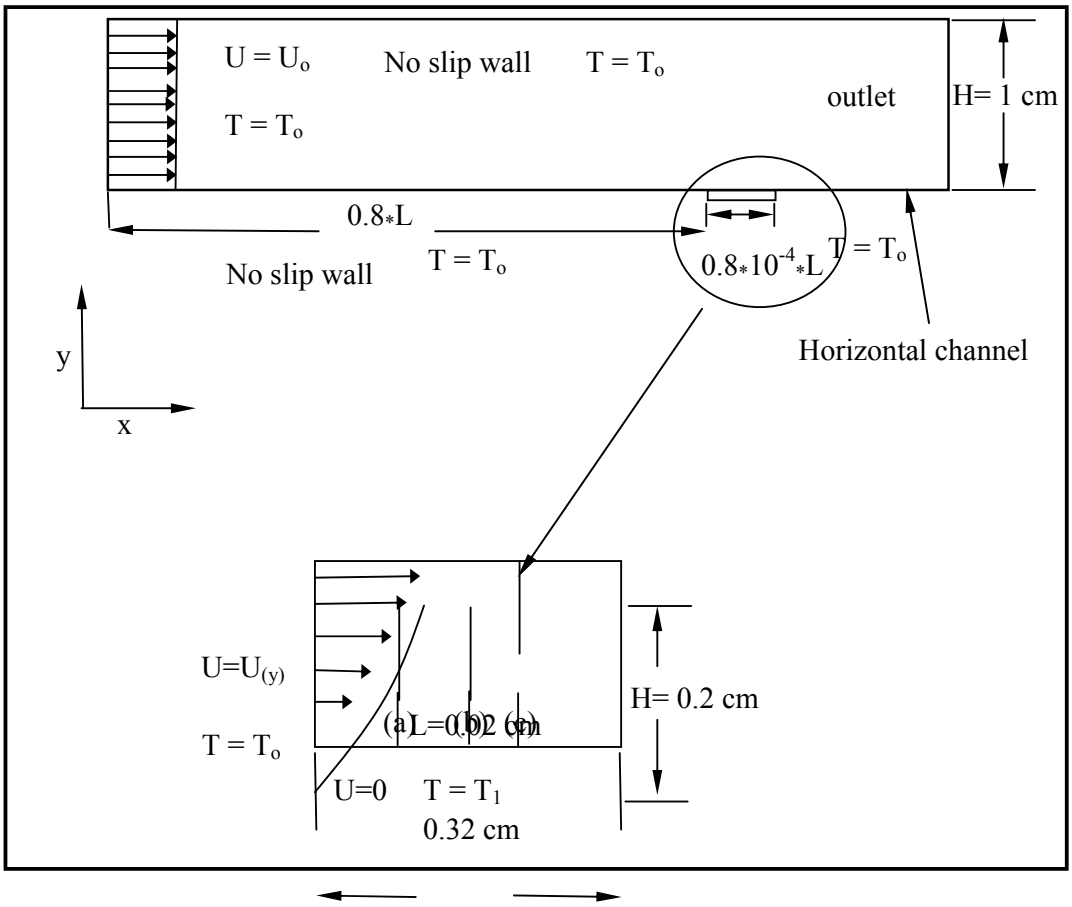

Fig.(2-1)Geometry and boundary conditions of the full-length model and focused domain near the sensor. (a), (b), and (c): Sections where velocity profiles are considered for comparison, Ref. [15] .

concluded due to the small size and relatively low power consumption of such sensors, the buoyancy effect on the overall flow structure is generally negligible. However, its impact on the flow variables such as shear stresses can be significant because such quantities are local and depend on the gradients of the velocity profile next to the sensor. Due to the small dimension of the (MEMS) sensor, a multi scale modeling approach is adopted to examine the effect of buoyancy on the velocity and wall shear stress profiles.

Manca O. *et al*. [16], are studied numerically the effect of the heat wall position on steady state mixed convection in a channel with an open cavity. Three basic heating modes are considered: (a) the heated wall is on the inflow side (assisting flow); (b) the heated wall is on the outflow side (opposing flow); and (c) the heated wall is the horizontal surface of the cavity (heating from below), as shown in Fig. (2-2).

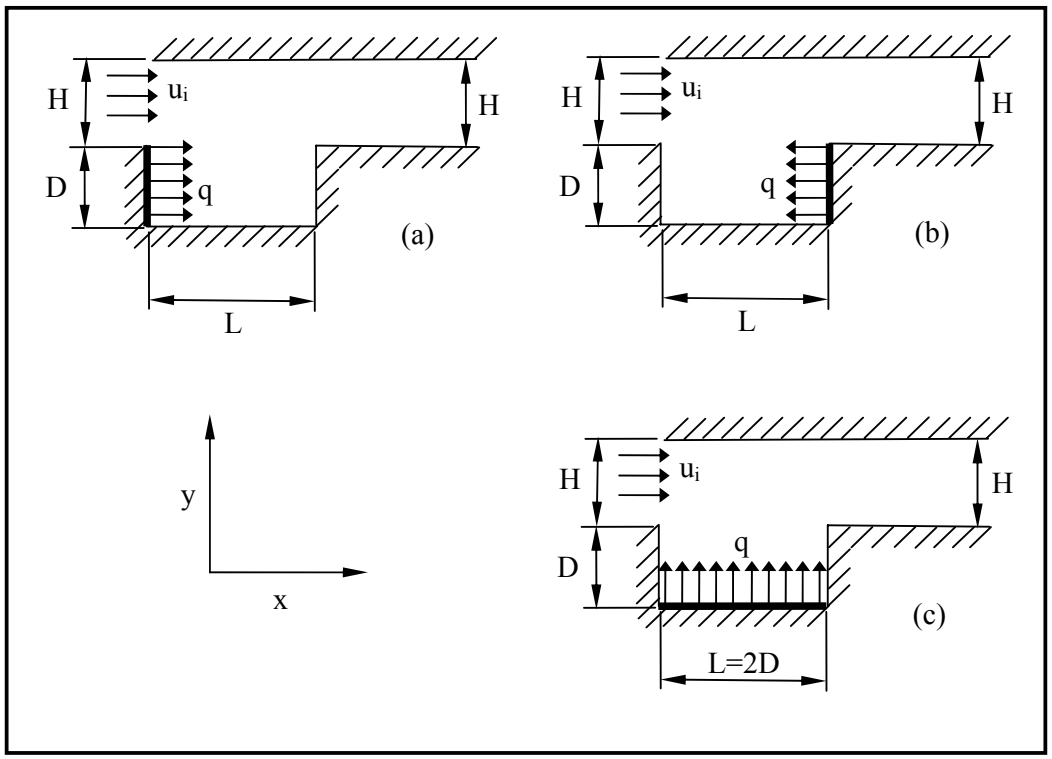

Fig. (2-2). Geometry under consideration: (a) assisting forced flow, (b) opposing forced flow, and (c) heating from below, Ref.[16].

For constant wall temperature, Reynolds of 100 and 1000, Richardson number of 0.1 and 100, Pr = 0.71 and the ratio between the channel and cavity heights (H/D) is in the range 0.1-1.5 and by using the finite element methods it was noticed that recirculating cells develop within the cavity, which improve the heat removal from the heat source for the opposing flow case. The present results show that the opposing forced flow configuration has the highest average Nusselt number among other

configurations for various (H/D). In addition, the results of this investigation illustrate that the maximum temperature values decrease as the Reynolds and Richardson numbers increase for all three configurations. Generally, the highest thermal performance is achieved in the opposing mode.

Khalil Khanafer. *et al*. [17], studied numerically Mixed convection heat transfer in two-dimensional open-ended enclosures, for three basic configurations. A wide range of pertinent parameters such Grashof number, Reynolds number, and the aspect ratio are varied as $10^2 \leq Re \leq 10^4$, $10^2 \leq Gr \leq 10^5$ and $0.25 \leq$ aspect ratio of the in closure (W/H) ≤ 1. The results show that the lower and the upper average Nusselt number increase almost linearly with the Reynolds numbers for the three configurations at low Grashof number. In addition, for low Grashof number, the results show that the lower average Nusselt number is the highest for the 45º flow angle of attack and is the lowest for the 90º flow angle of attack. However, the upper Nusselt number is found to be the highest for the 90º flow angle of attack and is the lowest for the 45º flow angle of attack. For high Grashof number, the results show that the lower and the upper average Nusselt number are the highest for the 45º flow angle of attack and are the lowest for the 90º flow angle of attack at various Reynolds numbers as shown in Fig. (2-3).

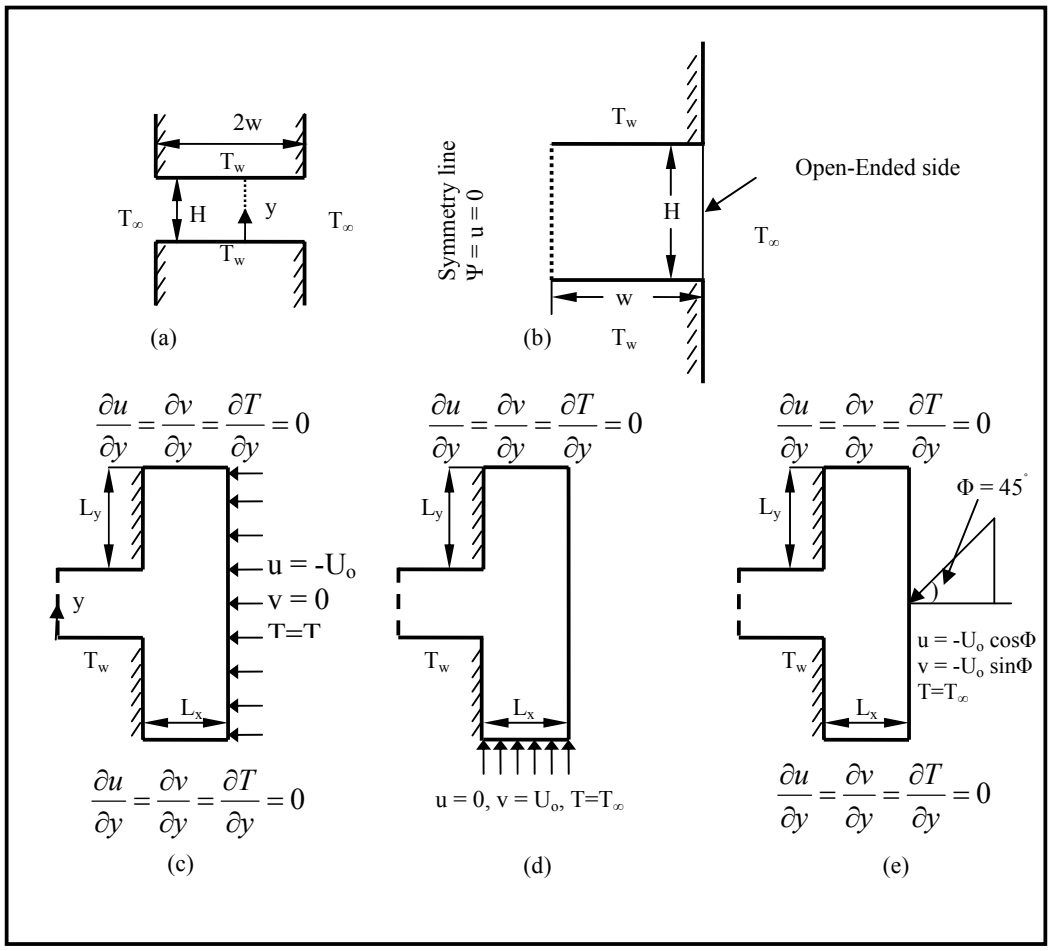

Fig. (2-3). (a) Physical domain, (b) physical domain utilizing the symmetry condition, (c) horizontal flow, (d) vertical flow, and (e) inclined flow, Ref. [17].

2.2 Vertical flat plate:

Kumari and Nath [1], studied the development of the mixed convection flow of an incompressible laminar viscous fluid over semi-infinite vertical plate when the fluid in the external stream is set in to motion impulsively, for Prandtl number of 0.7 and Richardson number range from 0 up to 3. by both analytically and numerical similarity solution concluded there is a smooth transition from the early flow development to the final steady state. The surface shear stress and the heat transfer increase and decrease with time when the buoyancy parameter is greater or less than a certain value. Both the surface shear stress and heat transfer increase with the buoyancy parameter after the

start of the motion. The surface shear stress and heat transfer for the constant heat flux case are greater than those of the constant wall temperature case.

Satish Kumar and Masayoshi Shimo [2], studied analytically the steady stat mixed convection over an isothermal vertical heated flat plate, for the Prandtl number of 0.7 and buoyancy parameter Richardson number range of 0.01 to 0.5. Shooting method can be used to solve for similarity solution for constant temperature case. The result for this case of buoyancy adding a forced convective flow over an isothermal vertical flat plate, the Nusselt number and wall shear stress (normalized by their values for forced convection) increase as the buoyancy parameter increase.

Manning and Qureshi [12], studied empirically the laminar aiding mixed convection over a vertical isothermal heated surface, for prandtl number range from 0.01 up to 100. the results for constant wall temperature case and for adding flow Nusselt number and wall shear stress increase as the free and forced convection parameter increases as the empirical relation ship (B.1) shows.

Chamkha. *et al*. [18], studied mixed convection flow over vertical plate with localized heating (cooling), magnetic field and suction (injection) for the Prandtl number of 0.7, magnetic parameter was varied from 0 up to 4, Richardson number was varied from -0.5 up to 0.5 and mass transfer constant was varied from -1 up to 1. The nonlinear coupled parabolic partial differential equations governing the flow have been solved by using an implicit finite-difference Scheme results the effect of the localized heating or cooling is found to be very significant on the heat transfer, but its effect on skin friction is comparatively small. The buoyancy, magnetic and suction parameter increase the skin friction and

heat transfer. The positive buoyancy force (beyond a certain value) causes an overshoot in the velocity profile.

Ali M. and Al-Yousef F. [19], studied the laminar mixed convection from a continuously moving vertical surface wit suction or injection for the boundary layer equation subject to power law temperature and velocity boundary conditions. By using similarity solutions for Pr = 0.72 results that the heat transfer coefficient increase with increases of mixed convection terms, and Nusselt number increase with increases of temperature exponent with constant mixed convection parameter (Ri_x) and injection parameter.

Selim A. *et al*. [20], studied the effect of surface mass transfer on mixed convection flow past a heated vertical flat permeable plate with thermophoresis, for a non uniform surface mass flux through the permeable surface, with steady state uniform free stream, for Prandtl number of 0.7, Schmidt number about 10, local Richardson number range from 0 up to 5 and for thermophoretic parameter of 0.1, 0.5 and 1, by using similarity solution method, from the present investigation the following conclusions may be drawn:

1. in the mixed convection regime the value of the local skin-friction coefficient, the local Nusselt number and the local Stanton number increase when the value of the local Richardson number increases.
2. As Richardson number increases both the temperature and concentration boundary layers decreases in thickness.
3. Wall suction was found to decrease the strength of the stream wise flow and to decrease both the thermal and concentration boundary layer thicknesses.
4. As the Schmidt number increases, the concentration boundary layer becomes thinner and the surface mass flux increases.

5. As the thermophoretic parameter increases the surface mass flux increases.

Idiri M. and Souidi F. [21], studied the higher order boundary layer effect in an opposed mixed convection problem on a vertical flat plate, for water with study state uniform free stream flow of Prandtle about 6.7 and mixed convection parameter ($Re/Gr^{*2/5}$) rang from 0.1 up to 0.5 where Gr^* is modified Grashof number defined as $(g_*\beta_*q_*L^4/k_*\upsilon^2)$, with constant wall temperature, by using (THE MATCHED ASYMPTOTIC EXPANSIONS METHOD), concluded for fixed Gr_x^* the contribution of the higher order on Nusselt increases with increases of mixed convection parameter, also for fixed mixed convection parameter Nusselt number decreases as Gr_x^* gets larger and for moderate Grashof number, the wall shear stress decreases as mixed convection parameter increases.

Herbert Steinruck [22], examined the effect of the buoyancy on the laminar steady state boundary layer about vertical heated flat plate, by using similarity solution method for Prandtl number range from 0.2 up to 2 and mixed convection parameter which defined as $\lambda = \lim_{x\to\infty} \frac{Gr_x}{\mathrm{Re}^2}$ was varied from -1 for apposed flow to 1 for assisting flow, concluded that the heat transfer rate increase or decreases with the increases or decreases of mixed convection parameter respectively.

Ramos R. *et al*. [23], studied steady state mixed convection between two parallel vertical heated flat plates, for Prandtl number of 0.7, Richardson number of (1/64, 1/10.66, 1/96, 1/160 and 1/240), with different value of Reynolds number, for constant heat flux and constant wall temperature, by using Generalized Integral Transform Technique (GITT), concluded the velocity closer to the channel walls is very high, due to the buoyancy effect, and the flat temperature profiles in regions

close to the channel center, but sharply decreasing profiles in positions closer to the walls, which means high temperatures gradients in these regions.

2.3 inclined flat plate:

Ping Cheng [24], studied combined free forced convection about horizontal and inclined surface in a saturated porous medium. For the parameter governing mixed convection from surface in porous media (Gr/Re) range from 0 up to 50. For constant heat flux case and inclination angles (0º and 45º) and by using similarity solution method concluded that the Nusselt number increase as increasing in mixed convection parameter and increases of inclination angle.

Rogerio Ramos [25], studied the steady state mixed convection in laminar flow between inclined parallel plats, by using the general integral transform technique which is employed in the hybrid numerical solution of the problem. For both constant wall temperature and constant heat flux and for Pr = 0.7, Re = 100 and 1600 and Ri = 1/37, concluded that the heat transfer rate and wall shear stress are increase with increases of buoyancy force and increasing of inclination angle.

Bahlaoui A. *et al*. [26], studied the steady state combined mixed convection and radiation in a channel discretely heated from below, for $Ra = 10^5$, Re = 50, inclination angle range of 0º up to 60º and emissive power by radiation (ε) of 0, 0.5 and 1, by using Alternate Direction Implicit Method (ADI), concluded that the Nusselt number increase with increases of inclination angle for different value of ε. This due to increases of natural convection effect by increases of inclination angle, total heat transfer cross the wall increases quickly with increases of (ε).

Yang H. Q. and Yang K. T. [27], studied the effect of laminar forced convection on natural convection from an inclined, heated plate situated inside the horizontal channel, for Ra of $5.2*10^3$, Re range of 0.12

to 120 to cover the range of natural convection dominant flow to the forced convection dominant flow, plate length fixed at L = 0.54H, where H is the high of the channel, inclination angle of 60º and 120º to determined the adding and opposing effect of the forced convection and Prandtl number of 0.71, numerically concluded that the forced convection is found to augment the heat transfer as well as to make the heat transfer rate more uniform on the upward facing side of the plate and the boundary condition, inclination angle, and offset position are found to have significant effect on the interaction of forced and natural convection.

Kumari M. *et al*. [28], studied numerically the mixed convection flow over a vertical wedge with magnetic field embedded in porous medium by using Keller box method for Prandtl number range from 0.72 up to 7, Richardson number range from 0 up to 10, magnetic field parameter range of 0 to 1, permeability parameter range of 0 to 0.5,and pressure gradient range of 0 to 1, concluded the skin friction and heat transfer are increases with the permeability of medium, buoyancy force, magnetic field and pressure gradient effects, while the effect of permeability and magnetic field on the heat transfer is very small. The heat transfer increases with Prandtl number but skin friction decreases. The buoyancy force which assist the forced convection flow causes an overshoot in the velocity profiles. Both skin friction and heat transfer increases with suction and the effect of injection is just the reverse.

2.4 Summery:

From the above research's concluded, that the mixed convection on horizontal flat plate, tangential component of the buoyancy force gives rise to a hydrostatic pressure distribution across the boundary layer which modify the forced convection boundary layer. As the boundary layer develops, the hydrostatic pressure at the plate surface also increase with increasing distance from the leading edge the buoyancy force either aid or appose the development of the forced convection boundary layer depending on wither the induced pressure gradient within the boundary layer is favorable or adverse.

The transport in aiding laminar mixed convection flow adjacent to a vertical or inclined surface, the direction of the forced flow is taken to be upward for the heated surface, this situation causes the flow to be predominately forced at the leading edge, primarily natural far downstream, and mixed in the middle, finally buoyancy force aid convective motion whereas if the surface heated to a temperature higher than the surroundings temperature and causes variation in the velocity and temperature field of the forced convection flows leading to variation in the Nusselt number and wall shear stress.

In the present work compares an analytical and a numerical analyses techniques that can used to solve for the case of convective flow aiding forced flow over inclined surface.

CHAPTER THREE

MATHEMATICAL MODEL

3.1 Introduction:

Problem of boundary layer mixed convection is investigated by employing many methods. Empirically with a high range of Prandtl number about from 0.01 up to 100, over a vertical isothermal heated surface by **Manning and Qureshi,** [12]. Experimentally with taking the buoyancy effect caused by heat generation from a microelectromechanical system (MEMS) based thermal shear stress sensor in a horizontal channel for steady state laminar flow by **Appukuttan,** [15]. Similarity solution method taking surface mass transfer effect on mixed convection flow past a heated vertical flat permeable plate by **Selim,** [20]. Numerical solution using (Matched Asymptotic Expansions Method) taking apposing flow effect on a vertical plate by **Idri and Souidi,** [21]. Hybrid similarity solution with taking shear stresses effect in the y-direction using (General Integral Transform Technique) for inclined two parallel flat plates by **Rogerio,** [25]. Alternate direction implicit method (ADI) with taking radiation effect in a horizontal channel by **Bahlaoui,** [26]. Numerical solution using (Keller box method) with taking Magnetic field effect over a vertical wedge with porous media by **Kumari**, [28]. In the present work is employing tow method, integral method for constant wall temperature cases in the first step, and similarity solution method for both constant wall temperature and constant heat flux in the second step , and to simplify the analyses there is some assumption are imposed.

3.2 Assumptions:

The present analysis is based on the following assumption:

1. Laminar two dimensional and study state incompressible fluid flow.
2. Newtonian fluid with constant properties except for the Buossinesq approximation.
3. Flow which gives the thermal boundary layer thickness and the hydrodynamic boundary layer thickness are equals.
4. Viscous shear force in the y-direction is negligible.
5. There are no pressure variations in the direction perpendicular to the plate.
6. The flow with constant wall temperature or constant heat flux.
7. The heat flow and temprature distribution over the inclined plat is independent of time, i.e.the heat flow is steady.
8. The temperature of the surrounding fluid is constant.
9. Impervious and no-slip walls.

3.3 Mixed Convection With Constant Free Stream Velocity:

3.3.1 Governing Momentum Equation:

Consider the plate shown in the figure (3-1), the governing equation of the flow formulated from consideration steady state laminar flow balance over the integral element (Δx and Δy), taken into account the assumption of the problem.

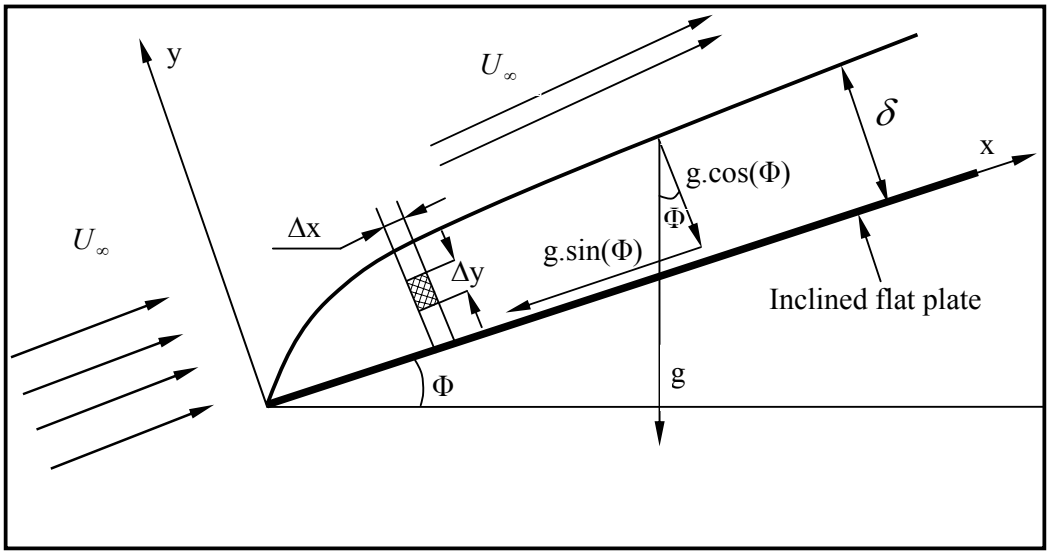

Fig (3-1)

Hence, for a two-dimensional steady state condition system and when the flow parallel to the flat plate.

The continuity equation [5] is defined as:

$$\frac{\partial u}{\partial x} + \frac{\partial v}{\partial y} = 0 \quad \text{……...……..(3.1)}$$

Integrating eq. (3.1) along the boundary layer:

$$\int_0^\delta \frac{\partial u}{\partial x} dy + \int_0^\delta \frac{\partial v}{\partial y} dy = 0$$

B.C $v = 0$ at $y = 0$, gives: $$v = -\int_0^\delta \frac{\partial u}{\partial x} dy \quad \text{……..…..(3.2)}$$

The momentum equation for mixed and natural convection [10] is defined

as the equilibrium of the net momentum in the left side and net shear force plus body forces in the right side as shown below;

$$\rho\cdot\left(u\frac{\partial u}{\partial x}+v\frac{\partial u}{\partial y}\right)=-\frac{\partial p}{\partial x}+\mu\frac{\partial^2 u}{\partial y^2}-\rho\cdot g\cdot\sin(\Phi) \qquad \text{……...……. (3.3)}$$

Assuming that the pressure gradient inside and outside the boundary layer is the same, thus:

$$\frac{\partial p}{\partial x}=-\rho_\infty\cdot g\sin(\Phi) \qquad \text{…….……(3.4)}$$

Substituting eq. (3.4) in to eq. (3.3) and using boussinesq approximation gives:

$$u\frac{\partial u}{\partial x}+v\frac{\partial u}{\partial y}=\upsilon\frac{\partial^2 u}{\partial y^2}+g.\beta.\sin(\Phi).(T-T_\infty) \qquad \text{……(3.5)}$$

Where the thermal expansivity [4] is defined as $\beta=\frac{1}{\rho}\left(\frac{\rho_\infty-\rho}{T-T_\infty}\right)$

Integrating eq. (3.5) along the boundary layer and adding and subtracting the term $\int_0^\delta u\ \frac{\partial v}{\partial y}dy$ gives:

$$\int_0^\delta u\frac{\partial u}{\partial x}dy+uv\Big|_0^\delta-\int_0^\delta u\frac{\partial v}{\partial y}dy=\upsilon\int_0^\delta\frac{\partial^2 u}{\partial y^2}dy+\int_0^\delta g.\beta.\sin(\Phi).(T-T_\infty)dy$$

B.C; $u=v=0$ at $y=0$, $u=U_\infty$ and $v=-\int_0^\delta\frac{\partial u}{\partial x}dy$ at $y=\delta$

Thus;

$$\int_0^\delta u\frac{\partial u}{\partial x}dy-U_\infty\int_0^\delta\frac{\partial u}{\partial x}dy-\int_0^\delta u\frac{\partial v}{\partial y}dy=\upsilon\int_0^\delta\frac{\partial^2 u}{\partial y^2}dy+\int_0^\delta g.\beta.\sin(\Phi).(T-T_\infty)dy$$

From (3.1) ; $\frac{\partial u}{\partial x}=-\frac{\partial v}{\partial y}$

Thus;

$$\frac{d}{dx}\int_0^\delta u(u-U_\infty)dy=v\frac{du}{dy}\Big|_0^\delta+\int_0^\delta g.\beta.\sin(\Phi).(T-T_\infty)dy \qquad \text{…… (3.6)}$$

But, $\frac{du}{dy}=0$ at $y=\delta$ Thus;

$$U_\infty{}^2\frac{d}{dx}\int_0^\delta\frac{u}{U_\infty}(1-\frac{u}{U_\infty})dy=-g.\beta.\sin(\Phi).\int_0^\delta(T-T_\infty)dy+\nu\left.\frac{du}{dy}\right|_{y=0} \quad \ldots.(3.7)$$

3.3.2 Boundary layer Thickness, Nusselt number and Shear Stress:

Solving eq. (3.7) by selected the velocity distribution profile for the forced convection flow [6] is defined as;

$$\frac{u}{U_\infty}=\frac{3}{2}\frac{y}{\delta}-\frac{1}{2}\frac{y^3}{\delta^3} \quad \ldots\ldots\ldots\ldots\ldots\ldots\ldots\ldots\ldots\ldots\ldots..(3.8)$$

Temperature distribution profile [5] is defined as;

$$\frac{T-T_\infty}{T_w-T_\infty}=1-\frac{3}{2}\frac{y}{\delta_t}+\frac{1}{2}\frac{y^3}{\delta_t{}^3} \quad \ldots\ldots\ldots\ldots\ldots\ldots\ldots\ldots\ldots\ldots..(3.9)$$

Where $\delta\equiv\delta_t$ from the assumption.

Substituting eqs. (3.9) and (3.8) in to eq. (3.7), gives;

$$\frac{39U_\infty{}^2}{280}\frac{d\delta}{dx}=-\frac{3}{8}g.\beta.\sin(\Phi).\theta_w\delta+\frac{3}{2}\frac{\nu\cdot U_\infty}{\delta} \quad \ldots\ldots\ldots\ldots\ldots\ldots\ldots\ldots..(3.10)$$

Solving the above differential equation by integration both sides gives:

$$\frac{\delta_{mix}}{x}=\frac{2}{(\mathrm{Re}_x)^{\frac{1}{2}}.(Ri_x\cdot\sin(\Phi))^{\frac{1}{2}}}\cdot\left[1-\exp[-5.4\cdot Ri_x\cdot\sin(\Phi)]\right]^{\frac{1}{2}} \quad \ldots\ldots\ldots(3.11)$$

Where as for the forced convection flow over a flat plate [5];

$$\frac{\delta_o}{x}=\frac{4.64}{\sqrt{\mathrm{Re}_x}} \quad \ldots\ldots\ldots\ldots\ldots\ldots\ldots\ldots\ldots\ldots\ldots\ldots\ldots\ldots\ldots\ldots (3.12)$$

Thus, the dimensionless boundary layer thickness ratio becomes;

$$\frac{\delta_{mix}}{\delta_o}=\frac{0.431}{[Ri_x\cdot\sin(\Phi)]^{\frac{1}{2}}}\cdot\left[1-\exp[-5.4\cdot Ri_x\cdot\sin(\Phi)]\right]^{\frac{1}{2}} \quad \ldots\ldots\ldots\ldots\ldots(3.13)$$

Since the heat balance on the plate surface [10], at $y = 0$ is defined as:

$$q = -k \cdot \left.\frac{dT}{dy}\right|_{y=0} = h \cdot (T_w - T_\infty) \qquad \text{……..……..(3.14)}$$

Thus; $h = \frac{3}{2} \cdot \frac{k}{\delta}$ ……(3.15)

Since; $Nu = \frac{h \cdot x}{k}$ ……..……..……(3.16)

Substituting eqs. (3.11) and (3.15) in to eq. (3.16), gives;

$$Nu_{mix} = \frac{3}{4} \cdot \sqrt{\mathrm{Re}_x \cdot Ri_x \cdot \sin(\Phi)} \cdot \frac{1}{\sqrt{1 - \exp[-5.4 \cdot Ri_x \sin(\Phi)]}} \qquad \text{……(3.17)}$$

Where as for the forced convection flow over a flat plate Nusselt number defined as [5]:

$$Nu_o = 0.332 \cdot \mathrm{Pr}^{1/3} \cdot \mathrm{Re}_x^{\,1/2} \qquad \text{……(3.18)}$$

Thus;

$$\frac{Nu_{mix}}{Nu_o} = \frac{\frac{3}{4} \cdot \sqrt{Ri_x \cdot \sin(\Phi)}}{0.332 \cdot \mathrm{Pr}^{\frac{1}{3}}} \cdot \frac{1}{\sqrt{1 - \exp[-5.4 \cdot Ri_x \sin(\Phi)]}} \qquad \text{……(3.19)}$$

Shear stress at the wall may be expressed in terms of a friction coefficient C_f [5] where:

$$\tau_w = \mu \cdot \left.\frac{du}{dy}\right|_{y=0} = C_f \frac{\rho \cdot U_\infty^{\,2}}{2} \qquad \text{…….....……(3.20)}$$

Substituting eqs. (3.8) and (3.12) in to eq. (3.20), gives.

$$\frac{C_f}{2} = \frac{3 \cdot \sqrt{[Ri_x \cdot \sin(\Phi)]}}{4 \cdot \sqrt{\mathrm{Re}_x}} \cdot \frac{1}{\sqrt{1 - \exp[-5.4 \cdot Ri_x \sin(\Phi)]}} \qquad \text{……..(3.21)}$$

Since; $St_x = \frac{Nu_{mix}}{\mathrm{Re}_x \cdot \mathrm{Pr}}$ ……(3.22)

Substituting eq. (3.18) in to eq. (3.22) gives:

$$St_x = \frac{C_f}{2 \cdot \mathrm{Pr}} = \frac{3 \cdot \sqrt{[Ri_x \cdot \sin(\Phi)]}}{4 \cdot \sqrt{\mathrm{Re}_x} \cdot \mathrm{Pr}} \cdot \frac{1}{\sqrt{1 - \exp[-5.4 \cdot Ri_x \sin(\Phi)]}} \qquad \text{……..……(3.23)}$$

The limits for eqs. (3.13), (3.19) and (3.23) respectively at $Ri_x \to 0$ means negligible buoyancy force effect which results:

$$\lim_{Ri_x \to 0} \frac{0.431}{[Ri_x \cdot \sin(\Phi)]^{\frac{1}{2}}} \cdot \left[1 - \exp[-5.4 \cdot Ri_x \cdot \sin(\Phi)\right]^{\frac{1}{2}} \approx 1 \qquad \text{……(3.24)}$$

$$\lim_{Ri_x \to 0} \frac{3}{4} \cdot \sqrt{\mathrm{Re}_x \cdot Ri_x \cdot \sin(\Phi)} \cdot \frac{1}{\sqrt{1 - \exp\left[-5.4 \cdot Ri_x \sin(\Phi)\right]}} = 0.323 \cdot \sqrt{\mathrm{Re}_x} \qquad \text{……(3.25)}$$

$$\lim_{Ri_x \to 0} \frac{3}{4} \cdot \frac{\sqrt{Ri_x \cdot \sin(\Phi)}}{\sqrt{\mathrm{Re}_x}} \cdot \frac{1}{\sqrt{1 - \exp\left[-5.4 \cdot Ri_x \sin(\Phi)\right]}} = \frac{0.323}{\sqrt{\mathrm{Re}_x}} \qquad \text{……(3.26)}$$

The limits for eqs. (3.13), (3.19) and (3.23) at $\Phi \to 0$ means horizontal flat plate which results:

$$\lim_{\Phi \to 0} \frac{0.431}{[Ri_x \cdot \sin(\Phi)]^{\frac{1}{2}}} \cdot \left[1 - \exp[-5.4 \cdot Ri_x \cdot \sin(\Phi)\right]^{\frac{1}{2}} \approx 1 \qquad \text{……(3.27)}$$

$$\lim_{\Phi \to 0} \frac{3}{4} \cdot \sqrt{\mathrm{Re}_x \cdot Ri_x \cdot \sin(\Phi)} \cdot \frac{1}{\sqrt{1 - \exp\left[-5.4 \cdot Ri_x \sin(\Phi)\right]}} = 0.323 \cdot \sqrt{\mathrm{Re}_x} \qquad \text{....(3.28)}$$

$$\lim_{\Phi \to 0} \frac{3}{4} \cdot \frac{\sqrt{Ri_x \cdot \sin(\Phi)}}{\sqrt{\mathrm{Re}_x}} \cdot \frac{1}{\sqrt{1 - \exp\left[-5.4 \cdot Ri_x \sin(\Phi)\right]}} = \frac{0.323}{\sqrt{\mathrm{Re}_x}} \qquad \text{…….(3.29)}$$

The limits for eqs. (3.13), (3.19) and (3.23) at $\Phi \to 90$ means vertical flat plate which results :

$$\lim_{\Phi \to 90} \frac{0.431}{[Ri_x \cdot \sin(\Phi)]^{\frac{1}{2}}} \cdot \left[1 - \exp[-5.4 \cdot Ri_x \cdot \sin(\Phi)\right]^{\frac{1}{2}} = \frac{.431}{Ri_x^{\frac{1}{2}}} \cdot \left[1 - \exp(-5.4 \cdot Ri_x)\right]^{\frac{1}{2}} \text{...(3.30)}$$

$$\lim_{\Phi \to 90} \frac{3}{4} \cdot \sqrt{\mathrm{Re}_x \cdot Ri_x \cdot \sin(\Phi)} \cdot \frac{1}{\sqrt{1 - \exp\left[-5.4 \cdot Ri_x \sin(\Phi)\right]}} = \frac{3}{4} \cdot \sqrt{\frac{Ri_x \cdot \mathrm{Re}_x}{1 - \exp(-5.4 \cdot Ri_x)}} \qquad \text{..(3.31)}$$

$$\lim_{\Phi \to 90} \frac{3}{4} \cdot \frac{\sqrt{\cdot Ri_x \cdot \sin(\Phi)}}{\sqrt{\mathrm{Re}_x} \cdot \mathrm{Pr}} \cdot \frac{1}{\sqrt{1 - \exp\left[-5.4 \cdot Ri_x \sin(\Phi)\right]}} = \frac{3}{4 \cdot \mathrm{Pr}} \cdot \sqrt{\frac{\dfrac{Ri_x}{1 - \exp(-5.4 \cdot Ri_x)}}{\mathrm{Re}_e}} \quad (3.32)$$

3.3.3 Hydrodynamic Boundary Layer Thickness and Shear Stress for The Assumption of (Pr >>> 1):

For this case temperature distribution profile is defined as:

$$\frac{T - T_\infty}{T_w - T_\infty} = 1 \qquad \text{……(3.33)}$$

Substituting eqs. (3.8) and (3.33) in to eq. (3.7) give:

$$\frac{39U_\infty{}^2}{280}\frac{d\delta}{dx} = -g.\beta.\sin(\Phi).\theta_w\delta + \frac{3}{2}\frac{\nu U_\infty}{\delta} \qquad \text{…….……(3.34)}$$

Integrating eq. (3.34) gives:

$$\frac{\delta}{x} = \frac{1.224}{(\mathrm{Re}_x)^{\frac{1}{2}}.(Ri_x \cdot \sin(\Phi))^{\frac{1}{2}}} \cdot \left[1 - \exp[-14.4 \cdot Ri_x \cdot \sin(\Phi)\right]^{\frac{1}{2}} \qquad \text{…..(3.35)}$$

Thus;

$$\frac{\delta}{\delta_o} = \frac{0.264}{[Ri_x \cdot \sin(\Phi)]^{\frac{1}{2}}} \cdot \left[1 - \exp[-14.4 \cdot Ri_x \cdot \sin(\Phi)\right]^{\frac{1}{2}} \qquad \text{……..(3.36)}$$

Substituting eqs. (3.8) and (3.35) in to eq. (3.19) gives:

$$\frac{C_f}{2} = \frac{3 \cdot \sqrt{[Ri_x \cdot \sin(\Phi)]}}{2.448 \cdot \sqrt{\mathrm{Re}_x}} \cdot \frac{1}{\sqrt{1 - \exp[-14.4 \cdot Ri_x \sin(\Phi)]}} \qquad \text{……(3.37)}$$

3.3.4 Boundary layer thickness and Nusselt number for The Assumption of (Pr <<< 1):

For this case velocity distribution profile is defined as:

$$\frac{u}{U_\infty} = 1 \qquad \text{……(3.38)}$$

The integral form of the energy equation [10] is defined as:

$$\frac{d}{dx}\int [u \cdot (T - T_\infty)]dy = -\alpha \cdot \left.\frac{dT}{dy}\right|_{y=0} \qquad \text{……(3.39)}$$

Substituting eqs. (3.9) and (3.38) in to eq. (3.39) gives:

$$\frac{3}{8}\cdot(T_w - T_\infty)\cdot U_\infty \cdot \frac{d\delta}{dx} = \frac{3}{2}\cdot\frac{\alpha\cdot(T_w - T_\infty)}{\delta} \qquad \text{……(3.40)}$$

Solving eq. (3.40) gives:

$$\frac{\delta}{x} = \frac{\sqrt{8}}{\sqrt{\mathrm{Pr}\cdot \mathrm{Re}_x}} \qquad \text{……(3.41)}$$

$$Nu_{mix} = 0.5303\cdot\sqrt{\mathrm{Pr}\cdot \mathrm{Re}_x} \qquad \text{……..…..(3.42)}$$

3.3.5 Boundary Layer Thickness and Nusselt Number with Constant Free Stream Velocity by Using Energy Equation:

Substituting eqs. (3.8) and (3.9) in to eq. (3.39) gives:

$$\frac{39}{280}\cdot U_\infty \cdot \frac{d\delta}{dx} = \frac{3}{2}\cdot\frac{\alpha}{\delta} \qquad \text{……..……(3.43)}$$

Integrating eq. (3.34) gives:

$$\frac{\delta}{x} = \frac{4.64}{\sqrt{\mathrm{Pr}\cdot \mathrm{Re}_x}} \qquad \text{……(3.44)}$$

Thus;

$$Nu_{mix} = 0.323\cdot\sqrt{\mathrm{Pr}\cdot \mathrm{Re}_x} \qquad \text{……..……...…… (3.45)}$$

$$\frac{C_f}{2} = \frac{0.323\cdot\sqrt{\mathrm{Pr}}}{\sqrt{\mathrm{Re}_x}} \qquad \text{…… (3.46)}$$

$$St = \frac{C_f}{2\cdot \mathrm{Pr}} \qquad \text{……..…….. (3.47)}$$

Equating eq. (3.25) with eq. (3.45) for Richardson number equal to zero gives Pr =1.

3.3.6 Velocity Profile with Buoyancy Effects:

Consider plate shown in the Fig. (3-2) the dimensionless equation of the velocity distribution is formulated from consideration steady state laminar flow balance and the boundary condition over the boundary layer thickness taken into account the assumption of the problem.

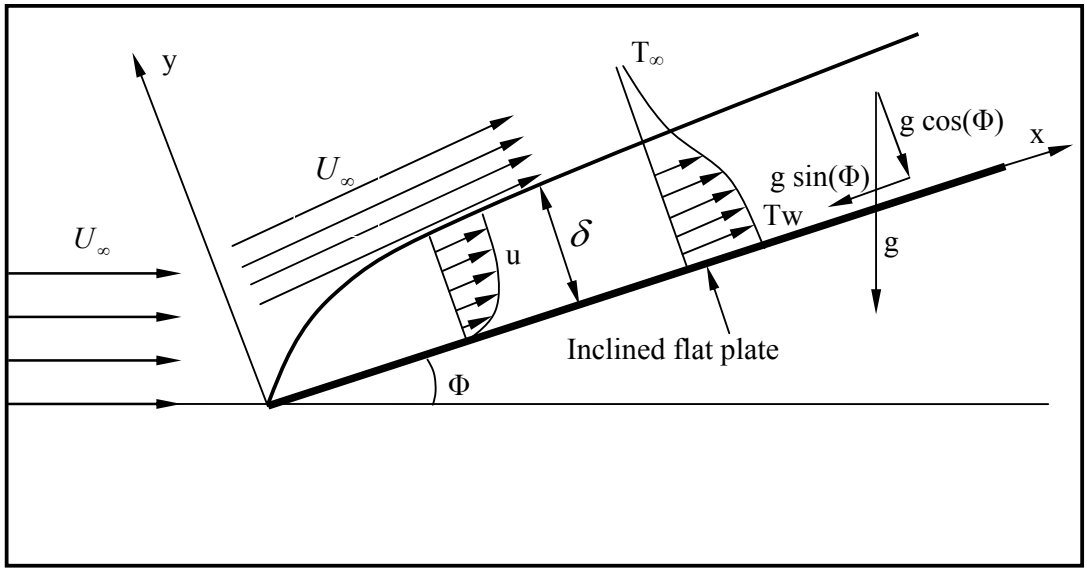

Fig (3-2)

Hence, for a two-dimensional steady state condition system, the boundary condition of the mixed flow condition:

1. $u = U_\infty$ at $y = \delta$
2. $u = 0$ at $y = 0$
3. $\frac{\partial u}{\partial y} = 0$ at $y = 0$
4. From eq. (3.5), $\frac{\partial^2 u}{\partial y^2} = -\frac{g.\beta.\sin(\Phi).(T_w - T_\infty)}{\upsilon}$ at $y = 0$

Let $\frac{u}{U_\infty} = a + by + cy^2 + dy^3$ ……(3.48)

Substitute the above boundary conditions in eq. (3.48) gives:

$$a = 0$$

$$b = \frac{g.\beta.\sin(\Phi).(T_w - T_\infty)\cdot\delta}{4\cdot\nu\cdot U_\infty} + \frac{3}{2}\cdot\frac{1}{\delta}$$

$$c = -\frac{g.\beta.\sin(\Phi).(T_w - T_\infty)}{2\cdot U_\infty\cdot\nu}$$

$$d = \frac{g.\beta.\sin(\Phi).(T_w - T_\infty)}{4\cdot U_\infty\cdot\nu}\cdot\frac{1}{\delta} - \frac{1}{2}\cdot\frac{1}{\delta^3}$$

Thus;

$$\frac{u}{U_\infty} = \frac{g.\beta.\sin(\Phi).(T_w - T_\infty)\cdot\delta^2}{4\cdot U_\infty\cdot\nu}\cdot\frac{y}{\delta}\cdot\left[1 - \frac{y}{\delta}\right]^2 + \frac{3}{2}\frac{y}{\delta} - \frac{1}{2}\frac{y^3}{\delta^3} \quad \text{….(3.49)}$$

3.3.6.1 Boundary layer thickness, Nusselt number and shear stress:

Substituting eqs. (3.9) and (3.49) in to eq. (3.39) gives:

$$\left[\frac{4}{105}\cdot\frac{g.\beta.\sin(\Phi)\cdot 3\cdot\delta^2}{4\cdot U_\infty\cdot\nu} + \frac{39}{280}\right]\cdot U_\infty\cdot\frac{d\delta}{dx} = \frac{3}{2}\cdot\frac{\alpha\cdot}{\delta} \quad \text{……..…..} \ (3.50)$$

Integrating eq. (3.50) and find the root by using MathCAD program gives:

$$\frac{\delta_{mix}}{x} = \frac{2}{\sqrt{\mathrm{Re}_x}}\cdot\sqrt{-\frac{39}{32}\cdot\frac{1}{Ri_x\cdot\sin(\Phi)} + \sqrt{\left(\frac{39}{32}\right)^2\cdot\frac{1}{(Ri_x\cdot\sin(\Phi))^2} + \frac{13440}{1024}\cdot\frac{1}{\mathrm{Pr}\cdot Ri_x\cdot\sin(\Phi)}}} \quad \text{..(3.51)}$$

Thus;

$$\frac{\delta_{mix}}{\delta_o} = \frac{2}{4.64}\cdot\sqrt{-\frac{39}{32}\cdot\frac{1}{Ri_x\cdot\sin(\Phi)} + \sqrt{\left(\frac{39}{32}\right)^2\cdot\frac{1}{(Ri_x\cdot\sin(\Phi))^2} + \frac{13440}{1024}\cdot\frac{1}{\mathrm{Pr}\cdot Ri_x\cdot\sin(\Phi)}}} \quad \text{…(3.52)}$$

$$\frac{Nu_{mix}}{\sqrt{\mathrm{Re}_x}} = \frac{3}{4}\cdot\frac{1}{\sqrt{-\frac{39}{32}\cdot\frac{1}{Ri_x\cdot\sin(\Phi)} + \sqrt{\left(\frac{39}{32}\right)^2\cdot\frac{1}{(Ri_x\cdot\sin(\Phi))^2} + \frac{13440}{1024}\cdot\frac{1}{\mathrm{Pr}\cdot Ri_x\cdot\sin(\Phi)}}}} \quad \text{..(3.53)}$$

$$\frac{Nu_{mix}}{Nu_o} = \frac{3}{4\cdot.332\cdot\mathrm{Pr}^{\frac{1}{3}}}\cdot\frac{1}{\sqrt{-\frac{39}{32}\cdot\frac{1}{Ri_x\cdot\sin(\Phi)} + \sqrt{\left(\frac{39}{32}\right)^2\cdot\frac{1}{(Ri_x\cdot\sin(\Phi))^2} + \frac{13440}{1024}\cdot\frac{1}{\mathrm{Pr}\cdot Ri_x\cdot\sin(\Phi)}}}} \quad \text{.(3.54)}$$

Substituting eqs. (3.49) and (3.51) in to eq. (3.20) gives:

$$\frac{C_f}{2}=\frac{Ri_x\cdot\sin(\phi)}{2\cdot\sqrt{\mathrm{Re}_x}}\cdot\sqrt{-\frac{39}{32}\cdot\frac{1}{Ri_x\cdot\sin(\Phi)}+\sqrt{\left(\frac{39}{32}\right)^2\cdot\frac{1}{(Ri_x\cdot\sin(\Phi))^2}+\frac{13440}{1024}\cdot\frac{1}{\mathrm{Pr}\cdot Ri_x\cdot\sin(\Phi)}}}+$$

$$\frac{3}{4\cdot\sqrt{\mathrm{Re}_x}}\cdot\frac{1}{\sqrt{-\frac{39}{32}\cdot\frac{1}{Ri_x\cdot\sin(\Phi)}+\sqrt{\left(\frac{39}{32}\right)^2\cdot\frac{1}{(Ri_x\cdot\sin(\Phi))^2}+\frac{13440}{1024}\cdot\frac{1}{\mathrm{Pr}\cdot Ri_x\cdot\sin(\Phi)}}}}$$

……(3.55)

Substituting eq. (3.53) in to eq. (3.22) gives:

$$St_x=\frac{3}{4\cdot\mathrm{Pr}\cdot\sqrt{\mathrm{Re}_x}}\cdot\frac{1}{\sqrt{-\frac{39}{32}\cdot\frac{1}{Ri_x\cdot\sin(\phi)}+\sqrt{\left(\frac{39}{32}\right)^2\cdot\frac{1}{(Ri_x\cdot\sin(\Phi))^2}+\frac{13440}{1024}\cdot\frac{1}{\mathrm{Pr}\cdot Ri_x\cdot\sin(\Phi)}}}}$$

……(3.56)

Thus;

$$St_x=\frac{1}{\mathrm{Pr}}\cdot\left[\frac{C_f}{2}-\frac{Ri_x}{2\cdot\sqrt{\mathrm{Re}_x}}\cdot\sqrt{-\frac{39}{32}\cdot\frac{1}{Ri_x\cdot\sin(\Phi)}+\sqrt{\left(\frac{39}{32}\right)^2\cdot\frac{1}{(Ri_x\cdot\sin(\Phi))^2}+\frac{13440}{1024}\cdot\frac{1}{\mathrm{Pr}\cdot Ri_x\cdot\sin(\Phi)}}}\right]$$

……(3.57)

3.4 Mixed Convection With Variable Free Stream Velocity:

3.4.1Governing equation:

Consider the plate shown in the Fig. (3-3) the governing equation of the flow is formulated from consideration steady state flow balance over the integral element (Δx and Δy), taken into account the assumption of the problem with variable free stream velocity.

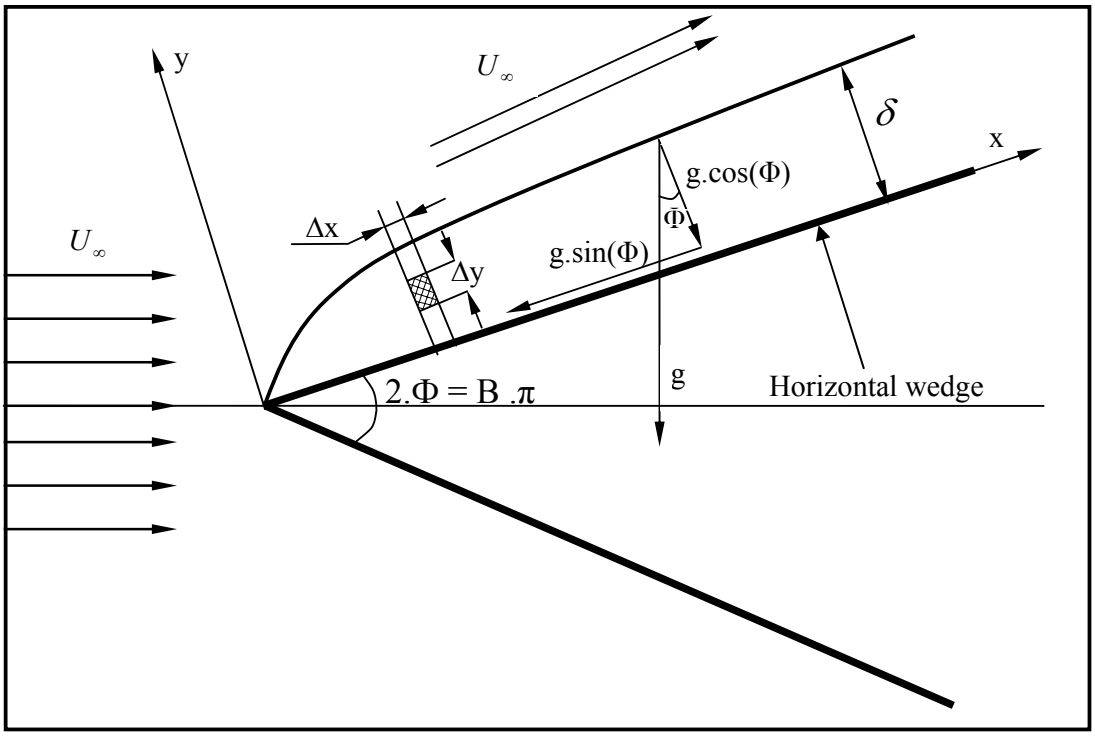

Fig.(3-3)

Hence, for a two-dimensional steady state condition system, the Bernoulli's equation with variable free stream is defined as [5] and [4]:

$$\frac{dp}{dx} = -\rho_\infty \cdot g \cdot \sin(\Phi) - \rho_\infty U_\infty \cdot \frac{dU_\infty}{dx} \qquad \text{……..(3.58)}$$

Substituting eq. (3.58) in eq. (3.3) and using the boussinesq approximation gives;

$$\rho\cdot\left(u\frac{\partial u}{\partial x}+v\frac{\partial u}{\partial y}\right)=\mu\frac{\partial^2 u}{\partial y^2}+\rho_\infty U_\infty\cdot\frac{dU_\infty}{dx}+g\cdot\rho.\beta.\sin(\Phi).(T-T_\infty)\quad..(3.59)$$

For incompressible flow; $\rho=\rho_\infty=c$ thus, eq. (3.59) becomes;

$$u\frac{\partial u}{\partial x}+v\frac{\partial u}{\partial y}=\nu\frac{\partial^2 u}{\partial y^2}+U_\infty\cdot\frac{dU_\infty}{dx}+g.\beta.\sin(\Phi).(T-T_\infty)\quad\ldots\ldots\ldots\ldots\ldots(3.60)$$

By integrate the momentum eq. (3.60) along the boundary layer add and subtract the term $\int_0^\delta u\frac{dv}{dy}dy$ gives :

$$\int_0^\delta u\frac{\partial u}{\partial x}dy+\int_0^\delta\frac{\partial(uv)}{\partial y}dy-\int_0^\delta U_\infty\frac{dU_\infty}{dx}dy-\int_0^\delta u\frac{dv}{dy}dy=\int_0^\delta\nu\frac{\partial^2 u}{\partial y^2}dy+\int_0^\delta g\cdot\beta\sin(\Phi)(T-T_\infty)dy$$

……..(3.61)

B.C;

$u=v=o$ at $y=0$ $\qquad u=U_\infty$ and $v=-\int_0^\delta\frac{du}{dx}dy$ at $y=\delta$

By substituting the boundary conditions and add and subtract the term $\int_0^\delta u\frac{dU_\infty}{dx}dy$ in to the eq. (3.61) gives:

$$\frac{d}{dx}(U_\infty{}^2\cdot\delta 2)+U_\infty\frac{dU_\infty}{dx}\cdot\delta 1=\nu\left.\frac{du}{dy}\right|_{y=0}-g\cdot\beta\cdot\sin(\Phi)\cdot\int_0^\delta(T-T_\infty)dy\quad(3.62)$$

Where δ_1; the displacements thickness $=\int_0^\delta(1-\frac{u}{U_\infty})dy$ ……..(3.63)

δ_2; the momentum thickness $=\int_0^\delta\frac{u}{U_\infty}(1-\frac{u}{U_\infty})dy$ ……..(3.64)

3.4.2 Boundary Layer Thickness , Nusselt Number and shear stresses with variable free stream velocity:

By solving the momentum and energy equations, the velocity distribution profile for the forced flow equation (3.8) and the temperature distribution profile also for the forced flow equation (3.9) are substituted in equations (3.39) and (3.62) gives;

$$\frac{39}{280}\frac{d(U_\infty{}^2\cdot\delta)}{dx}+\frac{3}{8}\cdot U_\infty\cdot\delta\frac{dU_\infty}{dx}=\nu\cdot U_\infty\cdot\frac{3}{2\delta}-\frac{3}{8}\cdot L\cdot\delta \qquad \text{…….(3. 65)}$$

$$\frac{39}{280}\frac{d(U_\infty\cdot\delta)}{dx}=\frac{3}{2}\frac{\alpha}{\delta} \qquad \text{…….(3.66)}$$

Let $U_\infty=C_1\cdot x^m,\delta=C_2\cdot x^n$ this gives;

$$\frac{39}{280}C_1{}^2C_2(2m+n)x^{2m+n-1}+\frac{3}{8}C_1{}^2C_2\cdot mx^{2m+n-1}=\frac{3}{2}\nu\frac{C_1}{C_2}x^{m-n}-\frac{3}{8}L\cdot C_2x^n \quad \text{....(3.67)}$$

$$\frac{13}{140}C_1\cdot C_2\cdot(m+n)x^{m+n-1}=\frac{\alpha}{C_2}x^{-n} \qquad \text{…….(3.68)}$$

Where $m=\dfrac{B}{2-B}$ and B is defined as the wedge angle factor [4],

Thus,

$$\frac{13}{140}\cdot C_2\cdot(m+n)x^{n-1}=\frac{\alpha}{C_2\cdot U_\infty}x^{-n} \qquad \text{.....(3.69)}$$

$$\frac{39}{280}C_2(2m+n)x^{n-1}+\frac{3}{8}C_2\cdot mx^{n-1}=\frac{3}{2}\frac{\nu}{C_2\cdot U_\infty}x^{-n}-\frac{3}{8}\frac{L}{U_\infty{}^2}\cdot C_2x^n \qquad \text{…...(3.70)}$$

from eq(3.69) $C_2{}^2=\dfrac{140\alpha\cdot x^{-2n+1}}{13(m+n)U_\infty}$ .....(3.71)

Substituting eq.(3.71) in to eq.(3.70) gives:

$$n=-\frac{1}{13}\frac{(61m-13m\cdot\mathrm{Pr}+35Gx\cdot\sin(\Phi))}{(1-\mathrm{Pr})} \qquad \text{..... (3.72)}$$

Since: $\frac{\delta^2}{x^2} = C_2{}^2 \cdot x^{2n-2}$ ……..... (3.73)

Substituting eq. (3.71) in eq. (3.73) gives:

$$\frac{\delta}{x} = \sqrt{\frac{140}{13(m+n)\,\mathrm{Pr}\cdot \mathrm{Re}_x}} \qquad \text{……......(3.74)}$$

Thus;

$$\frac{\delta_{mix}}{x} = \frac{2}{\sqrt{\mathrm{Re}_x}} \cdot \sqrt{\frac{(\mathrm{Pr}-1)}{\left(\frac{48}{35}\cdot m + Ri_x \cdot \sin(\Phi)\right)\cdot \mathrm{Pr}}} \qquad \text{.....(3.75)}$$

$$\frac{\delta_{mix}}{\delta_O} = \frac{2}{4.64} \sqrt{\frac{(\mathrm{Pr}-1)}{\left(\frac{48}{35}\cdot m + Ri_x \cdot \sin(\Phi)\right)\cdot \mathrm{Pr}}} \qquad \text{.....(3.76)}$$

$$\frac{Nu_{mix}}{\sqrt{\mathrm{R}_{ex}}} = \frac{3}{4} \frac{1}{\sqrt{\frac{(\mathrm{Pr}-1)}{\left(\frac{48}{35}\cdot m + Ri_x \cdot \sin(\Phi)\right)\cdot \mathrm{Pr}}}} \qquad \text{.....(3.77)}$$

$$\frac{Nu_{mix}}{Nu_o} = \frac{3}{4\cdot .332\cdot \mathrm{Pr}^{\frac{1}{3}}} \frac{1}{\sqrt{\frac{(\mathrm{Pr}-1)}{\left(\frac{48}{35}\cdot m + Ri_x \cdot \sin(\Phi)\right)\cdot \mathrm{Pr}}}} \qquad \text{…….(3.78)}$$

$$\frac{C_f}{2} = \frac{3}{4\cdot\sqrt{\mathrm{Re}_x}} \cdot \frac{1}{\sqrt{\frac{(\mathrm{Pr}-1)}{\left(\frac{48}{35}\cdot m + Ri_x \cdot \sin(\Phi)\right)\cdot \mathrm{Pr}}}} \qquad \text{…..……..(3.79)}$$

Substituting eq. (3.91) in to eq. (3.22) gives:

$$St_x = \frac{3}{4\cdot\sqrt{\mathrm{Pr}\cdot \mathrm{Re}_x}} \frac{1}{\sqrt{\frac{(\mathrm{Pr}-1)}{\left(\frac{48}{35}\cdot m + Ri_x \cdot \sin(\Phi)\right)}}} \qquad \text{…….(3.80)}$$

Thus;

$$St_x = \frac{C_f}{2\cdot \mathrm{Pr}} \qquad \text{……..(3.81)}$$

Solving the eqs. (3.69) and (3.70) Simultaneously by using MathCAD program to fined the root gives:

$n = \frac{1}{4}$, $m = \frac{1}{2}$

For $m = \frac{1}{2}$, gives: Φ = 60º

$$C1 = 1.985\nu\left[-\frac{45}{13}+\frac{\nu}{\alpha}\right]^{-\frac{1}{2}}\left[\frac{g\beta\sin(60)\cdot\theta_w}{\nu^2}\right]^{\frac{1}{2}} \quad \text{……(3.82)}$$

$$C2 = 2.75\left(\frac{\nu}{\alpha}\right)^{-\frac{1}{2}}\left[\frac{g\beta\sin(60)\cdot\theta_w}{\nu^2}\right]^{-\frac{1}{4}}\left[-\frac{45}{13}+\frac{\nu}{\alpha}\right]^{\frac{1}{4}} \quad \text{……..…(3.83)}$$

Thus;

$$U_\infty = 1.985\nu\left[-\frac{45}{13}+\frac{\nu}{\alpha}\right]^{-\frac{1}{2}}\left[\frac{g\beta\sin(60)\cdot\theta_w}{\nu^2}\right]^{\frac{1}{2}}\cdot x^{\frac{1}{2}} \quad \text{…..……(3.84)}$$

$$\frac{\delta_{mix}}{x} = 2.75\left[\frac{\left(-\frac{45}{13}+\mathrm{Pr}\right)}{(\mathrm{Pr})^2\cdot(Gr_x\cdot\sin(60))}\right]^{\frac{1}{4}} \quad \text{……..……..…….(3.85)}$$

or $$\frac{\delta_{mix}}{x} = \frac{2.75}{\sqrt{\mathrm{Re}_x}}\left[\frac{\left(-\frac{45}{13}+\mathrm{Pr}\right)}{(\mathrm{Pr})^2\cdot(Ri_x\cdot\sin(60))}\right]^{\frac{1}{4}} \quad \text{……..……..(3.86)}$$

$$\frac{\delta}{\delta_o} = \frac{2.75}{4.64}\left[\frac{\left(-\frac{45}{13}+\mathrm{Pr}\right)}{(\mathrm{Pr})^2\cdot(Ri_x\cdot\sin(60))}\right]^{\frac{1}{4}} \quad \text{…… (3.87)}$$

$$Nu_{mix} = 0.545(\mathrm{Pr})^{\frac{1}{2}}(Gr_x\cdot\sin(60))^{\frac{1}{4}}\left(-\frac{45}{13}+\mathrm{Pr}\right)^{-\frac{1}{4}} \quad \text{…… (3.88)}$$

or $$\frac{Nu_{mix}}{\sqrt{\mathrm{Re}_x}} = 0.545(\mathrm{Pr})^{\frac{1}{2}}(Ri_x\cdot\sin(60))^{\frac{1}{4}}\left(-\frac{45}{13}+\mathrm{Pr}\right)^{-\frac{1}{4}} \quad \text{…… (3.89)}$$

$$\frac{Nu_{mix}}{Nu_o}=\frac{0.545(\Pr)^{\frac{1}{2}}}{.332\cdot\Pr^{\frac{1}{3}}}(Ri_x\cdot\sin(60))^{\frac{1}{4}}\left(-\frac{45}{13}+\Pr\right)^{-\frac{1}{4}} \quad \text{……..(3.90)}$$

$$\frac{C_f}{2}=\frac{3}{2\cdot 2.75\cdot\sqrt{\mathrm{Re}_x}}\left[\frac{\left(-\frac{45}{13}+\Pr\right)}{(\Pr)^2\cdot(Ri_x\cdot\sin(60))}\right]^{-\frac{1}{4}} \quad \text{……(3.91)}$$

$$St\cdot\sqrt{\mathrm{Re}_x}=0.545(\Pr)^{\frac{-1}{2}}(Ri_x\cdot\sin(60))^{\frac{1}{4}}\left(-\frac{45}{13}+\Pr\right)^{-\frac{1}{4}} \quad \text{……(3.92)}$$

3.4.3 Boundary Layer Thickness, Nusselt Number and Shear Stress with Variable Free Stream Velocity by Using Energy Equation:

Energy equation (3.43)

$$\frac{39}{280}\cdot\frac{d(\delta\cdot U_\infty)}{dx}=\frac{3}{2}\cdot\frac{\alpha}{\delta} \quad \text{…… (3.93)}$$

$$U_\infty\cdot\delta\cdot d\delta+\delta^2 dU_\infty=\frac{140}{13}\cdot\alpha\cdot dx \quad \text{……(3.94)}$$

Let $\delta\cdot d\delta=A\cdot dx$ ……(3.95)

Integrating eq. (3.95) gives:

$$\delta^2=2\cdot A\cdot x \quad \text{……(3.96)}$$

Let $U_\infty=C\cdot x^m$ ……..(3.97)

Substituting eqs. (3.95), (3.96) and (3.97) in equation (3.94) gives:

$$C\cdot x^m\cdot A\cdot dx+2A\cdot x\cdot C\cdot m\cdot x^{m-1}dx=\frac{140}{13}\cdot\alpha dx \quad \text{…….(3.98)}$$

Simplifying eq. (3.98) gives:

$$A=\frac{140}{13}\cdot\frac{\alpha}{[1+2m]\cdot U_\infty} \quad \text{……..……...…..(3.99)}$$

Substituting eq. (3.99) in to eq. (3.96) gives:

$$\frac{\delta}{x}=\sqrt{\frac{280}{13\cdot[1+2m]}}\cdot\frac{1}{\sqrt{\Pr\cdot\mathrm{Re}_x}} \quad \text{……... (3.100)}$$

$$\frac{\delta}{\delta_o} = \sqrt{\frac{1}{1+2m}} \cdot \frac{1}{\sqrt{\Pr}} \qquad \text{……..……(3.101)}$$

$$Nu = \frac{3}{2 \cdot \sqrt{\frac{280}{13 \cdot [1+2m]}}} \cdot \sqrt{\Pr \cdot \mathrm{Re}_x} \qquad \text{…….……(3.102)}$$

$$\frac{Nu}{Nu_o} = \frac{3}{2 \cdot \sqrt{\frac{280}{13 \cdot [1+2m]}}} \cdot \frac{\sqrt{\Pr}}{0.332 \cdot \Pr^{\frac{1}{3}}} \qquad \text{……(3.103)}$$

Substituting eqs. (3.8) and (3.100) in eq. (3.20) gives:

$$\frac{C_f}{2} = \frac{3}{2} \cdot \frac{\sqrt{\Pr}}{\sqrt{\mathrm{Re}_x}} \cdot \frac{1}{\sqrt{\frac{280}{13 \cdot [1+2m]}}} \qquad \text{……..……..(3.104)}$$

Substituting eq. (3.102) in to eq. (3.22) gives:

$$St_x = \frac{3}{2 \cdot \sqrt{\frac{280}{13 \cdot [1+2m]}}} \cdot \frac{1}{\sqrt{\Pr \cdot \mathrm{Re}_x}} \qquad \text{…….……(3.105)}$$

Thus;

$$St_x = \frac{C_f}{2 \cdot \Pr} \qquad \text{……(3.106)}$$

3.5 Similarity Solution with Variable Free Stream Velocity for 60º Inclination angle and Constant Wall Temperature.

3.5.1 Dimensionless Momentum and Energy Equations.

The energy equation is defined as [10] :

$$u\ \frac{\partial T}{\partial x}+v\ \frac{\partial T}{\partial y}=\alpha\frac{\partial^2 T}{\partial y^2} \qquad \text{……(3.107)}$$

Eqs. (3.60) and (3.107) can be converting to dimensionless form by suggestion dimensionless variables:

$$x^*=\frac{x}{L}\ ,\ y^*=\frac{y}{L}\ ,\quad u^*=\frac{u\cdot L}{\nu}\quad ,\quad v^*=\frac{v\cdot L}{\nu}\ ,\quad U_\infty{}^*=\frac{U_\infty\cdot L}{\nu}$$

$$\theta=\frac{T-T_\infty}{T_w-T_\infty}$$

Substituting the dimensionless parameter in to eqs. (3.60) and (3.107) get the dimensionless form of the momentums and energy equations:

$$u^*\frac{\partial u^*}{\partial x^*}+v^*\frac{\partial u^*}{\partial y^*}=\frac{\partial^2 u^*}{\partial y^{*2}}+U^*{}_\infty\cdot\frac{dU^*{}_\infty}{dx^*}+\frac{g.\beta.\sin(\Phi).(T-T_\infty)L^3}{\nu^2} \quad \text{..(3.108)}$$

$$u^*\frac{\partial\theta}{\partial x^*}+v^*\frac{\partial\theta}{\partial y^*}=\frac{1}{\Pr}\frac{\partial^2\theta}{\partial y^{*2}} \qquad \text{…… (3.109)}$$

Where for the forced flow the similarity variable [3] is defined as:

$$\eta=y\sqrt{\frac{U_\infty}{\nu\cdot x}} \qquad \text{……(3.110)}$$

And free stream velocity for inclined surface [4] is defined as:

$$U^*{}_\infty=c\cdot x^{*m} \qquad \text{…… (3.111)}$$

By substituting the dimensionless variable in to eq. (3.110) gives:

$$\eta=\sqrt{c}\cdot y^*\cdot x^{*\frac{m-1}{2}} \qquad \text{…… (3.112)}$$

dimensionless stream function [3] is defined as:

$$\Psi^*=\int u^*\cdot dy^* \qquad \text{……..(3.113)}$$

Substituting the dimensionless variables and eq. (3.111) in to eq.(3.113) gives:

$$\Psi^* = \sqrt{c} \cdot x^{*\frac{m+1}{2}} \cdot f \quad \text{…….. (3.114)}$$

$$u^* = c \cdot x^{*m} \cdot f' \quad \text{…….. (3.115)}$$

$$v^* = -\sqrt{c} \cdot x^{*\frac{m-1}{2}} \left[\frac{m+1}{2} f - \frac{m-1}{2} \eta \cdot f' \right] \quad \text{……..……(3.116)}$$

Substituting eqs. (3.112), (3.114), (3.115) and (3.116) in eqs. (3.108) and (3.109) to convert the partial differential equations in to ordinary differential equations gives:

$$f''' + \frac{m+1}{2} f \cdot f'' + m \cdot (1 - f'^2) + \frac{\theta}{x^{*2m-1}} = 0 \quad \text{…… (3.117)}$$

$$\theta'' + \Pr \cdot \left(\frac{1+m}{2} f \cdot \theta' \right) = 0 \quad \text{..…… (3.118)}$$

Equation (3.117) valid only For $m = \frac{1}{2}$ thus;

$$f''' + \frac{3}{4} f \cdot f'' + \frac{1}{2} \cdot (1 - f'^2) + \theta = 0 \quad \text{…… (3.119)}$$

$$\theta'' + \Pr \cdot \frac{3}{4} f \cdot \theta' = 0 \quad \text{…….. (3.120)}$$

B.C; $f(0) = 0$, $f'(0) = 0$, $f'(\infty) = 1$, $\theta(0) = 1$, $\theta(\infty) = 0$

For $m = \frac{1}{2}$, gives: Φ = 60º

Where $c = \sqrt{Gr_l \cdot \sin(60)}$ ……..……(3.121)

Thus,

$$\Psi^* = \sqrt{Gr_l \cdot \sin(60)} \cdot x^{*\frac{3}{4}} \cdot f \quad \text{……..(3.122)}$$

$$u^* = \sqrt{Gr_l \cdot \sin(60)} \cdot x^{*\frac{1}{2}} \cdot f' \quad \text{…….……(3.123)}$$

$$v^* = -\sqrt{Gr_l \cdot \sin(60)} \cdot x^{*\frac{-1}{4}} \left[\frac{3}{4} f + \frac{1}{4} \eta \cdot f' \right] \quad \text{……(3.124)}$$

By using (MathCAD) program can be solving the ordinary differential equations (3.119) and (3.120) simultaneously.

Substituting eq. (3.112) in eq. (3.14) gives:

$$h = -k \sqrt[4]{\frac{g \cdot \beta \cdot (T_w - T_\infty) \cdot \sin(60)}{\nu^2}} \cdot x^{-\frac{1}{4}} \cdot \theta' \quad \text{…… (3.125)}$$

Thus,

$$\frac{Nu_{mix}}{\sqrt{\mathrm{Re}_x}} = -\left[Ri_x \cdot \sin(60) \right]^{1/4} \cdot \theta' \quad \text{……..(3.126)}$$

$$C_f = \frac{2 \cdot f''(0) \cdot \left(Ri_x \cdot \sin(60) \right)^{\frac{1}{4}}}{\sqrt{\mathrm{Re}_x}} \quad \text{...…….(3.127)}$$

But when $c = \mathrm{Re}_L$ eq.(3.119), (3.126) and (3.127) becomes:

$$f''' + \frac{3}{4} f \cdot f'' + \frac{1}{2} \cdot (1 - f'^2) + Ri_L \cdot \sin(60) \cdot \theta = 0 \quad \text{…….(3.128)}$$

$$\frac{Nu_{mix}}{\sqrt{\mathrm{Re}_x}} = -\left(\frac{x}{L} \right)^{1/4} \cdot \theta'(0) \quad \text{……..……..(3.129)}$$

$$C_f = \frac{2 \cdot f''(0) \cdot \left(\frac{x}{L} \right)^{\frac{1}{4}}}{\sqrt{\mathrm{Re}_x}} \quad \text{…….. ...…….(3.130)}$$

By using (MathCAD) program can be solving the ordinary differential equations (3.120) and (3.128) simultaneously.
Where:
B.C; $f(0) = 0$, $f'(0) = 0$, $f'(\infty) = 1$, $\theta(0) = 1$, $\theta(\infty) = 0$

3.6 Similarity Solution with Variable Free Stream Velocity for 60° Inclination Angle and Constant Heat Flux.

From definition for constant heat flux (variable wall temperature) condition $T_w - T_\infty = A \cdot x^n$ [4] and [10].

We suppose:

$$U^*_\infty = c \cdot x^{*m} \quad \text{..... (3.131)}$$

$$\eta = y^* \cdot \sqrt{c} \cdot x^{*\frac{m-1}{2}} \quad \text{..... (3.132)}$$

$$c = \sqrt{\frac{g \cdot \beta \cdot A \cdot x^{*n} \cdot \sin(\phi) \cdot L^3}{\nu^2}} \quad \text{.....(3.133)}$$

Substituting the dimensionless variables and eq. (3.133) in eq. (3.113) gives:

$$\Psi^* = \sqrt[4]{\frac{g \cdot \beta \cdot A \cdot \sin(\phi) \cdot L^3}{\nu^2}} \cdot x^{*\frac{2m+n+2}{4}} \cdot f \quad \text{..... (3.134)}$$

$$u^* = \sqrt{\frac{g \cdot \beta \cdot A \cdot \sin(\phi) \cdot L^3}{\nu^2}} \cdot x^{*\frac{2m+n}{2}} \cdot f' \quad \text{..... (3.135)}$$

$$v^* = -\sqrt[4]{\frac{g \cdot \beta \cdot A \cdot \sin(\phi) \cdot L^3}{\nu^2}} \cdot x^{*\frac{2m+n-2}{4}} \left[\frac{2m+n+2}{4} f - \frac{2m+n-2}{4} \eta \cdot f' \right] \text{...(3.136)}$$

Substituting eqs. (3.132), (3.134), (3.135) and (3.136) in eqs. (3.108) and (3.109) to convert the partial differential equations in to ordinary differential equations gives:

$$f''' + \frac{2m+n+1}{4} f \cdot f'' + \frac{2m+n}{2} \cdot (1 - f'^2) + \frac{\theta}{x^{*2m-1}} = 0 \quad \text{..... (3.137)}$$

$$\theta'' + \Pr \cdot \left(-n \cdot \theta \cdot f' + \frac{2m+n+2}{4} \cdot f \cdot \theta' \right) = 0 \quad \text{..... (3.138)}$$

Eq. (3.137) valid only For $m = \frac{1}{2}$ and for constant heat flux $n = \frac{1}{5}$ thus;

For $m = \frac{1}{2}$, gives: Φ = 60º

$$f''' + \frac{4}{5} f \cdot f'' + \frac{3}{5} \cdot (1 - f'^2) + \theta = 0 \quad \text{…… (3.139)}$$

$$\theta'' + \Pr \cdot \left(-\frac{1}{5} \cdot \theta \cdot f' + \frac{4}{5} \cdot f \cdot \theta' \right) = 0 \quad \text{…….. (3.140)}$$

B.C; $f(0) = 0$, $f'(0) = 0$, $f'(\infty) = 1$, $\theta(0) = 1$, $\theta(\infty) = 0$

By using (MathCAD) program can be solving the ordinary differential eqs. (3.139) and (3.140) simultaneously.

Substituting eq. (3.132) in eq. (3.14) gives:

$$h = -k \sqrt[4]{\frac{g \cdot \beta \cdot (T_w - T_\infty) \cdot \sin(60)}{\nu^2}} \cdot x^{-\frac{1}{4}} \cdot \theta' \quad \text{…… (3.141)}$$

Thus:

$$\frac{Nu_{mix}}{\sqrt{\mathrm{Re}_x}} = -\left[Ri_x \cdot \sin(60) \right]^{1/4} \cdot \theta' \quad \text{……..(3.142)}$$

$$C_f = \frac{2 \cdot f''(0) \cdot \left(Ri_x \cdot \sin(60) \right)^{\frac{1}{4}}}{\sqrt{\mathrm{Re}_x}} \quad \text{...…….(3.143)}$$

Chapter four

Results and Discussion

4.1 Mixed Convection with Constant Free Stream Velocity:

4.1.1 Uniform free stream parallel to the flat plate:

Generally, the variation of hydrodynamic, heat transfer and shear stress along the flat plate may be affected by many factors such as surface temperature, Prandtl number, Richardson number and inclination angle.

4.1.2 Hydrodynamic:

Boundary layer thickness ratio along the inclined flat plate obtained by equation (3.13) is plotted in Figs.(4-1) and (4-2), for Pr = 1 boundary layer thickness' ratio decreases with gradually increases of Richardson number and inclination angle, due to the increases of buoyancy force effect by increases of adding flow component.

Variation of the thickness' ratio along vertical plate obtained by equation (3.30) with Richardson number is plotted in Fig.(4-3), the maximum decreasing in boundary layer thickness ratio with the increases of Richardson number approximately occurs with $0.1 < Ri_x < 3$ which limited maximum adding flow region because of the maximum common effect of both free and forced convection limited in this region as shown in Fig. (1-6).

Boundary layer thickness' ratio obtained from equation (3.36) is plotted in Figs.(4-4) and (4-5), for Pr >>> 1, thickness ratio decreases with the increases of Richardson number and inclination angle due to the increases of buoyancy force component effect on the flow.

4.1.3 Heat transfer:

Increasing of Nusselt number along the inclined surface obtained from the equation (3.17) is plotted in Figs. (4-6) and (4-7), for the same Reynolds number, Pr = 1 and inclination angle range from 0º up to 90º, Nusselt number increases with the increases of Richardson number and

inclination angle due to the increases of buoyancy force effect on the flow which increases the heat transfer rate.

Increases of Nusselt number with Richardson number along the vertical surface obtained from equation (3.31) is plotted in Fig. (4-8) for Pr = 1, when ($Ri_x \longrightarrow 0$) ie. Reynolds number is very high, forced convection is dominated and there is no effect of buoyancy force on the flow as shown in point (A), then Nusselt number increases with the increases of Richardson number due to the increases of buoyancy force effect which increases heat transfer rate.

The effect of the buoyancy force term component ($Ri_{x*}\sin(\Phi)$) on Nusselt number ratio obtained from equation (3.19) is plotted in Fig.(4-9), the ratio increases with the increases of ($Ri_{x*}\sin(\Phi)$) for assisting flow and decrease with the decreases of ($Ri_{x*}\sin(\Phi)$) for opposing flow and equals to one when the buoyancy force component equals to zero as shown in point (A).

Increasing of Nusselt number along the flat plate obtained from equations (3.42) and (3.45) is plotted in Fig.(4-10) Nusselt number increases with the increases of Prandtl number due to the increases of momentum diffusivity with respect to the thermal diffusivity also the figure shows that the Nusselt number approach's to the real value when the velocity distribution profile approach's to the real condition as shown in point (A).

4.1.4 Shear stress:

Increasing of Stanton number along the flat plate obtained from eq. (3.23) is plotted in Figs.(4-11) and (4-12), for Pr = 1, Stanton number increases with the increases of Richardson number and inclination angle due to the increases of heat transfer rate by increases the buoyancy effet.

The effect of buoyancy force term component and Prandtl number on Stanton number obtained from equation (3.23) is plotted in Fig.(3-13) Stanton number decreases with the increases of Prandtl number and always increases with the increases of buoyancy force term component ($Ri_x * \sin(\Phi)$) due to the increases of buoyancy force effect.

Stanton number along the vertical flat plate with buoyancy force term and Prandtl number obtained from equation (3.32) is plotted in Fig. (4-14), for different Prandtl number when (Ri_x 0) i.e. Reynolds number is very high, forced convection is dominated and there is no effect of buoyancy force on the flow, Stanton number have the same value of the forced convection condition and increases with the increases of Richardson number due to the increases of heat transfer rate by increases of buoyancy force effect and decreases with the increases of Prandtl number due to the increases of momentume difusivity withrespect to the thermal difusivity.

4.2 Velocity Distribution profile with Buoyancy Effect:

4.2.1 hydrodynamic:

Boundary layer thickness ratio along the flat plate obtained from equation (3.52) is plotted in Figs. (4-15) and (4-16) for Pr = 1 the ratio is decrease with the increases of Richardson number and inclination angle due to the increases of buoyancy effect which increases the flow rate, while the ratio by equation (3.52) is greater than the ratio by equation (3.13) because of the velocity distribution profile is approach's to the real condition by the effect of the buoyancy force.

4.2.2 Heat Transfer:

Nusselt number along the flat plate obtained from equation (3.53) is plotted in Figs.(4-17) and (4-18) for Pr = 1 and the velocity distribution profile contained the buoyancy force effect, the Nusselt number increases

with the increases of Richardson number and inclination angle due to the increases of the flow rate by the increases of buoyancy effect which increases the heat transfer rate.

Variation of Nusselt number along the plate obtained from equation (3.53) with buoyancy forced component and Prandtl number is plotted in Fig. (4-19), Nusselt number increase with the increases of Prandtl number due to the increases of momentum diffusivity with respect to the thermal diffusivity and Nusselt number equals to Nu_o when Richardson number approach's to zero at point (A) and then increase with the increases of Richardson number due to the increases of buoyancy force effect.

Nusselt number ratio along the plate obtained from equation (3.54) with buoyancy forced component and Prandtl number is plotted in Fig. (4-20), Nusselt number ratio increase with the increases of Prandtl number and the ratio is always greater than one when the rang of Richardson number approachs to the mixed convection range due to the effect of the buoyancy force.

The problem of mixed convection over vertical flat plate which solved by Ref, [12] in equation (B.1), and solved by equation (3.53) are plotted in Figs. (4-21), (4-22) and (4-23), shows the difference in increasing of Nusselt number with the increases of Prandtl number where the carves are identical with the increasing of Prandtl for small range from 0.1 to 15 and begin to increase with equation (3.53) for high range of Prandtl number because of the absence of the shear stress effect in equation (3.53).

4.2.3 Shear Stress:

Variation of Stanton number along the flat plate obtained from the equation (3.56) is plotted in Figs. (4-24) and (4-25) for Pr = 10 and the

buoyancy effect on the velocity distribution profile the Stanton number increase with the increases of Richardson number and inclination angle due to the increases of heat transfer rate by increases the buoyancy effect on the flow.

Variation of Stanton number along the flat plate with buoyancy force component and Prandtl number obtained from equation (3.56) is plotted in Figs. (3.26) and (3.27), Stanton number increase with the increases of buoyancy force component which increases the heat transfer rate and decrease with the increases of Prandtl number due to the increases of the momentum diffusivity with respect to the thermal diffusivity.

4.3 Mixed convection with variable free stream velocity:

4.3.1 hydrodynamic:

Boundary layer thickness ratio along the plate obtained from equation (3.76) is plotted in Figs.(4-28) and (4-29) for inclination angle range from 5º to 90º and Prandtl number of 1.1 the thichness ratio decreases with the increases of inclination angle and Richardson number due to the increases of buoyancy force effect on the flow while the ratio approach's to one with negligible buoyancy effect and Prandtl approach's to one as shown in Fig. (4-30).

Figs.(4-31) and (4-32) show the prandtl number effect on the thickness ratio for inclination angle of 70º, the ratio decreases with the increases of Richardson number due to the increases of buoyancy force and increase with the increases of Prandtl number.

4.3.2 Heat transfer:

Nusselt number along the plate for equation (3.77) is plotted in Figs. (4-33) and (4-34) for inclination angle range from 5º up to 90º and Pr = 2, Nusselt number increase with the increases of inclination angle

and Richardson number due to the increases of heat transfer rate by increases buoyancy force effect on the flow.

Fig.(4-35) shows for inclination angle of 60º Nusselt number increase with the increases of Richardson number due to the increases of buoyancy force effect and decrease with small range of Prandtl and then constant for large increases of Prandtl number.

Nusselt number ratio along the plate obtained from equation (3.78) is plotted in Figs.(4-36, a and b) for Pr = 2 and 10 respectively Nusselt ratio increases with the increases of Richardson number and inclination angle due to the increases of buoyancy force effect on the flow, for inclination angle range from 5º to 90º and Richardson number range from 0.1 to 10 the Nusselt ratio increases with the increase of Richardson number and inclination angle due to the increases of buoyancy effect on the flow and decrease with the increases of Prandtl number as show in Fig. (4-37).

4.3.3 Shear stress:

Stanton number along the plate obtained from equation (3.80) is plotted in Figs.(4-38) and (4-39) for inclination angle range from 5º to 90º and Pr = 2, Stanton number increases with the increases of the Richardson number and inclination angle due to the increases of heat transfer rate by the increases of buoyancy effect on the flow.

4.4 Mixed Convection with Variable Free Stream Velocity and inclination angle of 60º:

4.4.1 Hydrodynamic:

Boundary layer thickness ratio along the plate with inclination of angle of 60˚ obtained from equation (3.87) is plotted in Figs. (4-40) and (4-41) pulse increasing of the thickness ratio for Prandtl number range from 3.462 to 4 and then decreasing with increases of Prandtl number due

to the increases of momentum diffusivity with respect to the thermal diffusivity and always decreases with the increases of Richardson number due to the increases of buoyancy effect on the flow.

4.4.2 Heat transfer:

Nusselt number along the plate of inclination angle of 60˚ obtained from equation (3.89) is plotted in Figs.(4-42, a and b) and (4-43) pulse decreasing of Nusselt number for Prandtl number range from 3.462 to 6 and then increases with the increases of Prandtl number due to the increases of momentum diffusivity with respect to the thermal diffusivity, while Nusselt number always increases with the increases of Richardson number due to the increases of buoyancy effect.

Nusselt number ratio along the plate of inclination angle of 60˚ obtained by equation (3.90) is plotted in Figs.(4-44), (4-45) and (4-46) Nusselt ratio decreases with the increases of Prandtl number but always greater than one for mixed region of Richardson number range due to the buoyancy effect on the flow.

4.4.3 Shear Stress:

Stanton number along the plate with inclination angle of 60˚ for equation (3.92) is plotted in Figs.(4-47), (4-48) and (4-49), Stanton number decrease with the increases of Prandtl number and increases with the increases of Richardson number due to the increases of heat transfer rate by the increases of buoyancy effect on the flow.

4.5 Variable free stream from energy equation:

4.5.1 Hydrodynamic:

Boundary layer thickness ratio along the flat plate obtained from equation (3.101) is plotted in Figs. (4-50) and (4-51) the ratio decreases with the increases of Prandtl due to the increases of momentum diffusivity with respect to the thermal diffusivity, the figure shows the

small effect of inclination angle on the boundary layer thickness' with respect to the Prandtl effect with the absence of the buoyancy effect.

4.5.2 Heat transfer:

Nusselt number along the flat plate obtained from equation (3.102) is plotted in Fig. (4-52) Nusselt number increases with the increases of Prandtl number due to the increases of momentum diffusivity with respect to the thermal diffusivity and also increases with the increases of inclination angle but with small range due to the absence of the buoyancy effect on the flow.

4.5.3 Shear stress:

Stanton number along the flat plate obtained from equation (3.105) is plotted in Fig. (4-53) Stanton number decreases with the increases of Prandtl number due to the increases of momentum diffusivity with the respect to the thermal diffusivity and there is a few increases with the increases of inclination angle due to the absence of buoyancy effect.

4.6 Similarity Solution with Variable Free Stream Velocity for 60° Inclination Angle and Constant Wall Temperature:

4.6.1 Hydrodynamic:

Dimensionless velocity distribution profile along the plate of inclination angle of 60º from the selected run of the exact similarity solution of the equation (3.119) is plotted in Fig.(4-54) for inclination angle of 60º and Prandtl of 0.6, 1, 3, 15, 50 and 100, the profile decrease with the increases of Prandtl number, while the profile increases with the increases of similarity variable (η) and then equals to one when (η) represented as infinite value, i.e., far of the surface but with negligible buoyancy effect on the flow there is no effect of Prandtl number on the velocity profile as shown in Fig. (4-55) while the Prandtl number effect

increases with the increases of buoyancy effect on the flow as shown in Fig. (4-56).

4.6.2 Heat transfer:

Dimensionless temperature distribution profile along the plate of inclination angle of 60º for selected rune of the exact similar solution of the equation (3.120) is plotted in Fig. (4-57), the profile variant with variation of Prandtl number and the temperature decrease with the increases of similarity variable (η) far of the surface.

Variation of dimensionless heat transfer factor along the plate of inclination angle of 60º for the exact similar solution of equation (3.120) is plotted in Fig.(4-58) for the Prandtl number of 0.6, 1, 3, 15, 50 and 100 dimensionless heat transfer factor decrease with the increases of Prandtl number due to the increases of momentum diffusivity with respect to the thermal diffusivity.

Nusselt number along the plate of inclination angle of 60º for the solution of equation (3.126) is plotted in Fig. (4-59) for the Prandtl number of 0.6, 1, 3, 15, 50 and 100 Nusselt number increases with the increases of buoyancy force term component due to the increases of buoyancy effect on the flow and increases with the increases of Prandtl number due to the increases of momentum diffusivity with respect to the thermal diffusivity.

4.6.3 Shear stress:

Variation of shear stress factor along the plate of inclination angle of 60º is plotted in Figs. (4-60) and (4-62) for the exact similar solution of eq. (3.119) and eq. (3.127) for Prandtl number of 0.6, 1, 3, 15, 50 and 100, coefficient of friction decreases with the increases of Prandtl number and increase with the increases buoyancy effect on the flow but with negligible buoyancy effect on the flow there is no effect of Prandtl

number on the coefficient of friction as shown in Figs. (4-61) and (4-63) which plotted by the selected run for the exact similar solution of eq. (3.128) and eq. (3.130), while the Prandtl number effect increases with the increases of buoyancy effect on the flow.

4.7 Similarity Solution with Variable Free Stream Velocity for 60º inclination Angle and Constant Heat flux:

4.7.1 Hydrodynamic:

Dimensionless velocity distribution profile along the plate of inclination angle of 60º with constant heat flux from the selected rune of the exact similarity solution of the equation (3.139) is plotted in Fig. (4-64) for inclination angle of 60º and Prandtl of 0.6, 1, 3, 15, 50 and 100 the profile decreases with the increases of Prandtl number, while the profile increases with the increases of similarity variable (η) and then equals to one when (η) represented as infinite value, i.e. far of the surface.

4.7.2 Heat transfer:

Dimensionless temperature distribution profile along the plate of inclination angle of 60˚ with constant heat flux for selected rune of the exact similar solution of the equation (3.140) is plotted in Fig. (4-65), the profile variant with variation of Prandtl number and the temperature decreases with the increases of similarity variable (η) far of the surface.

Variation of dimensionless heat transfer factor along the plate of inclination angle of 60˚ with constant heat flux for the exact similar solution of equation (3.140) is plotted in Fig. (4-66) for the Prandtl number of 0.6, 1 ,3 ,15, 50 and 100 dimensionless heat transfer factor decreases with the increases of Prandtl number due to the increases of momentum diffusivity with respect to the thermal diffusivity.

Nusselt number along the plate of inclination angle of 60º with constant heat flux for equation (3.142) is plotted in Fig. (4-67) for the

Prandtl number of 0.6, 1, 3, 15, 50 and [100, Nusselt number increases with the increases of buoyancy force term component due to the increases of buoyancy effect on the flow and increases with the increases of Prandtl number due to the increases of momentum diffusivity with respect to the thermal diffusivity.

For comparison the similarity solution for both constant wall temperature and constant heat flux with inclination angle of 60º is ploted in Fig. (4-70). The results shows that the Nusselt number are always increases with increases of Richardson number, the results shows also that the Nusselt number for constant wall temperature are less than Nusselt number for constant heat flux with about 15% for any value of Prandtl number, these results are identical to that presented by **Schlichting,** [4] and **Holman,** [5]. for both conditions of free and forced convection alone with constant wall temperature and constant heat flux.

4.7.3 Shear stress:

Variation of shear stress along the plate of inclination angle of 60º with constant heat flux is plotted in Figs. (4-68) and (4-69) for the exact similar solution of equation (3.139) and equation (3.143) for Prandtl number of 0.6, 1, 3, 15, 50 and 100, coefficient of friction decreases with the increases of Prandtl number and increases with the increases of flow rate due to the increases buoyancy effect on the flow.

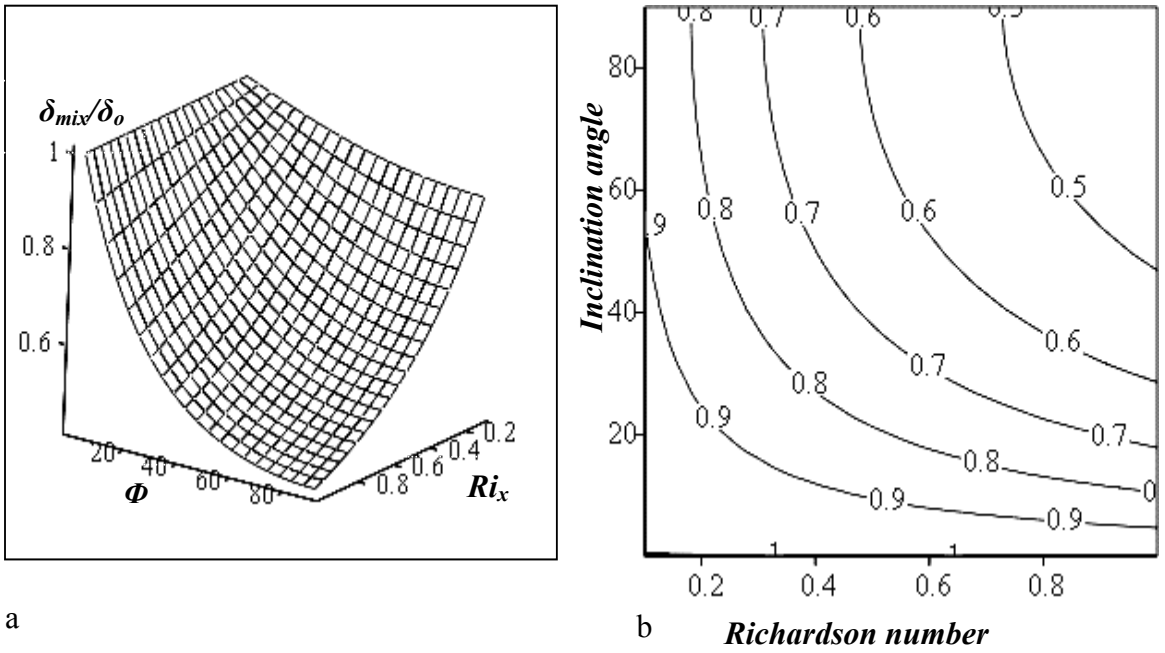

a b

Fig. (4-1): Variation of boundary layer thickness ratio (δ_{mix}/δ_o) with Richardson number range of 0 to 1 and inclination angle range of 0.1˚ to 90˚ for Pr =1, by eq. (3.13).

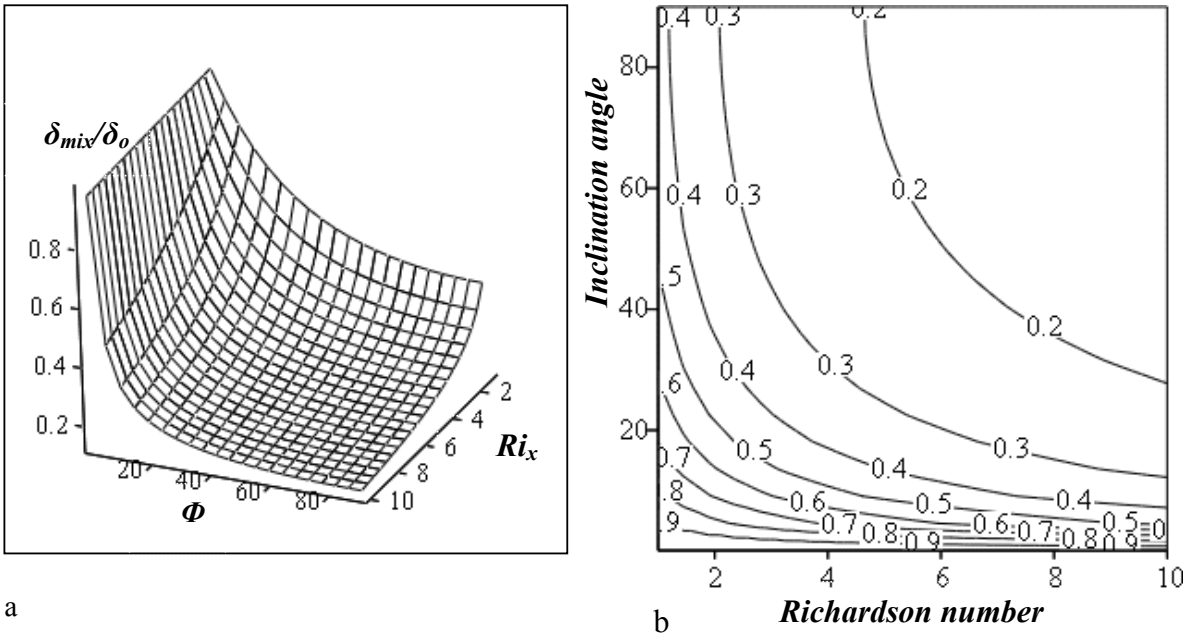

a b

Fig. (4-2): Variation of boundary layer thickness ratio (δ_{mix}/δ_o) with Richardson number range of 1 to 10 and inclination angle range of 0.1˚ to 90˚ for Pr =1, by eq. (3.13).

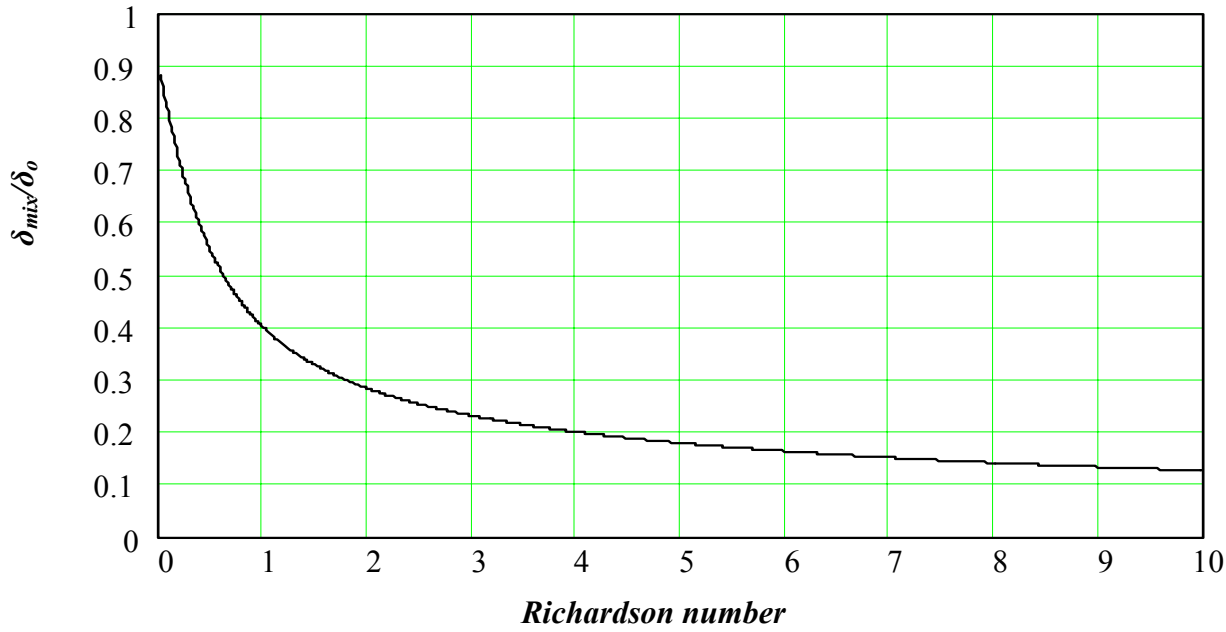

Fig. (4-3): Variation of boundary layer thickness ratio with Richardson number range of 0 to 10 for vertical flat plate and Pr = 1, eq. (3.30).

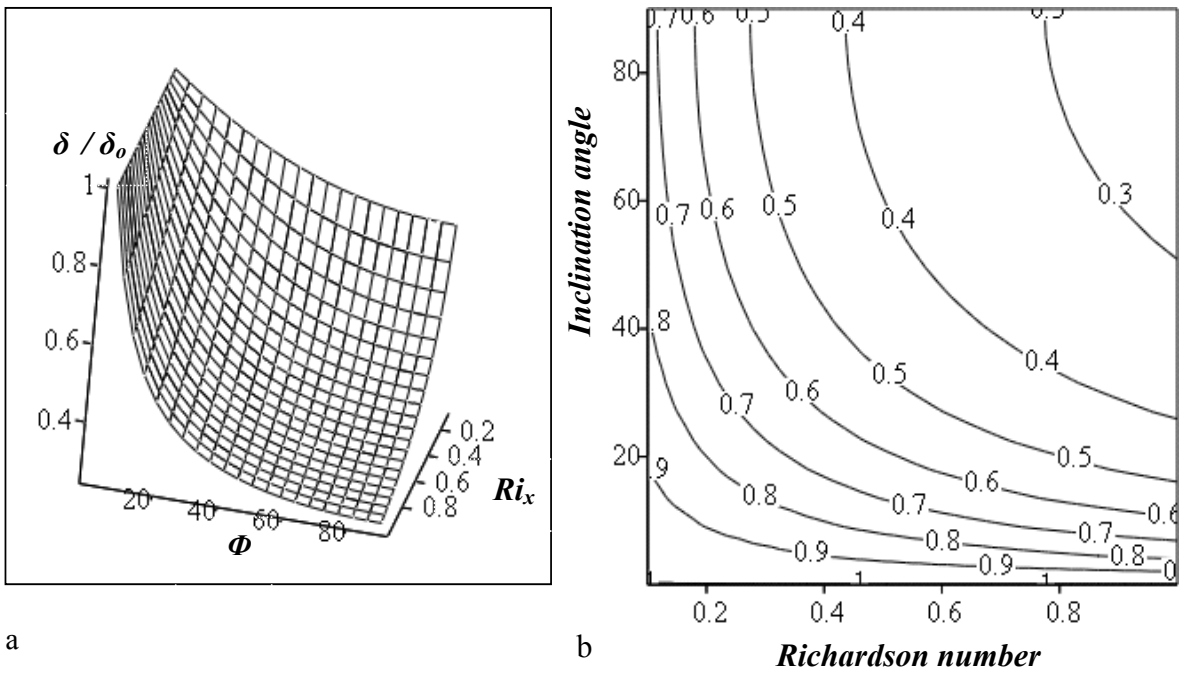

Fig. (4-4): Variation of boundary layer thickness ratio (δ / δ_o) with Richardson number range of 0.1 to 1 and inclination angle range of 0.1˚ to 90˚ and Pr >>> 1 eq. (3.36).

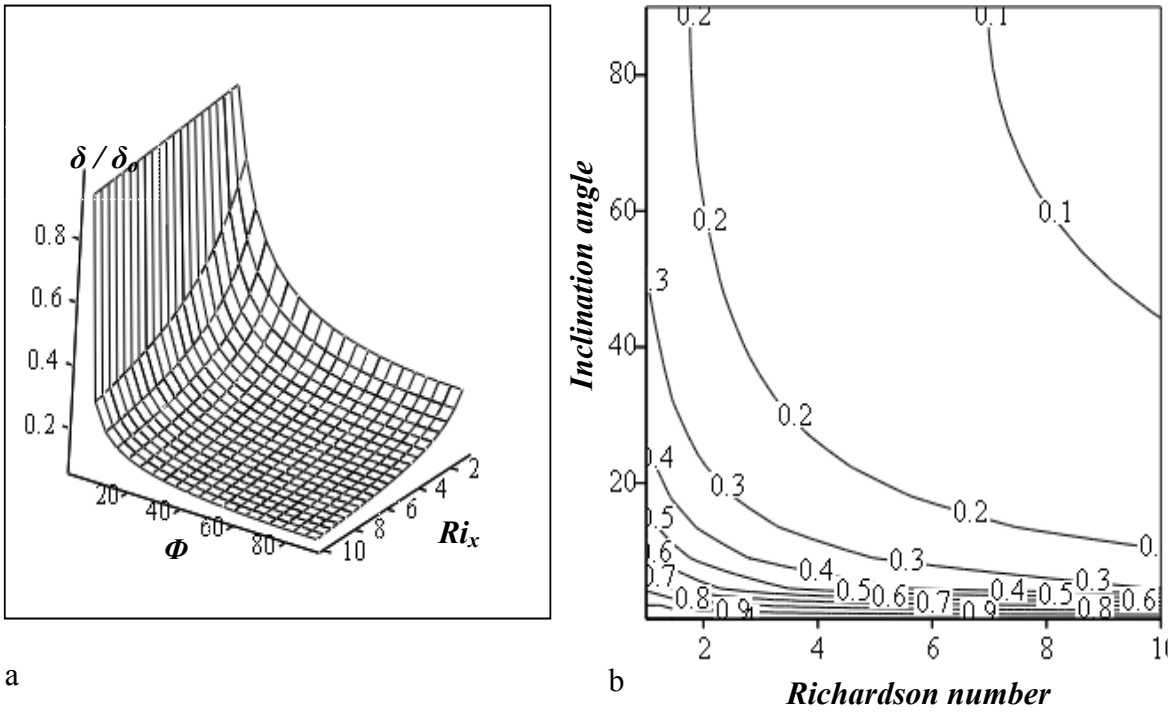

Fig. (4-5): Variation of boundary layer thickness ratio (δ / δ_o) with Richardson number range of 1 to 10 and inclination angle range of 0.1˚ to 90˚ and Pr >>> 1 , eq. (3.36).

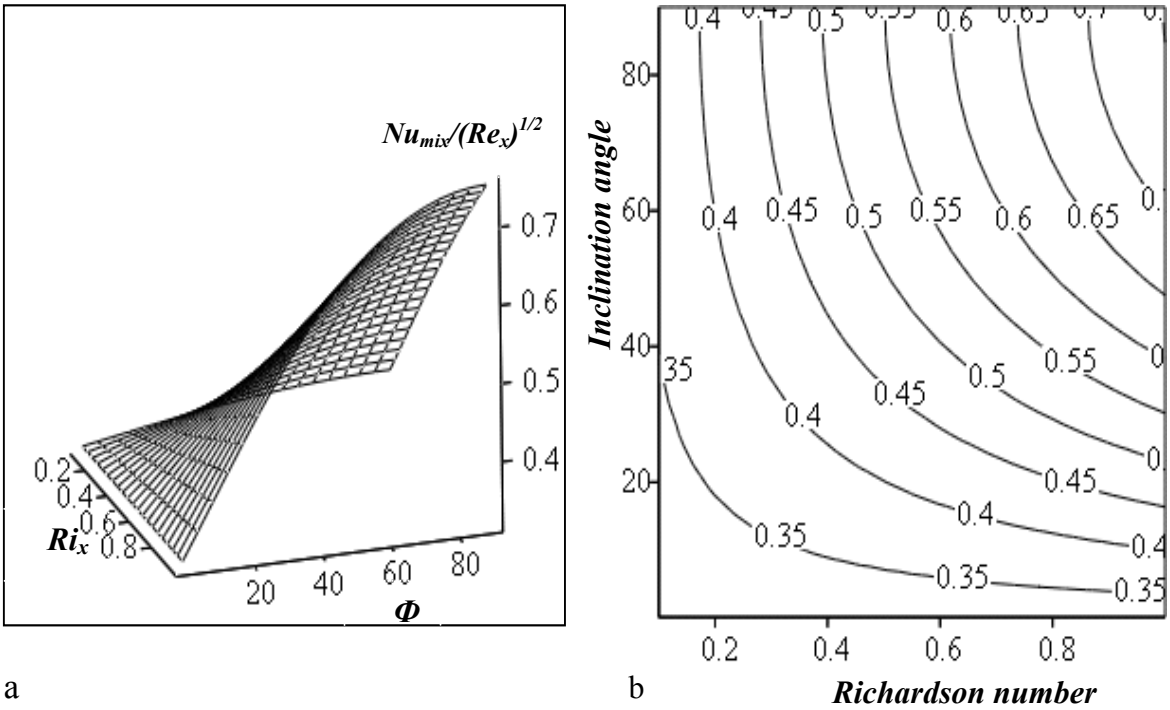

Fig. (4-6): Variation of ($Nu_{mix}/(Re_x)^{1/2}$) with Richardson number range of 0 to 1 and inclination angle range of 0.1˚ to 90˚ for Pr =1, by eq. (3.17).

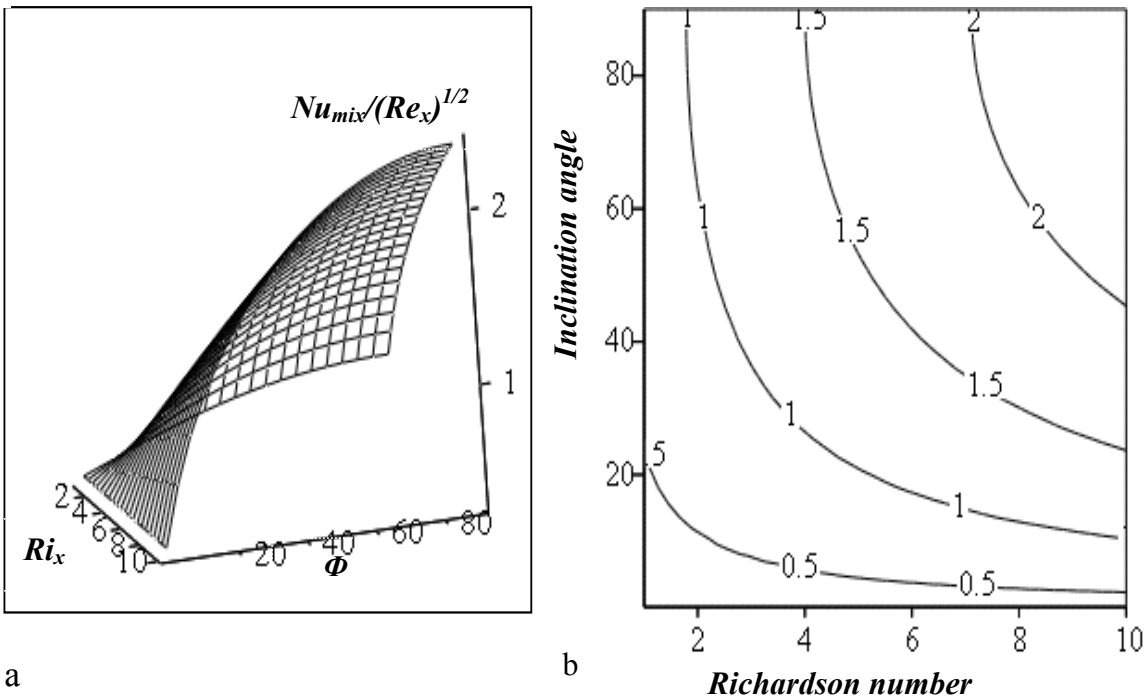

Fig. (4-7): Variation of $(Nu_{mix}/(Re_x)^{1/2})$ with Richardson number range of 1 to 10 and inclination angle range of 0.1˚ to 90˚ for Pr =1, by eq. (3.17).

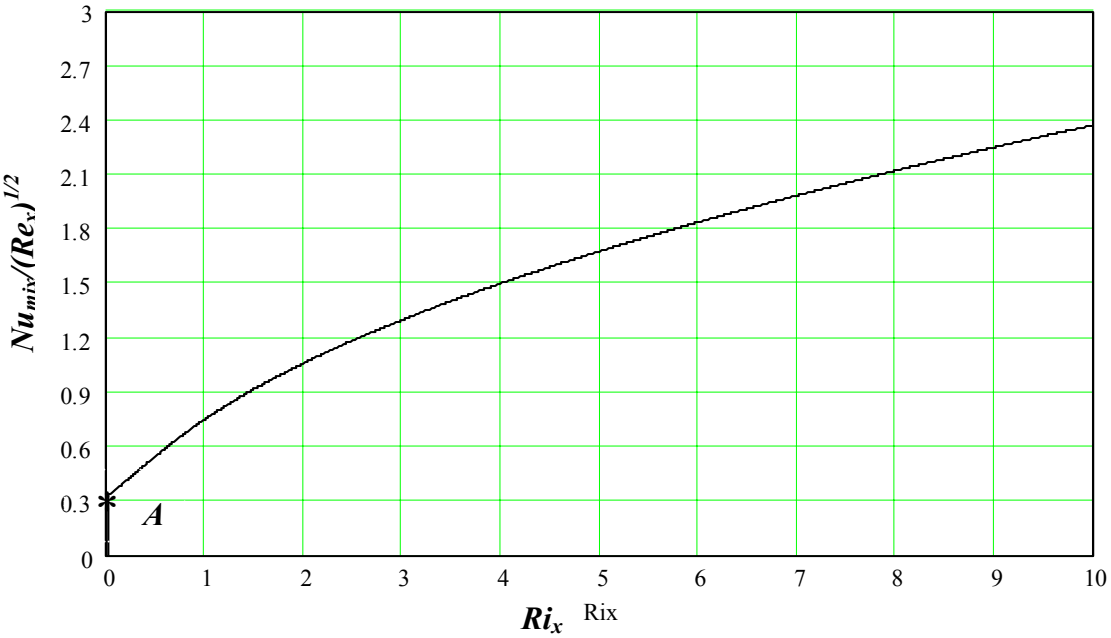

Fig. (4-8): Variation of $(Nu_{mix}/(Re_x)^{1/2})$ with Richardson number range of 0 to 10, for vertical flat plate and Pr =1, by eq. (3.31).

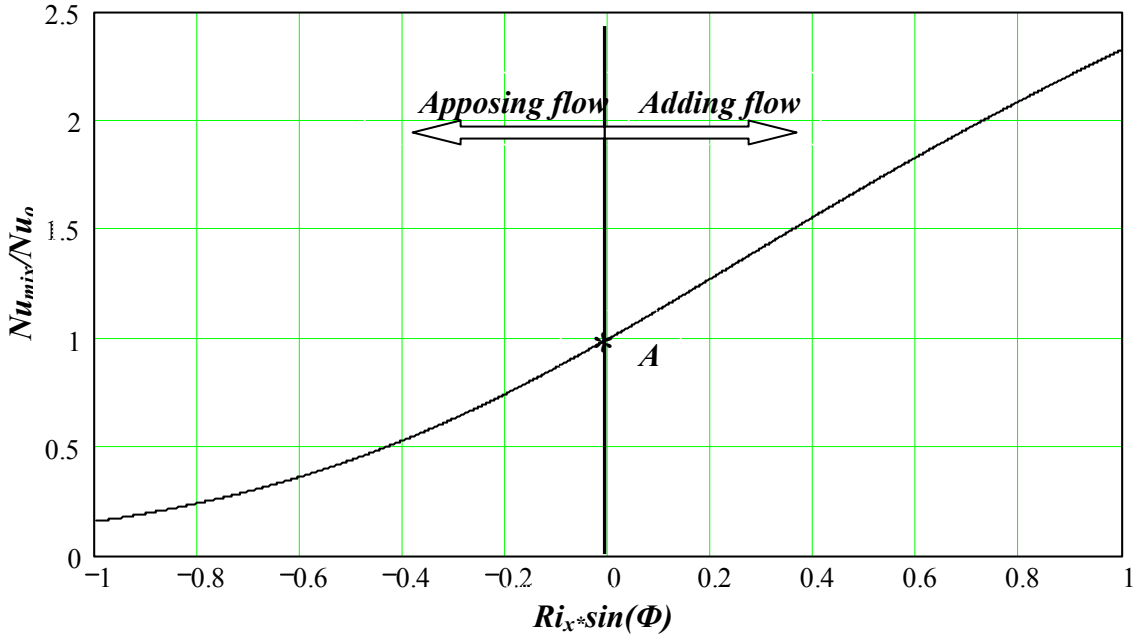

*Fig. (4-9): Variation of (Nu_{mix}/Nu_o) with (Ri_x*sin (Φ)) for Pr =1, eq. (3.19).*

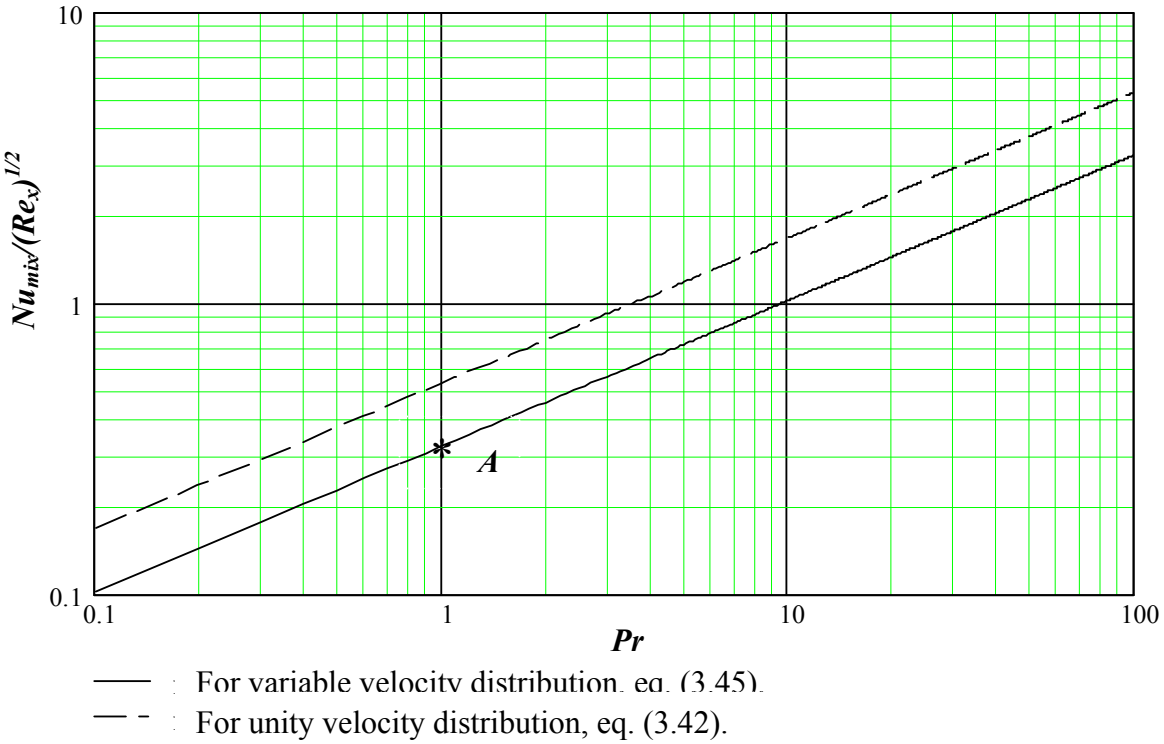

Fig. (4-10): Variation of $(Nu_{mix}/(Re_x)^{1/2})$ with Prandtl number range of 0.1 to 100 for $Ri_x \longrightarrow 0$, by eqs. (3.42, 3.45).

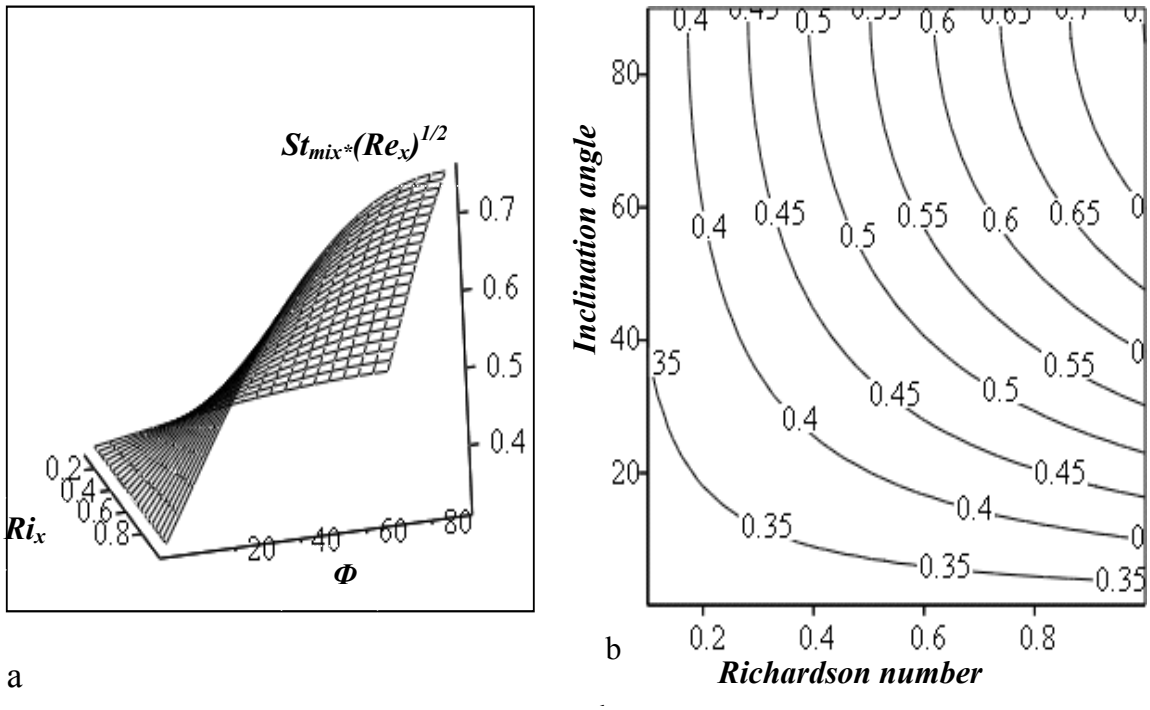

Fig. (4-11): Variation of ($St_{mix*}(Re_x)^{1/2}$) with Richardson number range of 0 to 1 and inclination angle range of 0.1˚ to 90˚ for Pr =1, by eq. (3.23).

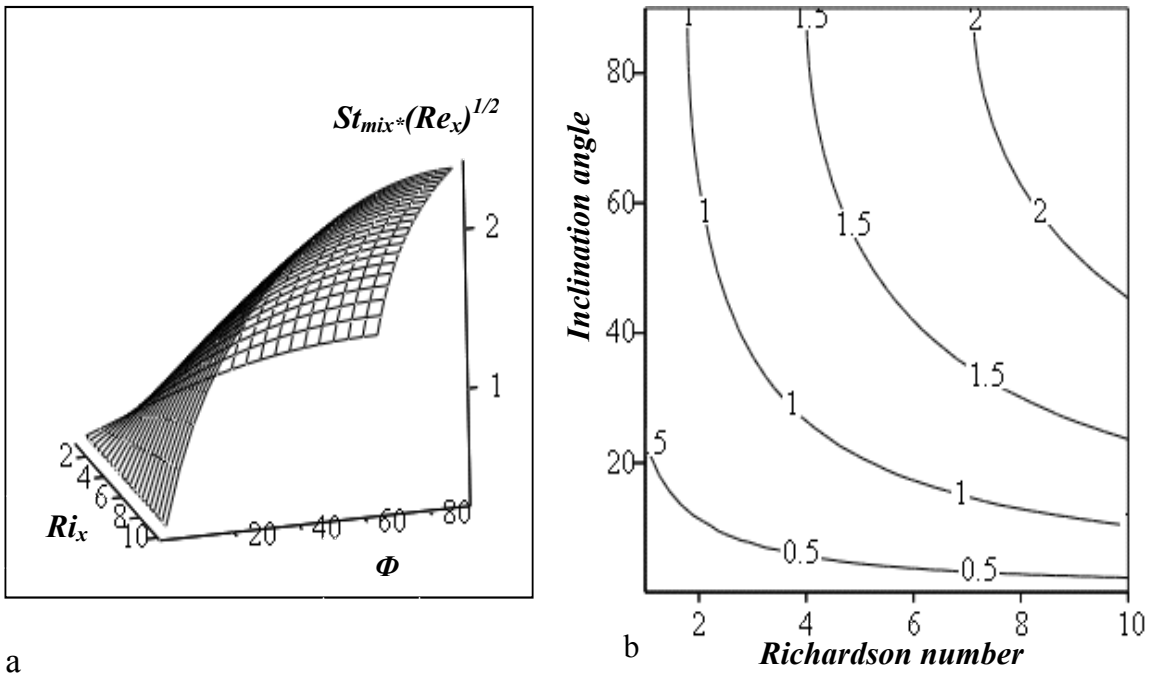

Fig. (4-12): Variation of ($St_{mix*}(Re_x)^{1/2}$) with Richardson number range of 1 to 10 and inclination angle range of 0.1˚ to 90˚ for Pr =1, by eq. (3.23).

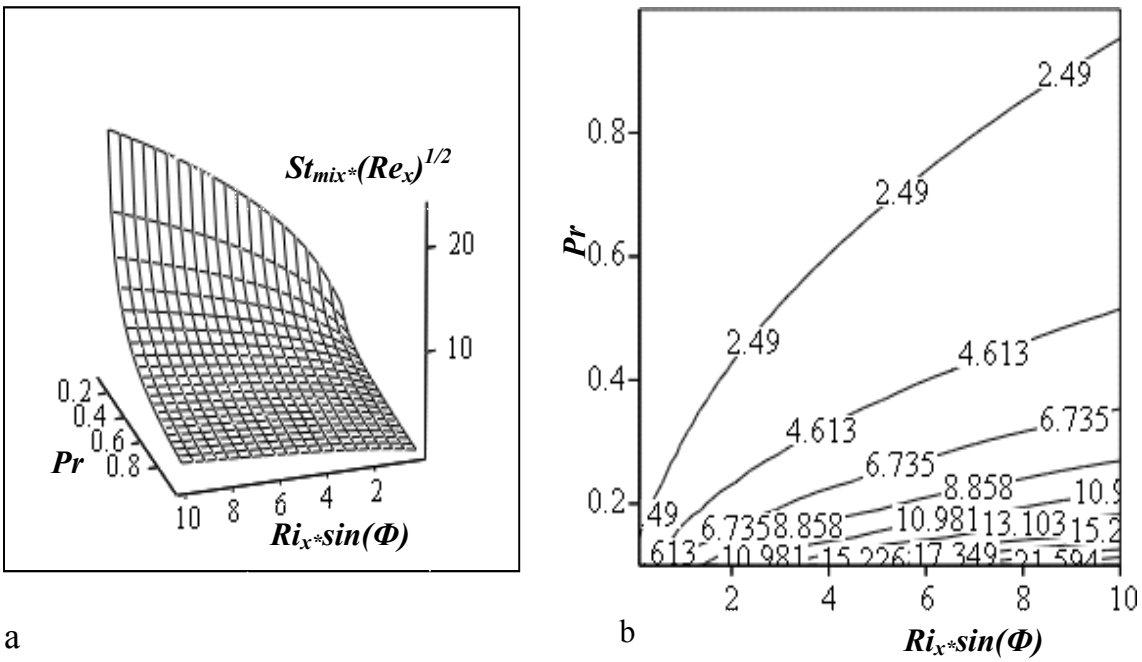

Fig. (4-13): Variation of ($St_{mix*}(Re_x)^{1/2}$) with ($Ri_{x*}sin(\Phi)$) range of 1 to 10 and Prandtl number range of 0.1 to 1, by eq. (3.23).

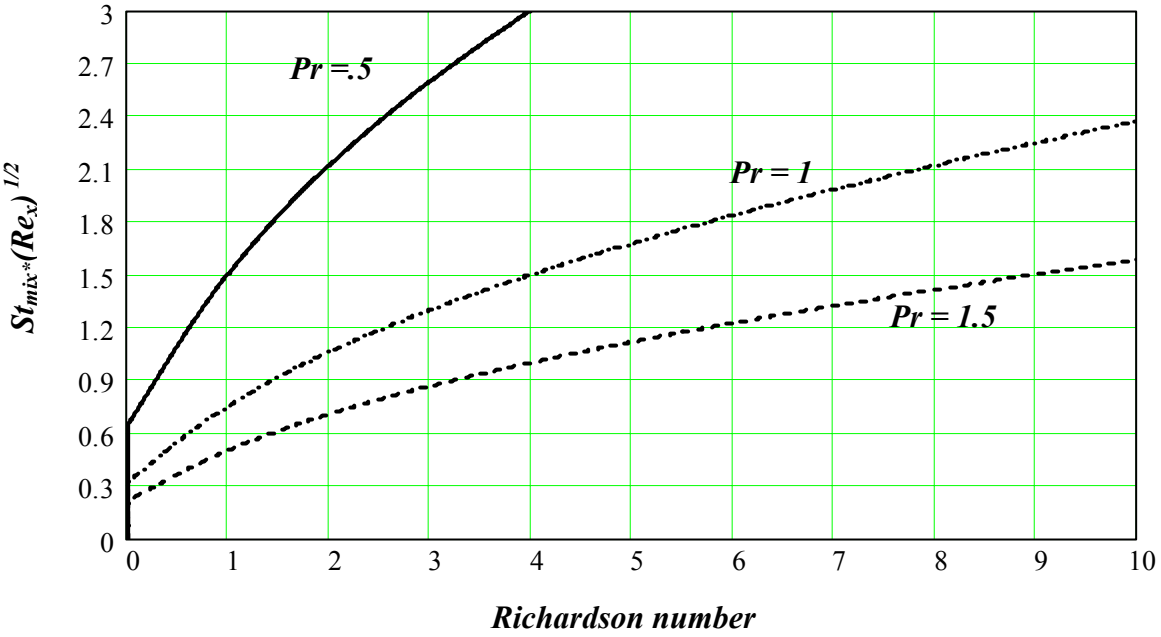

Fig.(4-14): Variation of ($St_{mix*}(Re_x)^{1/2}$) with Richardson number range of 0 to 10 for vertical flat plate and Pr = 0.5,1 and 1.5, by eq. (3.32).

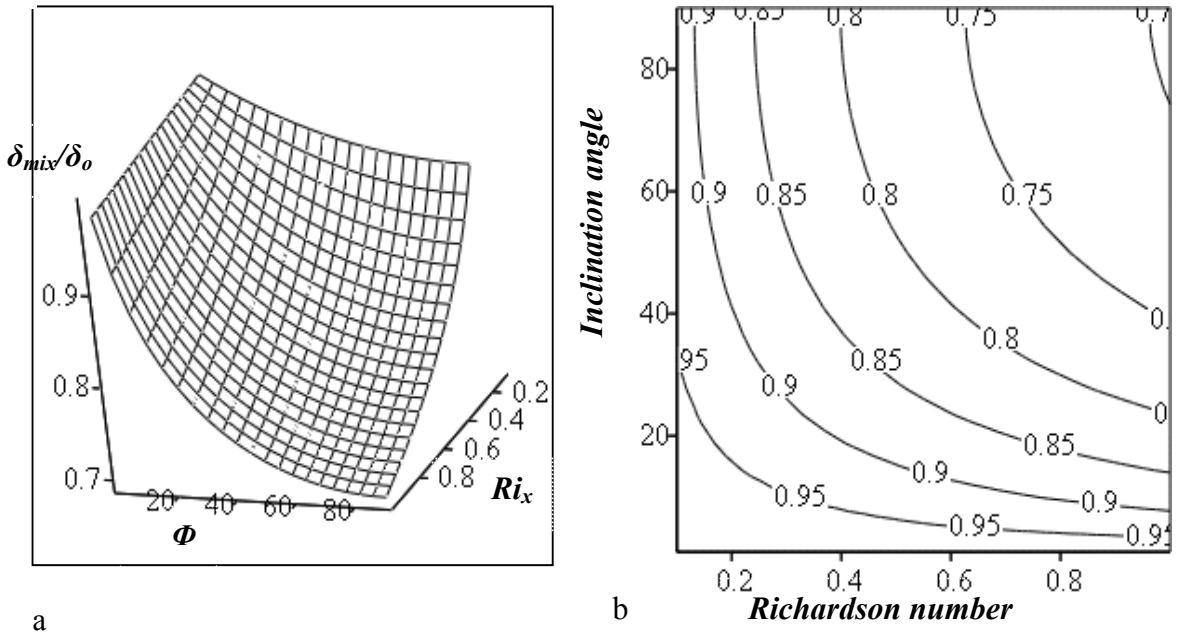

a b

Fig. (4-15): Variation of boundary layer thickness ratio (δ_{mix}/δ_o) with Richardson number range of 0.1 to 1 and inclination angle range of 1˚ to 90˚ for Pr =1, by eq. (3.52).

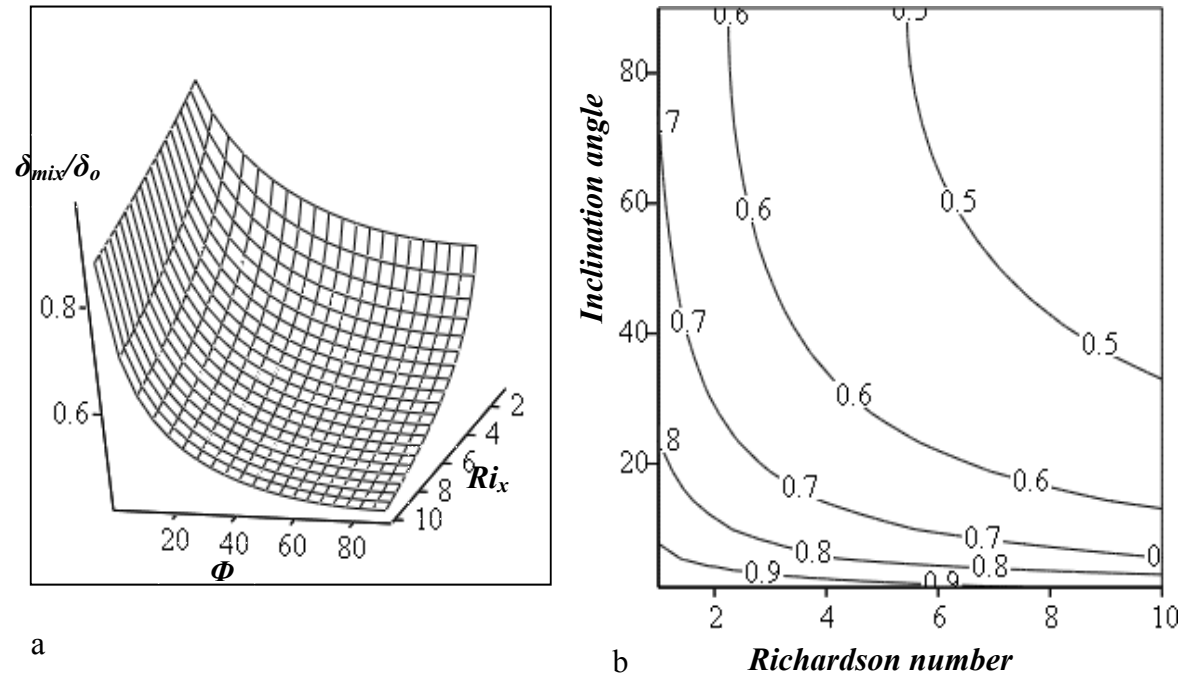

a b

Fig. (4-16): Variation of boundary layer thickness ratio (δ_{mix}/δ_o) with Richardson number range of 1 to 10 and inclination angle range of 1˚ to 90˚ for Pr =1, by eq. (3.52).

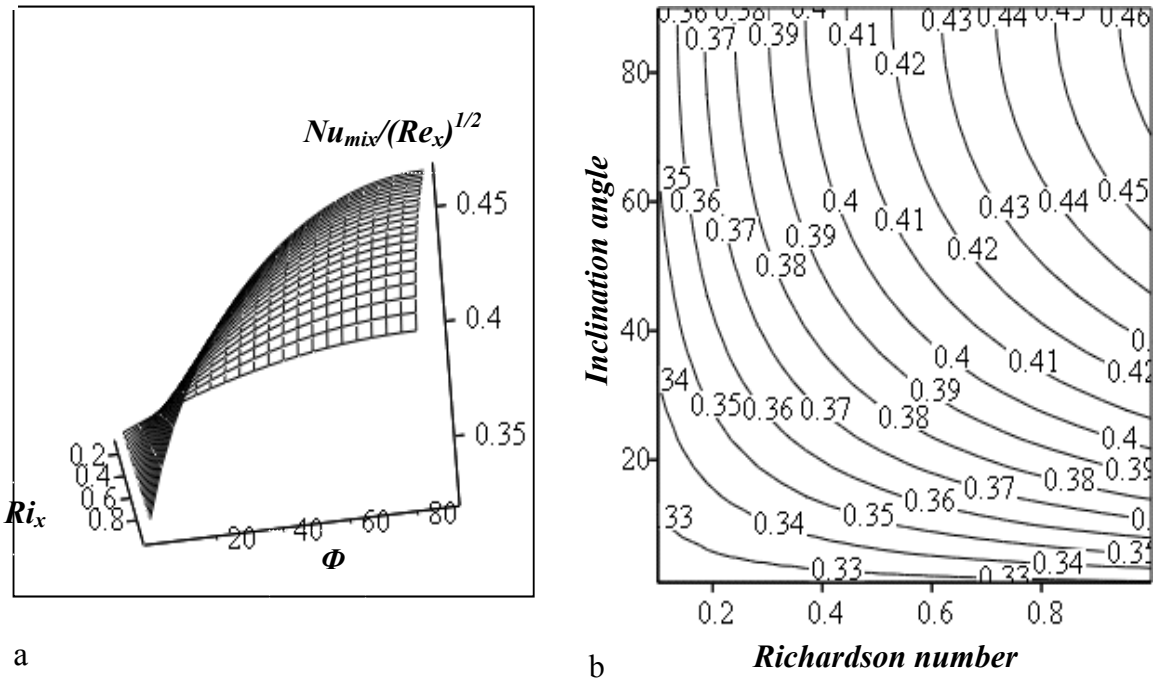

Fig. (4-17): Variation of $(Nu_{mix}/(Re_x)^{1/2})$ with Richardson number range of 0.1 to 1 and inclination angle range of 1˚ to 90˚ for Pr =1, by eq. (3.53).

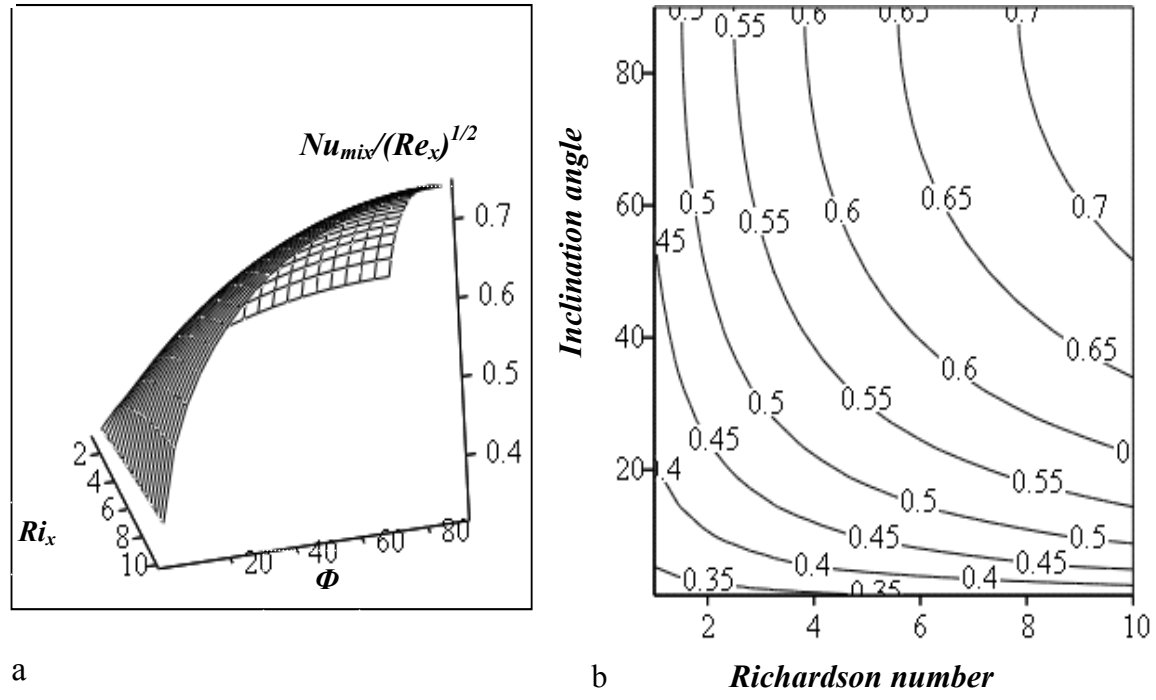

Fig. (4-18): Variation of $(Nu_{mix}/(Re_x)^{1/2})$ with Richardson number range of 1 to 10 and inclination angle range of 1˚ to 90˚ for Pr =1, by eq. (3.53).

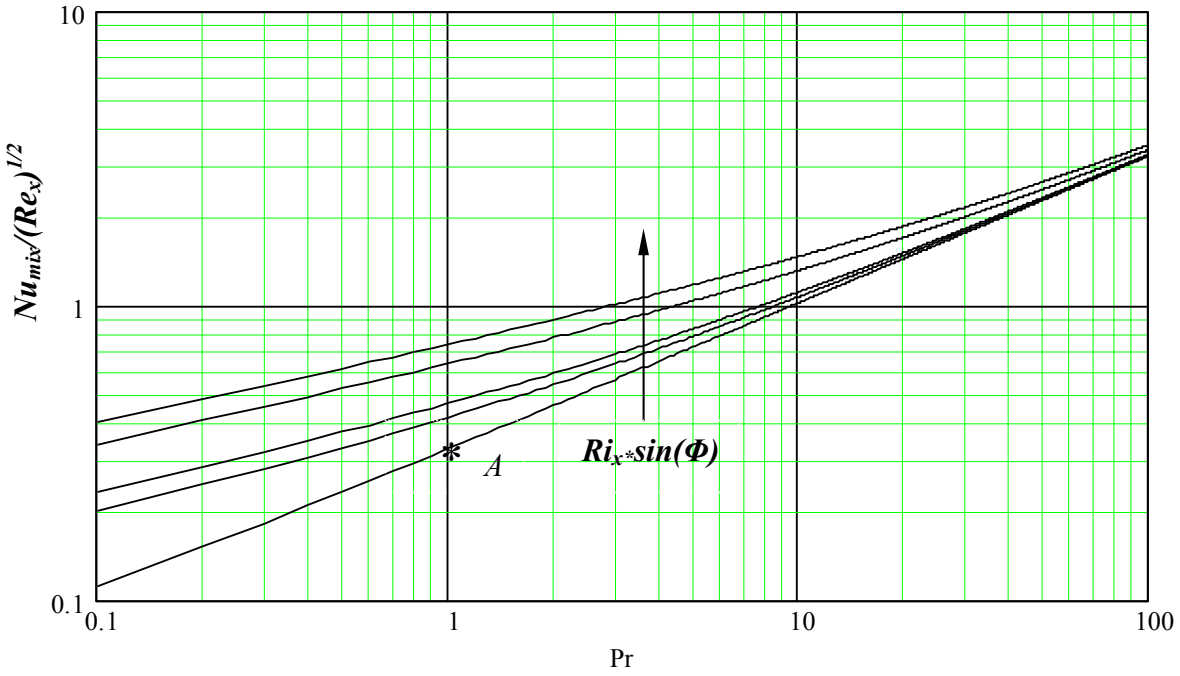

Fig. (4-19): Variation of $(Nu_{mix}/(Re_x)^{1/2})$ with Prandtl number range of 0.1 to 100 and $Ri_x*sin(\Phi) = 0.01, 0.5, 1, 5, 10$, by eq. (3.53).

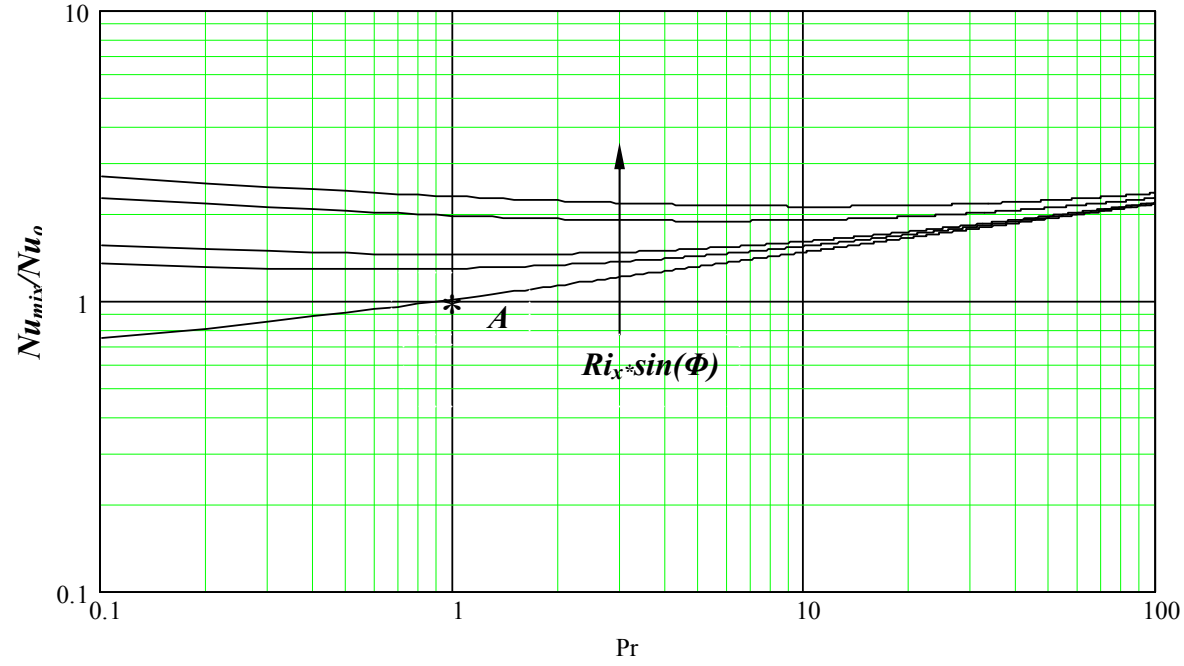

Fig. (4-20): Variation of (Nu_{mix}/Nu_o) with Prandtl number range of 0.1 to 100 and for $Ri_x*sin(\Phi) = 0.01, 0.5, 1, 5, 10$, by eq. (3.54).

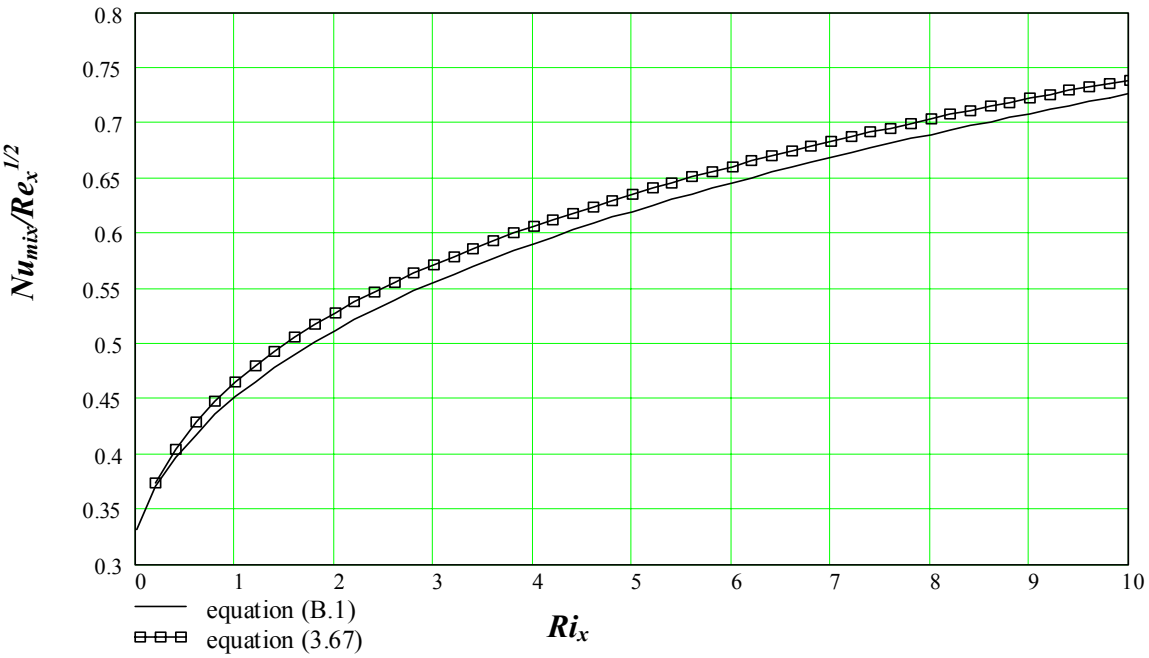

Fig. (4-21): Variation of Nusselt number with Richardson number for vertical plate and Pr = 1, by eqs. (3.53, B.1).

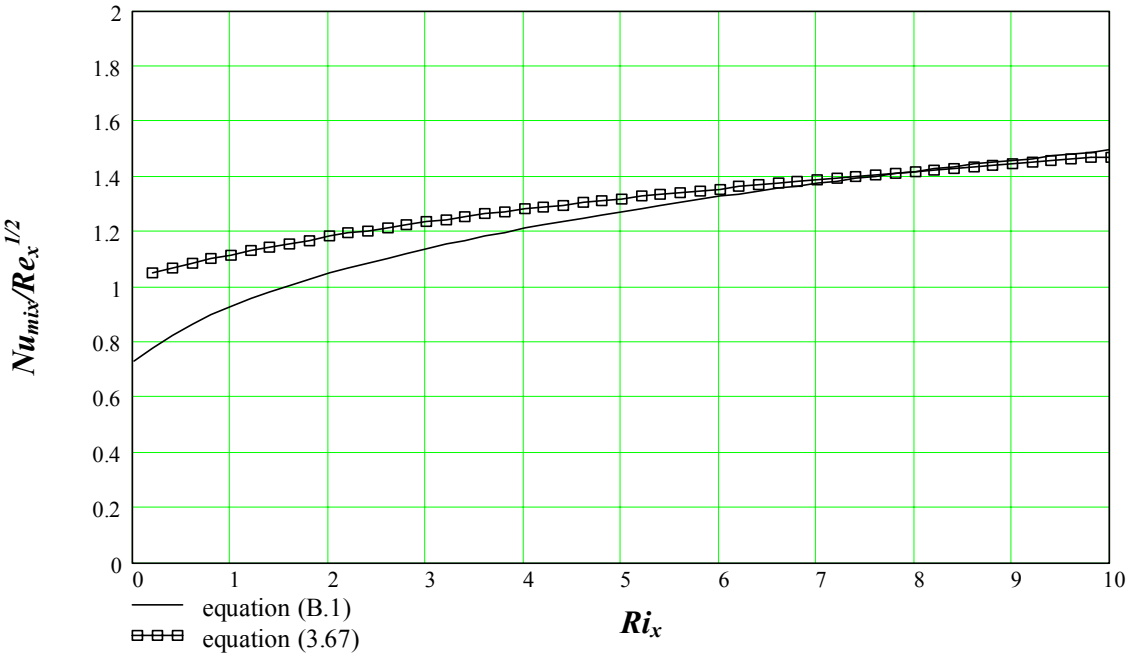

Fig. (4-22): Variation of Nusselt number with Richardson number for vertical plate and Pr = 10, by equations (3.53, B.1).

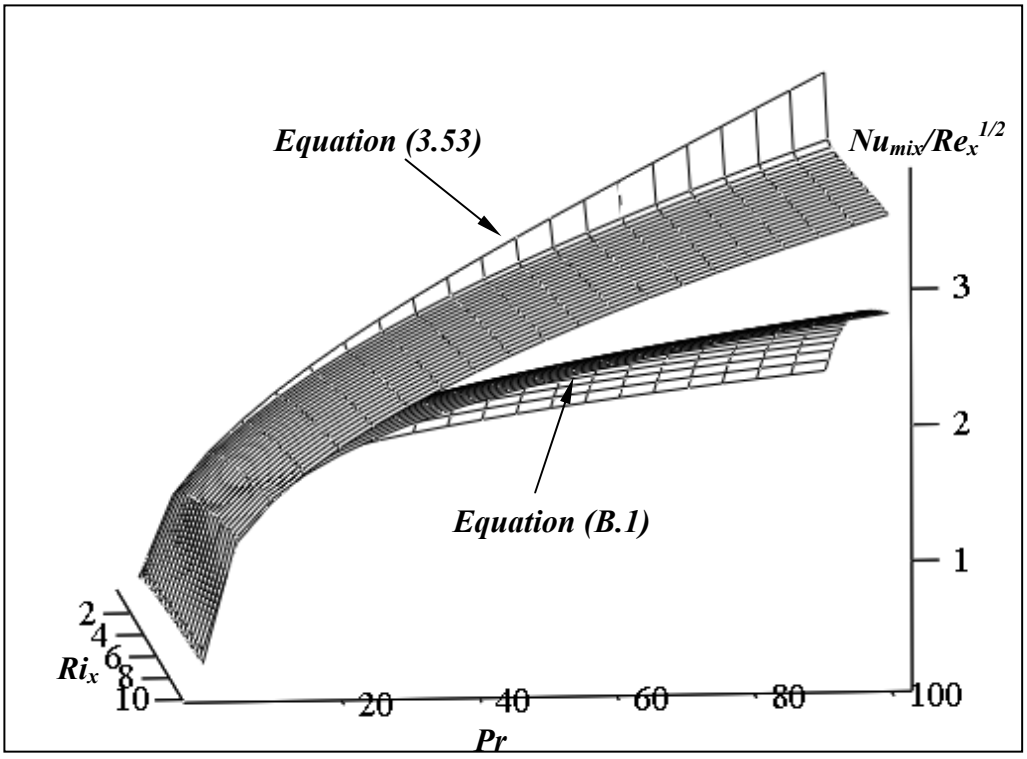

Fig. (4-23): Variation of Nusselt number with Richardson number and Pr number for vertical plate, by eqs. (3.53 and B.1).

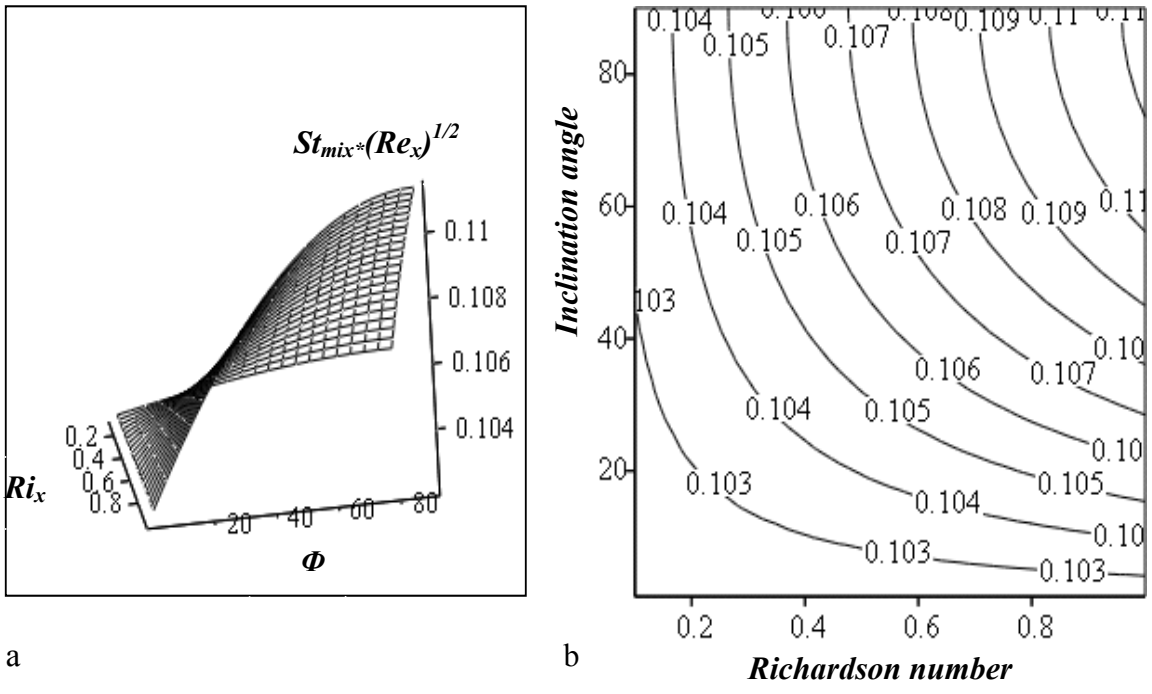

Fig. (4-24): Variation of ($St_{mix}*(Re_x)^{1/2}$) with Richardson number range of 0.1 to 1 and inclination angle range of 1˚ to 90˚ for Pr =10, by eq. (3.56).

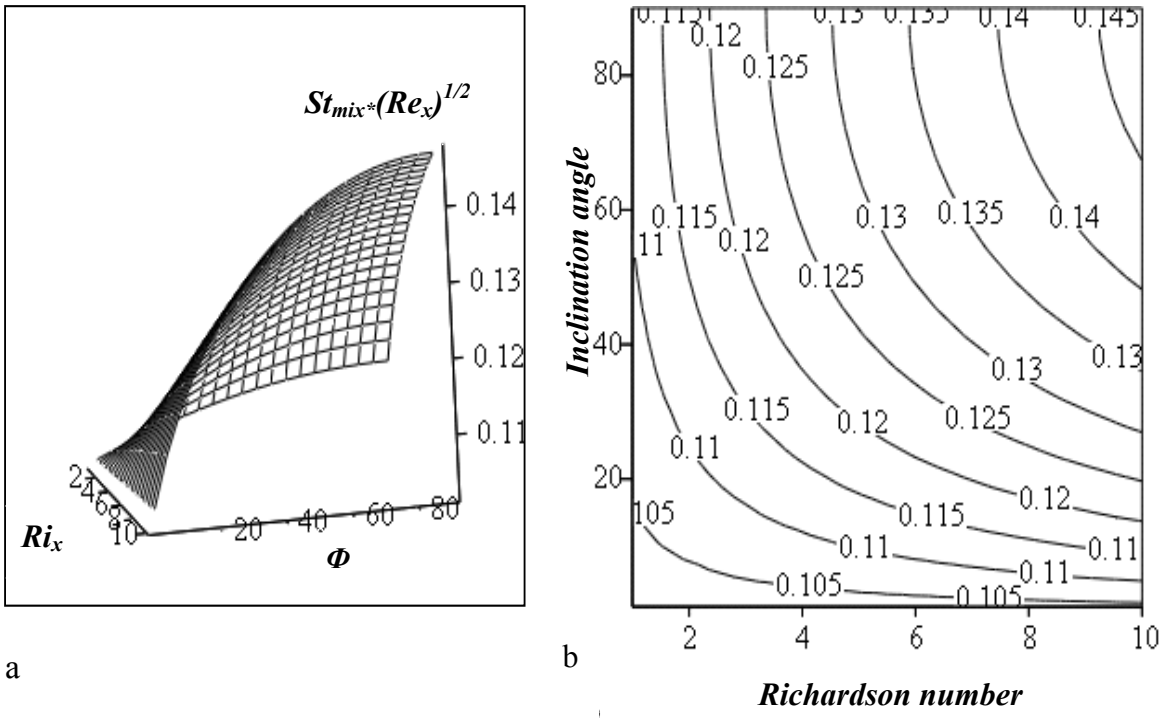

Fig. (4-25): Variation of ($St_{mix}*(Re_x)^{1/2}$) with Richardson number range of 1 to 10 and inclination angle range of 1˚ to 90˚ for Pr =10, by eq. (3.56).

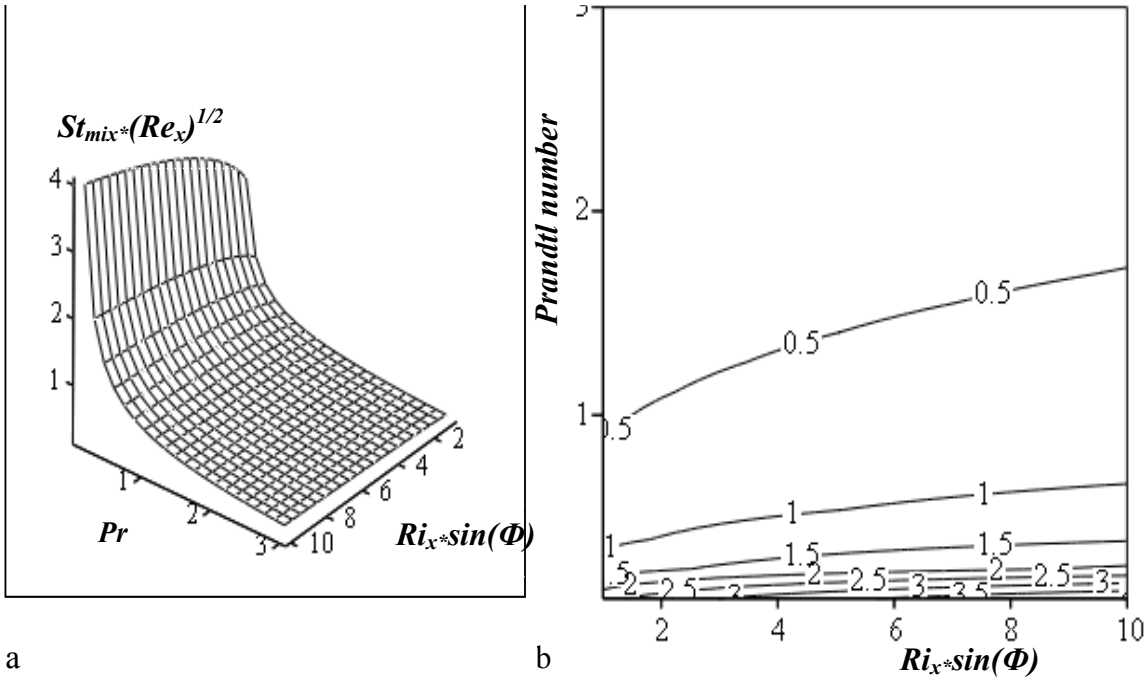

Fig. (4-26): Variation of ($St_{mix}*(Re_x)^{1/2}$) with ($Ri_x*sin(\Phi)$) range of 1 to 10 and Prandtl number range of 0.1 to 3, by eq. (3.56).

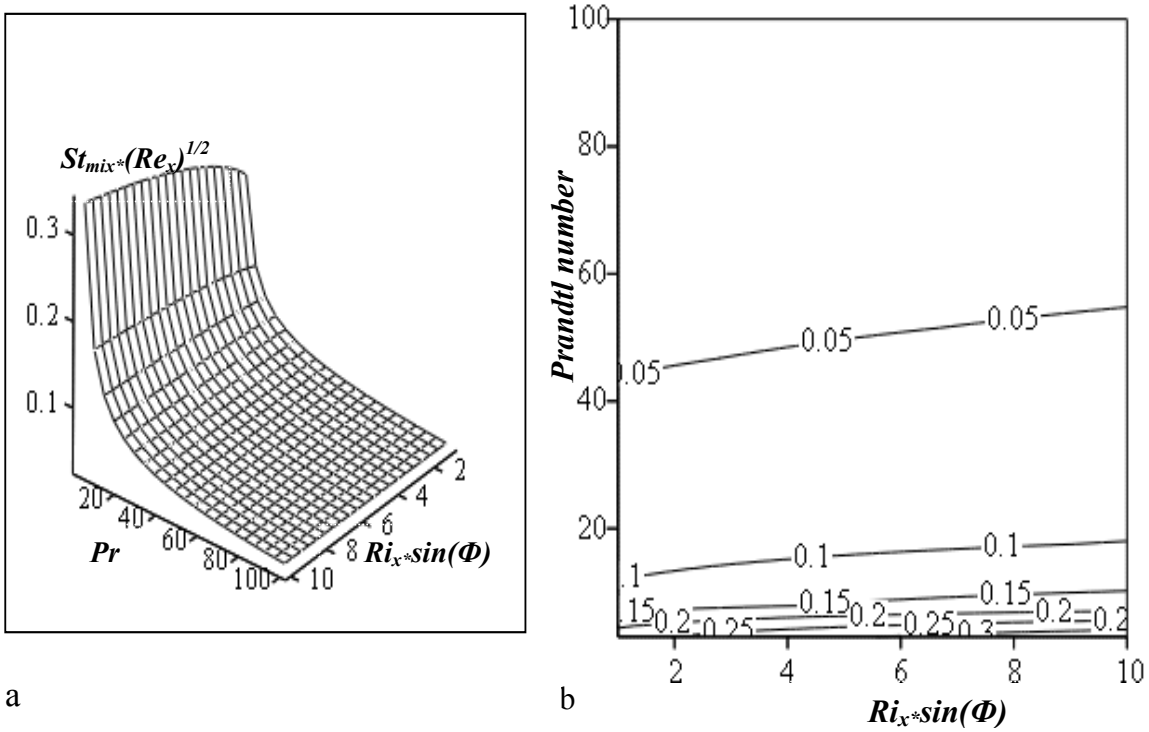

Fig. (4-27): Variation of $(St_{mix}*(Re_x)^{1/2})$ with $(Ri_x*sin(\Phi))$ range of 1 to 10 and Prandtl number range of 3 to 100, by eq. (3.56).

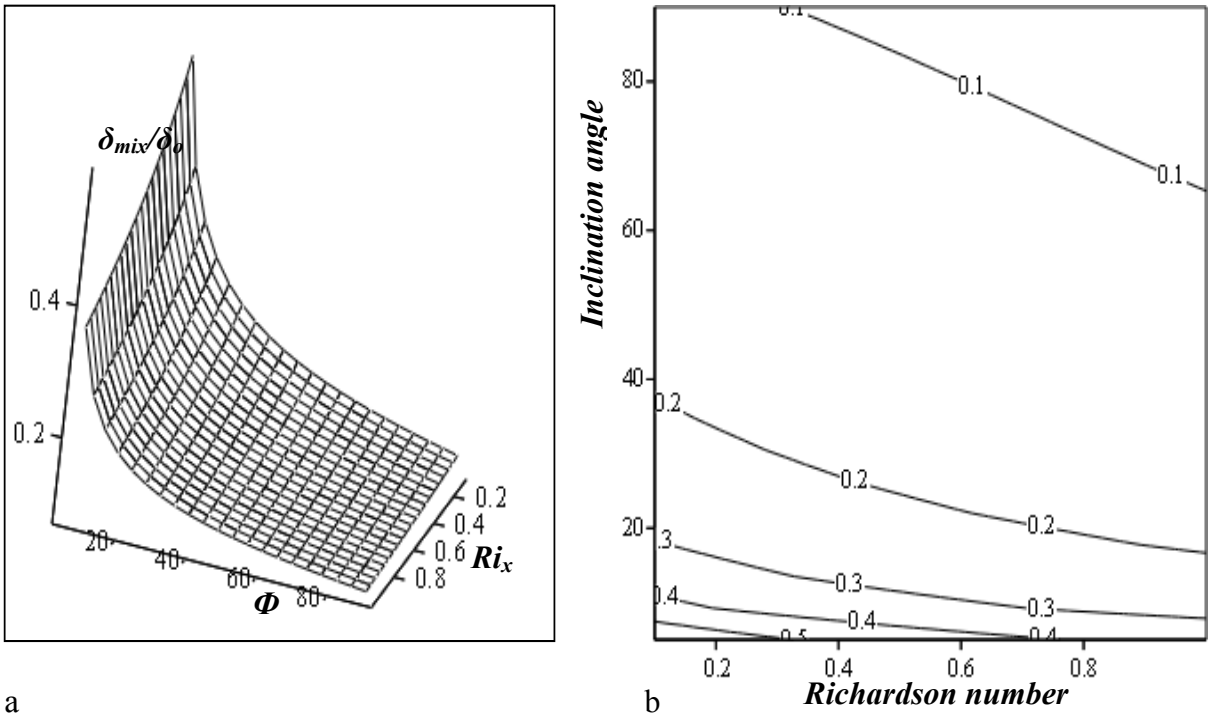

Fig. (4-28): Variation of boundary layer thickness ratio (δ_{mix}/δ_o) with Richardson number range of 0.1 to 1 and Inclination angle range of 5˚ to 90˚ for Pr =1.1, eq. (3.76).

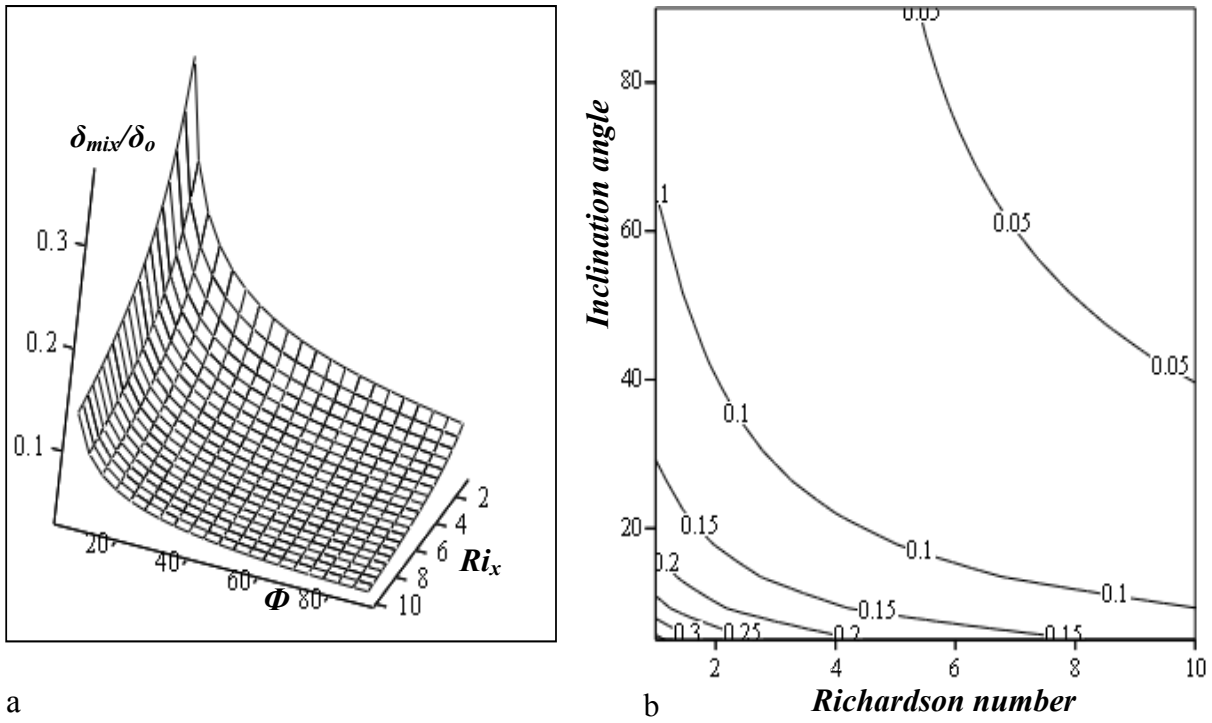

Fig. (4-29): Variation of boundary layer thickness ratio (δ_{mix}/δ_o) with Richardson number range of 1 to 10 and Inclination angle range of 5˚ to 90˚ for Pr =1.1, eq. (3.76).

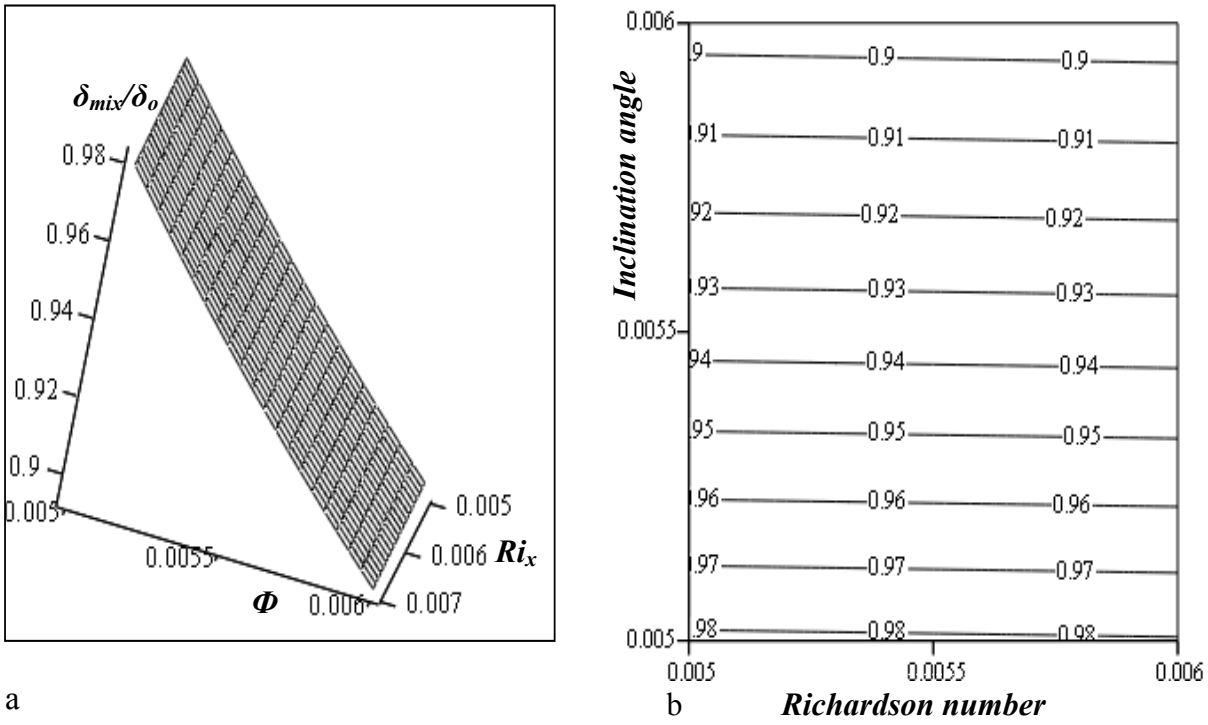

Fig. (4-30): Variation of boundary layer thickness ratio (δ_{mix}/δ_o) with Richardson number range of 0.005 to 0.006 and Inclination angle range of 0.005˚ to 0.006˚ for Pr = 1.0002 eq. (3.76).

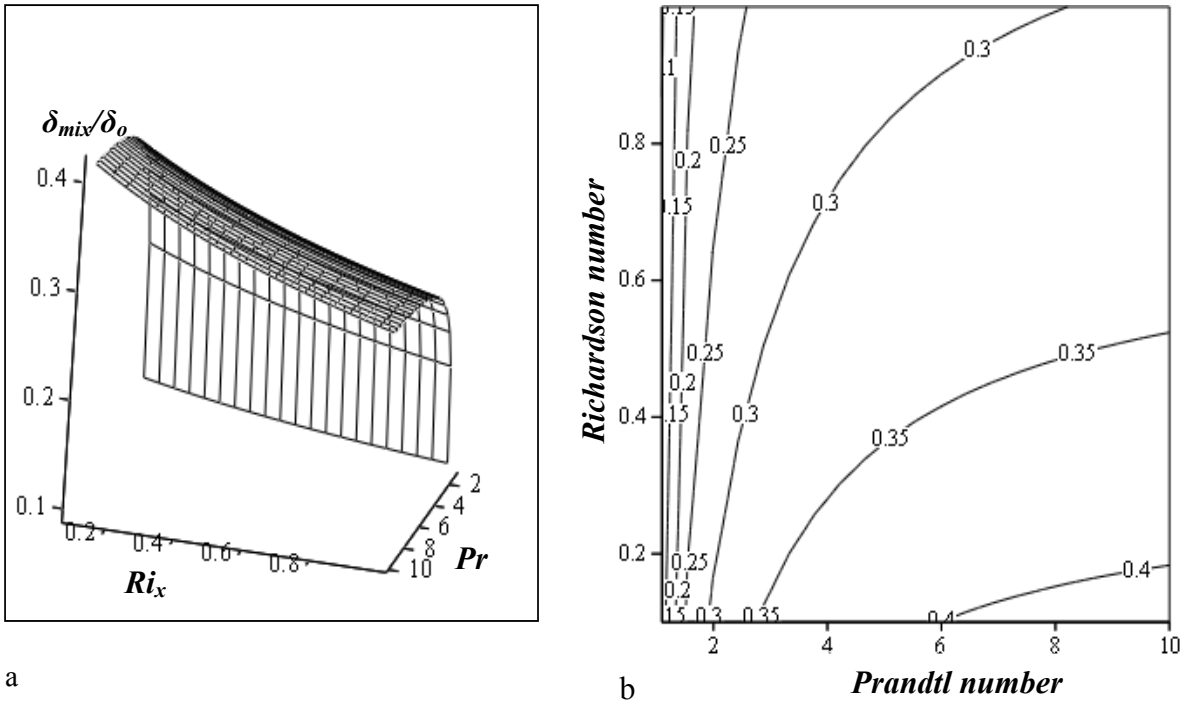

a b

Fig. (4-31): Variation of boundary layer thickness ratio (δ_{mix}/δ_o) with Prandtl number range of 1.1 to 10 and Richardson number range of .01 to 1 for Φ =70˚, eq. (3.76).

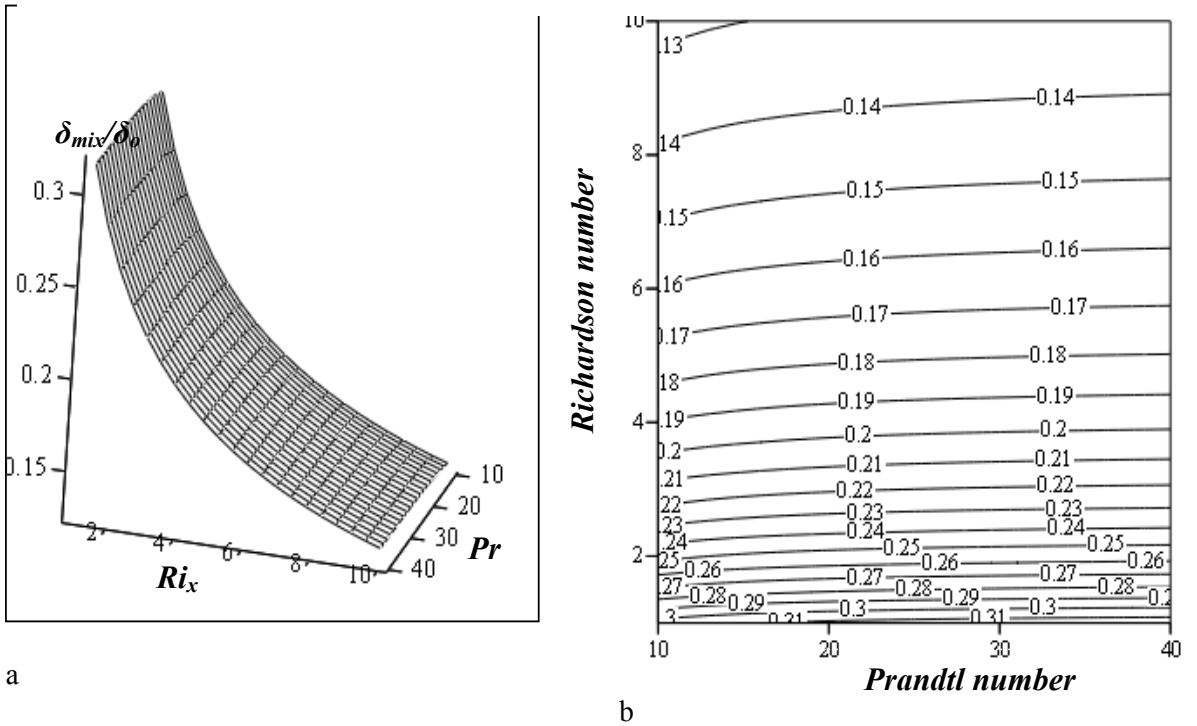

a b

Fig. (4-32): Variation of boundary layer thickness ratio (δ_{mix}/δ_o) with Prandtl number range of 10 to 40 and Richardson number range of 1 to 10 for Φ =70˚, eq. (3.76).

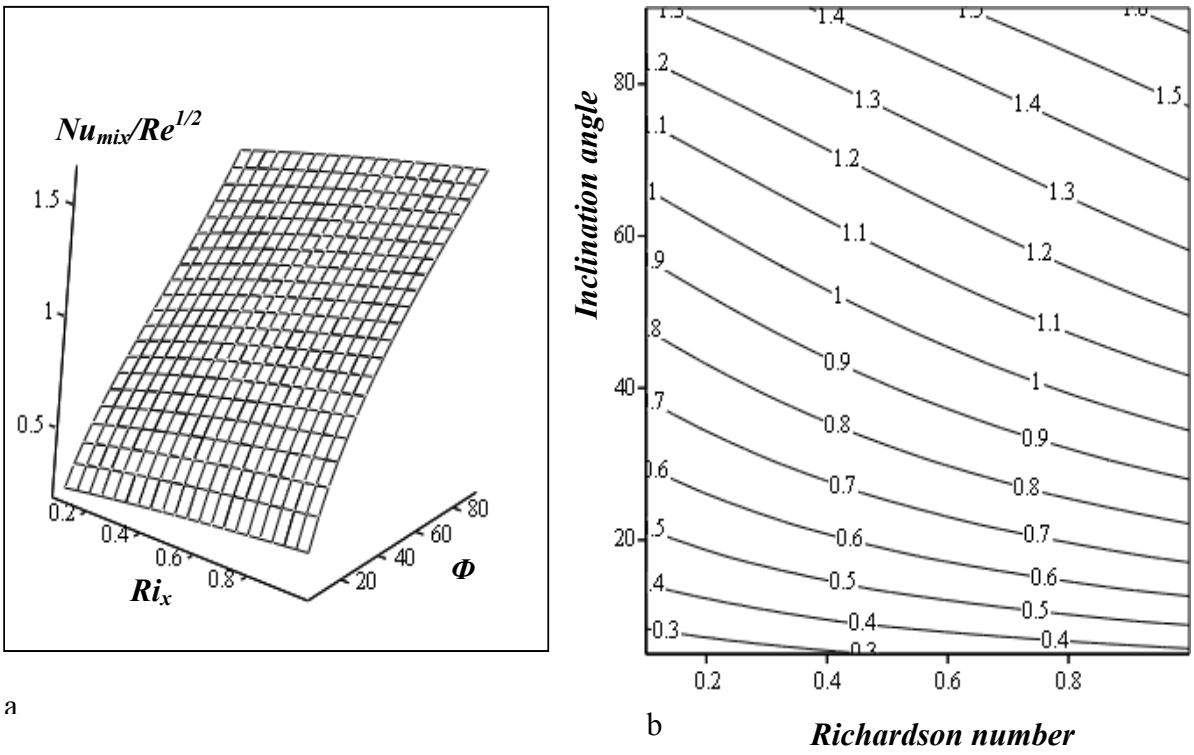

Fig. (4-33): Variation of ($Nu_{mix}/(Re_x)^{1/2}$) with Richardson number range of 0.1 to 1 and Inclination angle range of 5˚ to 90˚ for Pr =2, eq. (3.77).

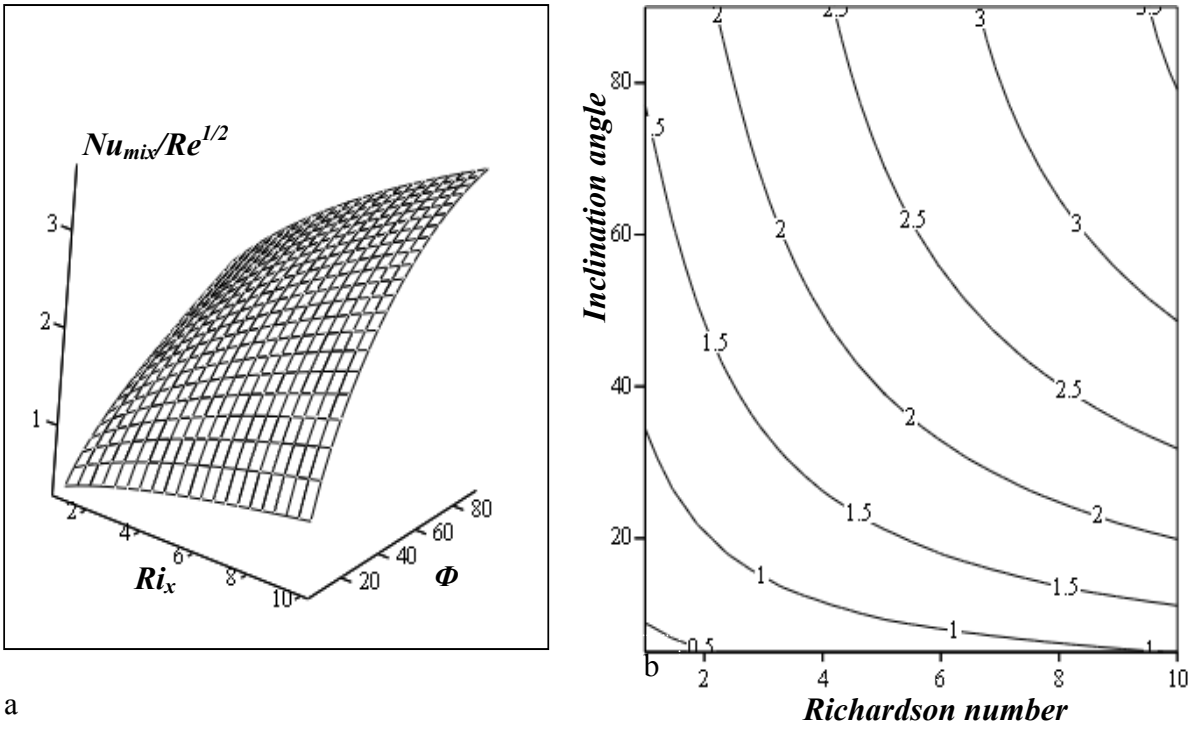

Fig. (4-34): Variation of ($Nu_{mix}/(Re_x)^{1/2}$) with Richardson number range of 1 to 10 and Inclination angle range of 5˚ to 90˚ for Pr =2, eq. (3.77).

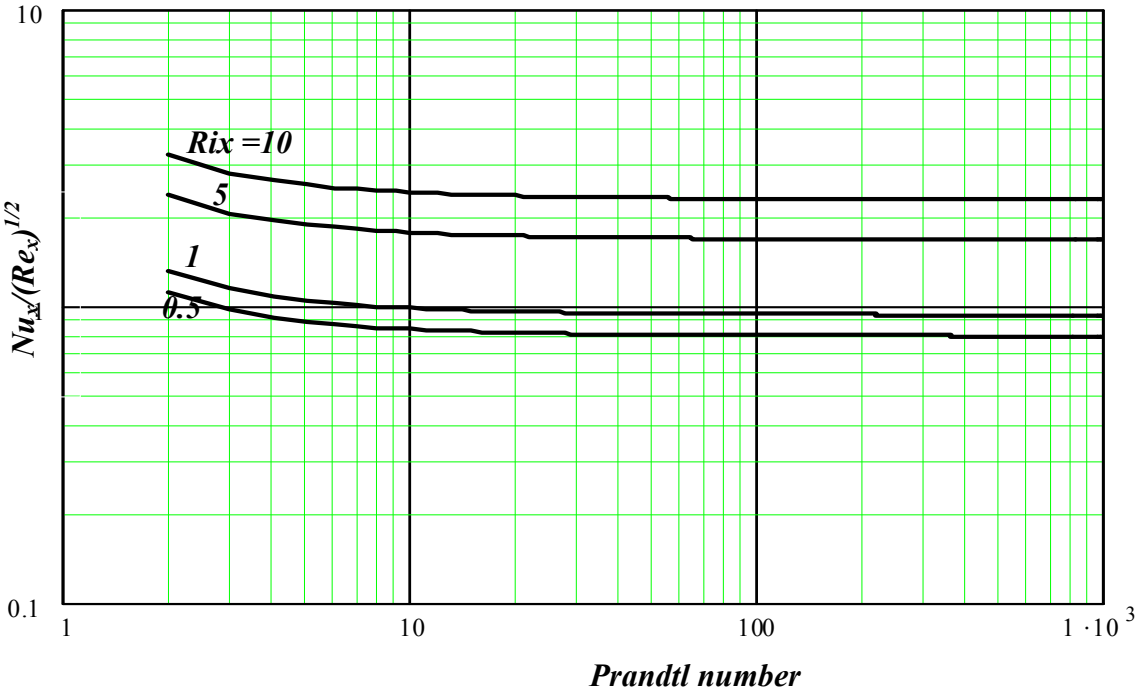

Fig. (4-35): Variation of ($Nu_{mix}/(Re_x)^{1/2}$) with Richardson of 0.5, 1, 5 and 10 and Prandtl number range of 1 to 1000 for Φ = 60˚, eq. (3.77).

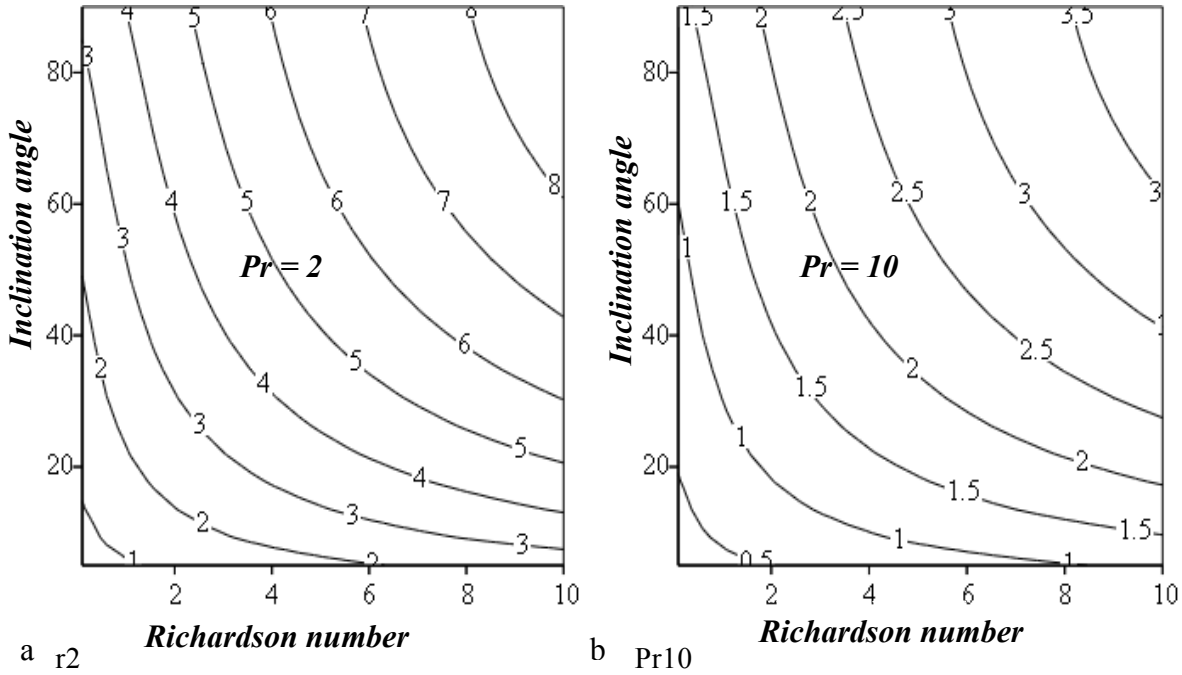

Fig. (4-36) a,b : Variation of (Nu_{mix}/Nu_o) with Richardson range of 0.1 to 10 Inclination angel range of 5˚ to 90˚ for Pr = 2 and 10 respectively eq. (3.78).

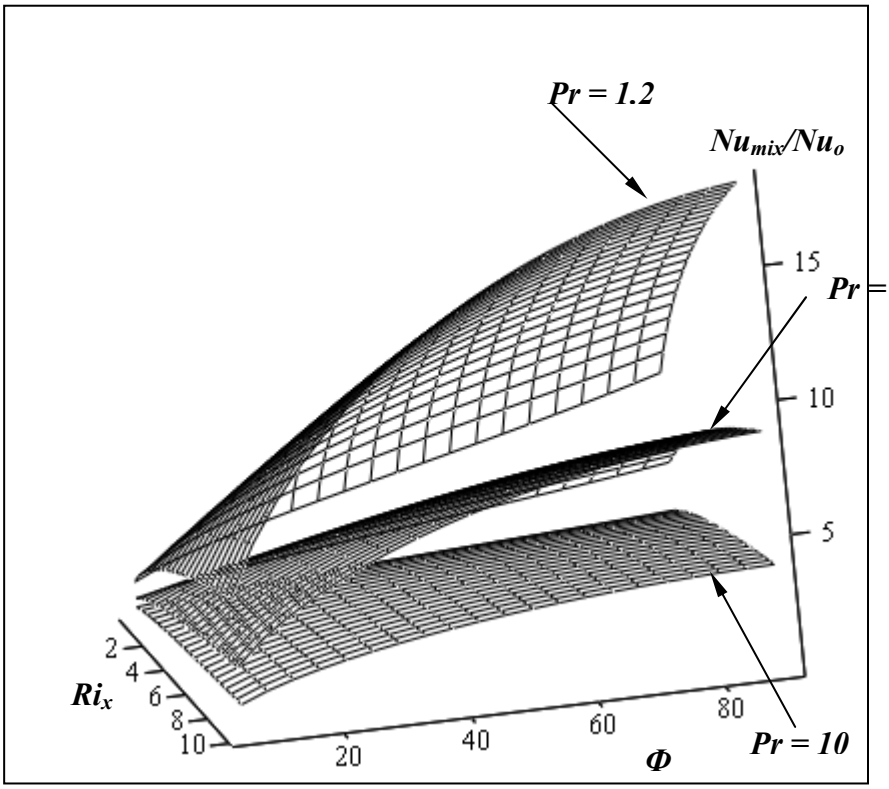

Fig. (4-37) Variation of (Nu_{mix}/Nu_o) with Richardson range of 0.1 to 10 and Inclination angel range of 5˚ to 90˚ for Pr = 1.2, 2 and 10 respectively, by eq. (3.78).

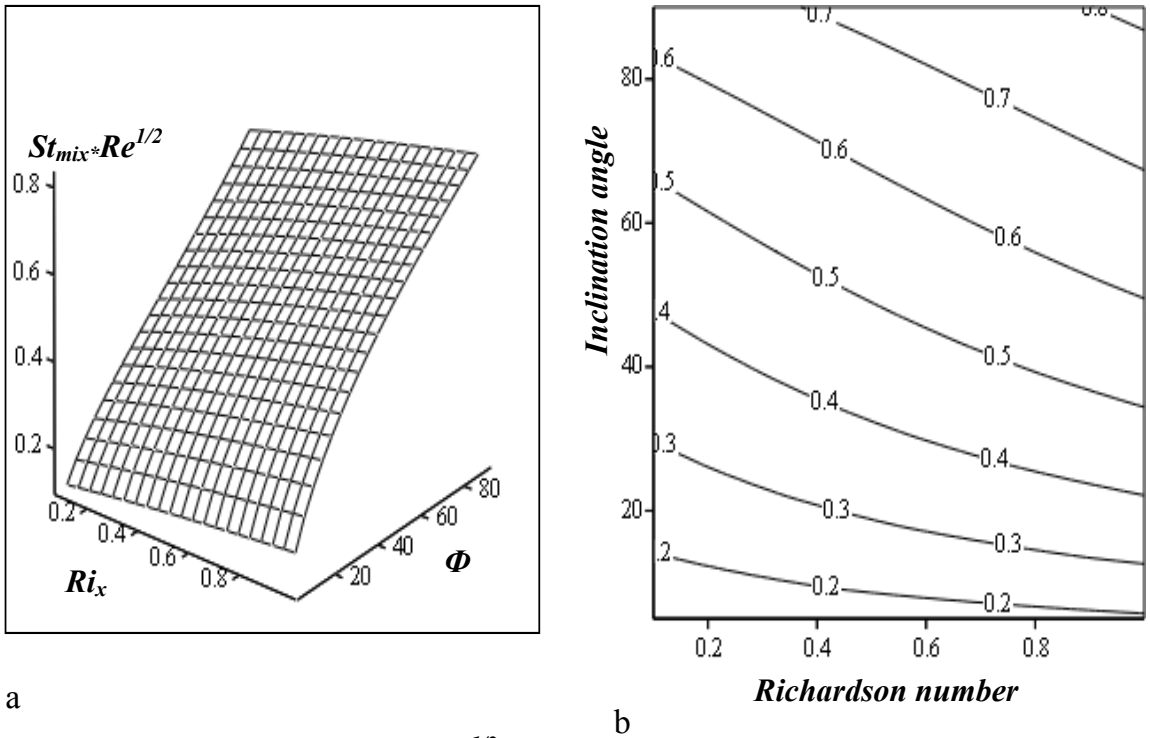

a b

Fig. (4-38): Variation of ($St_{mix}*(Re_x)^{1/2}$) with Richardson number range of 0.1 to 1 and Inclination angel range of 5˚ to 90˚ for Pr =2, eq. (3.80).

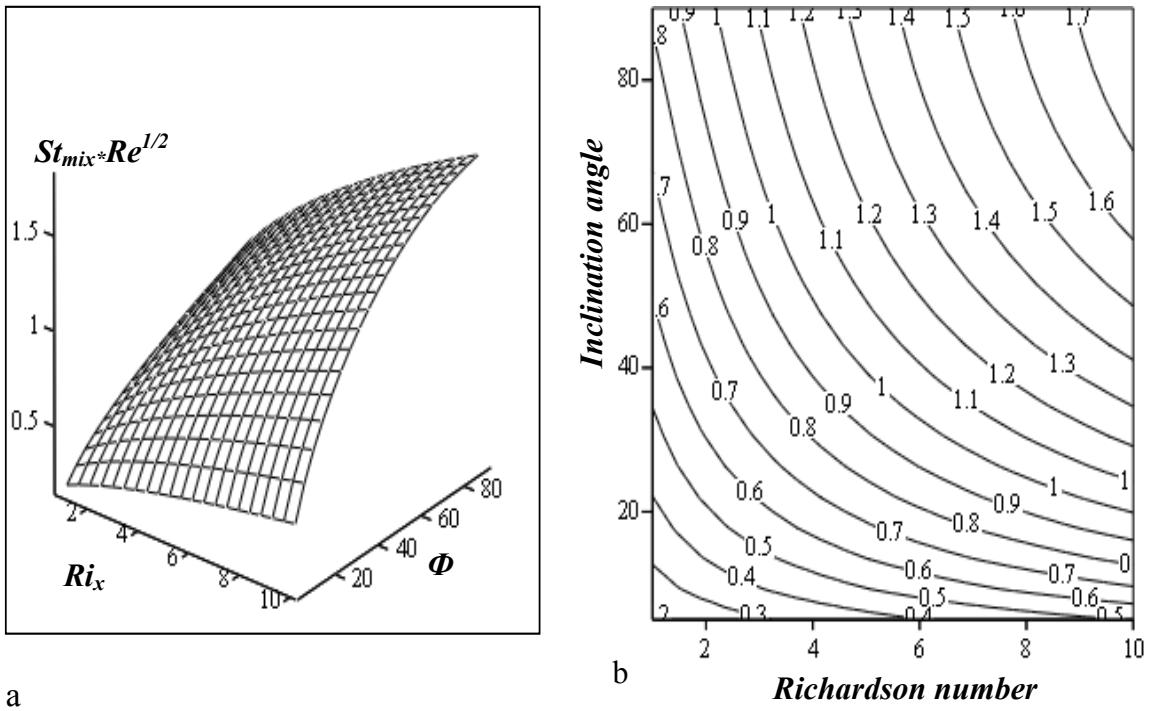

a

Fig. (4-39): Variation of ($St_{mix}*(Re_x)^{1/2}$) with Richardson number range of 1 to 10 and Inclination angel range of 5 ˚ to 90˚ for Pr =2, eq. (3.80).

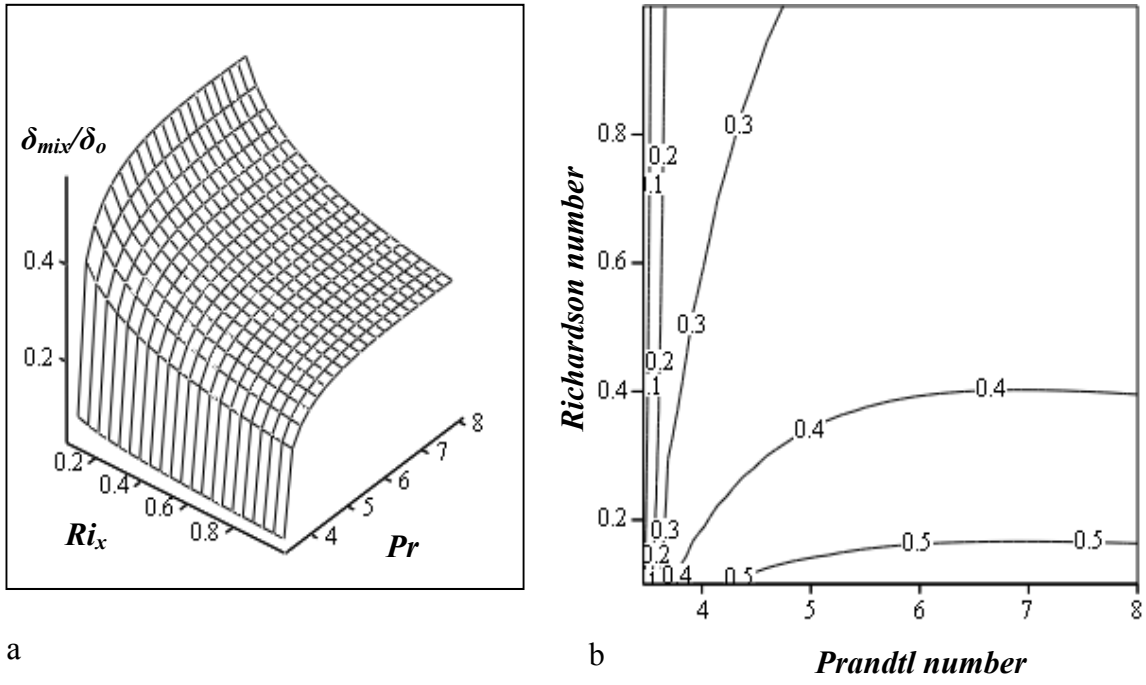

a

Fig. (4-40): Variation of boundary layer thickness ratio (δ_{mix}/δ_o) with Richardson number range of .01 to 1 and Prandtl number range of 3.462 to 8 for Φ = 60˚, eq. (3.87).

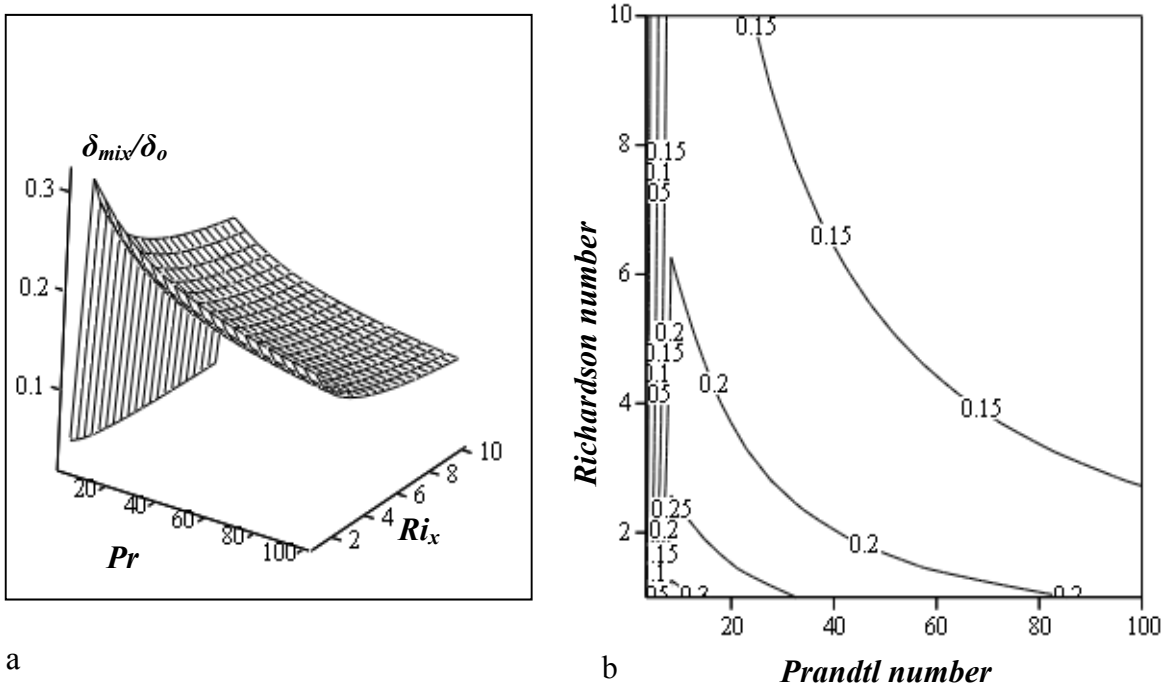

a b

Fig (4-41): Variation of boundary layer thickness ratio (δ_{mix}/δ_o) with Richardson number range of 1 to 10 and Prandtl number range of 3.462 to 100 for $\Phi = 60^\circ$, eq. (3.87).

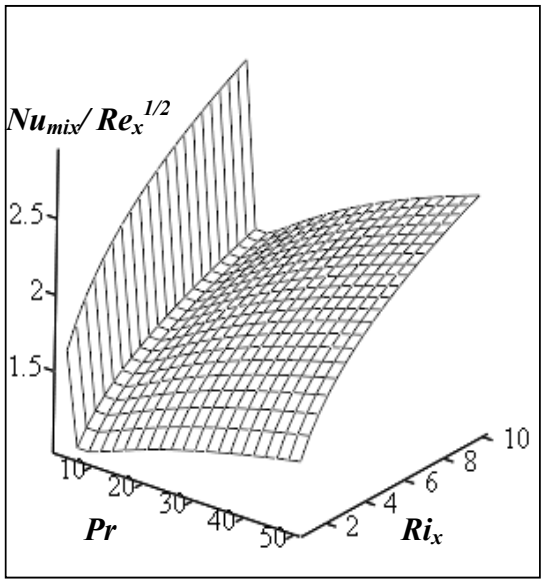

Fig. (4-42,a): Variation of $(Nu_{mix}/(Re_x)^{1/2})$ with Richardson number range of 1 to 10 and Pr range of 3.6 to 50 for $\Phi = 60^\circ$, eq. (3.89).

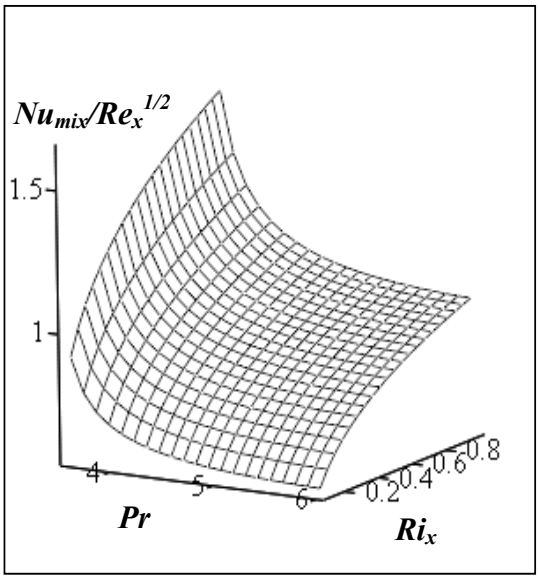

Fig.(4-42,b): Variation of $(Nu_{mix}/(Re_x)^{1/2})$ with Richardson number range of 0.1 to 1 and Pr range of 3.6 to 6 for $\Phi = 60^\circ$, eq. (3.89.)

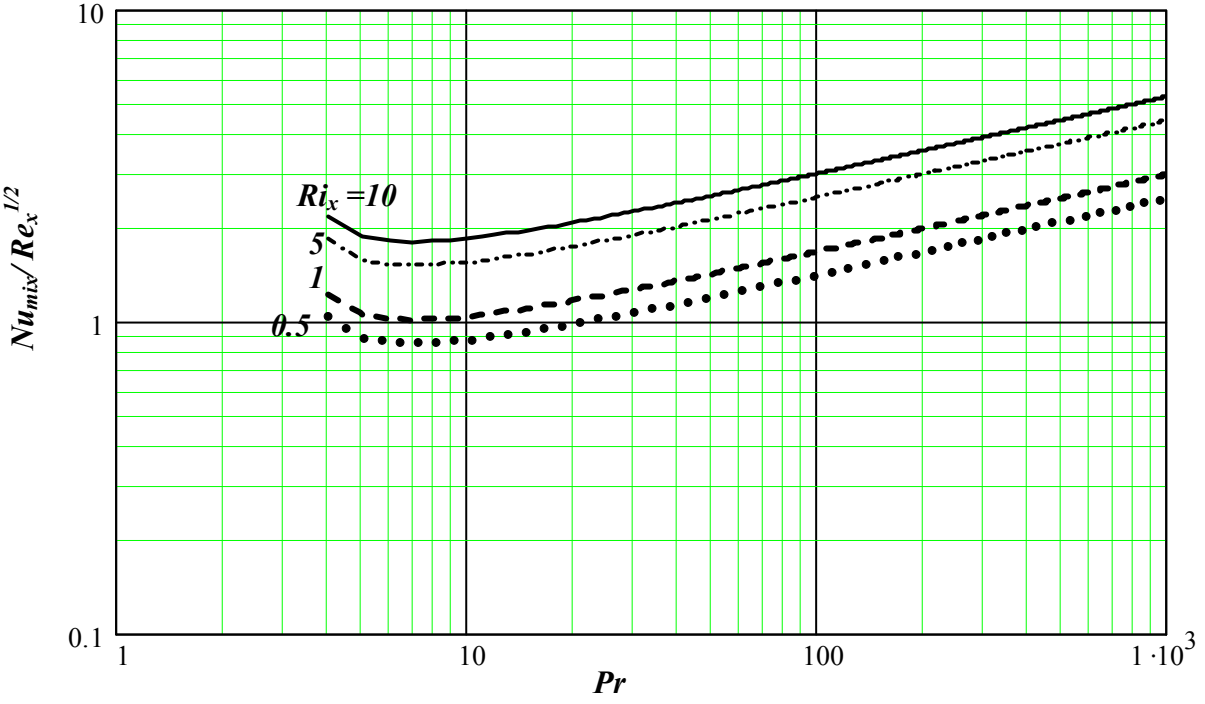

Fig. (4-43): Variation of $(Nu_{mix}/(Re_x)^{1/2})$ with Richardson of 0.5, 1, 5 and 10 and Prandtl number range of 1 to 1000 for $\Phi = 60^\circ$, eq. (3.89).

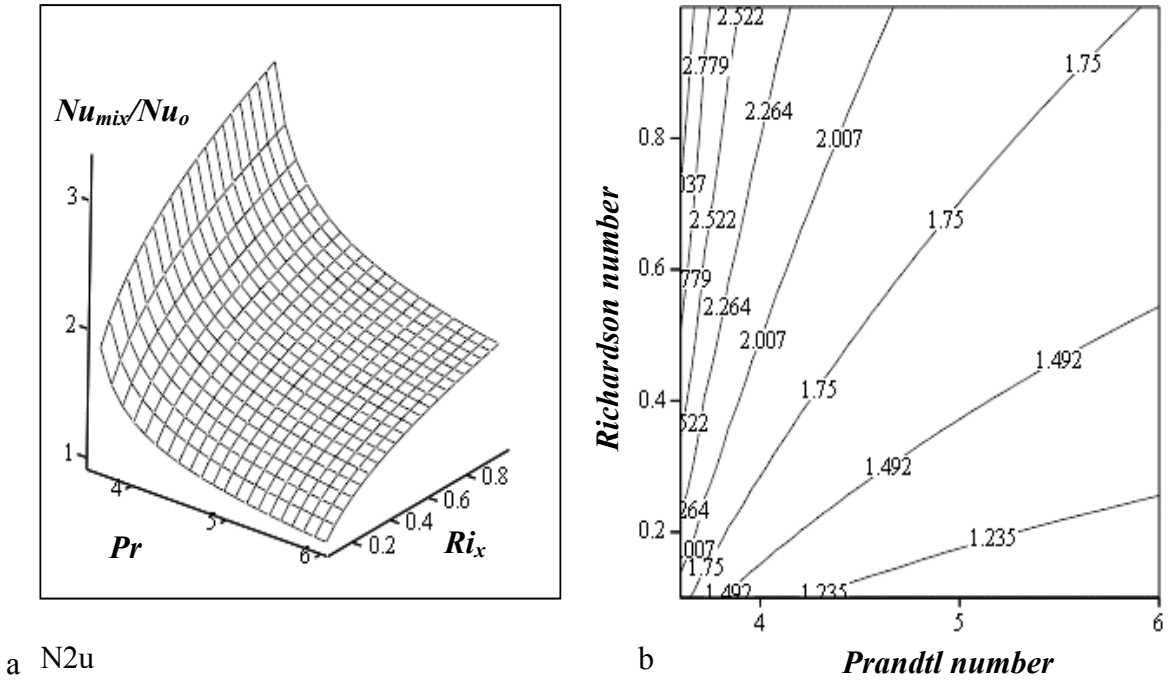

a N2u b

Fig. (4-44): Variation of (Nu_{mix}/Nu_o) with Richardson range of 0.1 to 1 and inclination angle of 60° for Pr = 3.6 to 6, eq. (3.90).

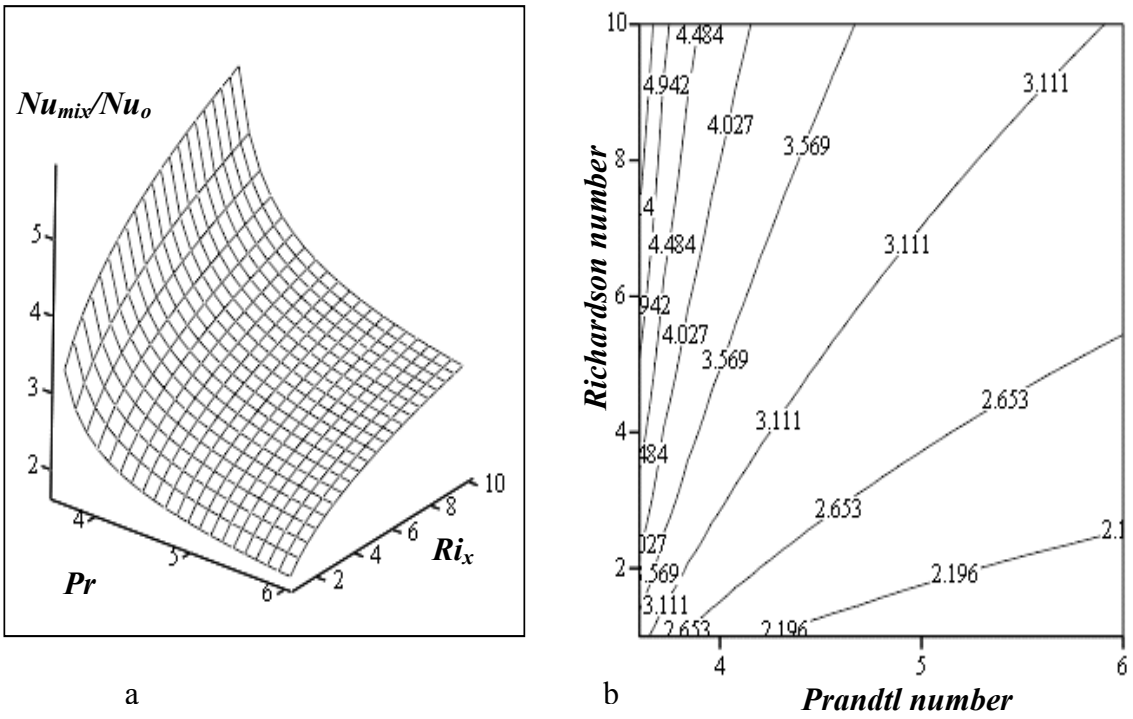

Fig. (4-45): Variation of (Nu_{mix}/Nu_o) with Richardson range of 1 to 10 and inclination angle of 60˚ for Pr = 3.6 to 6, eq. (3.90).

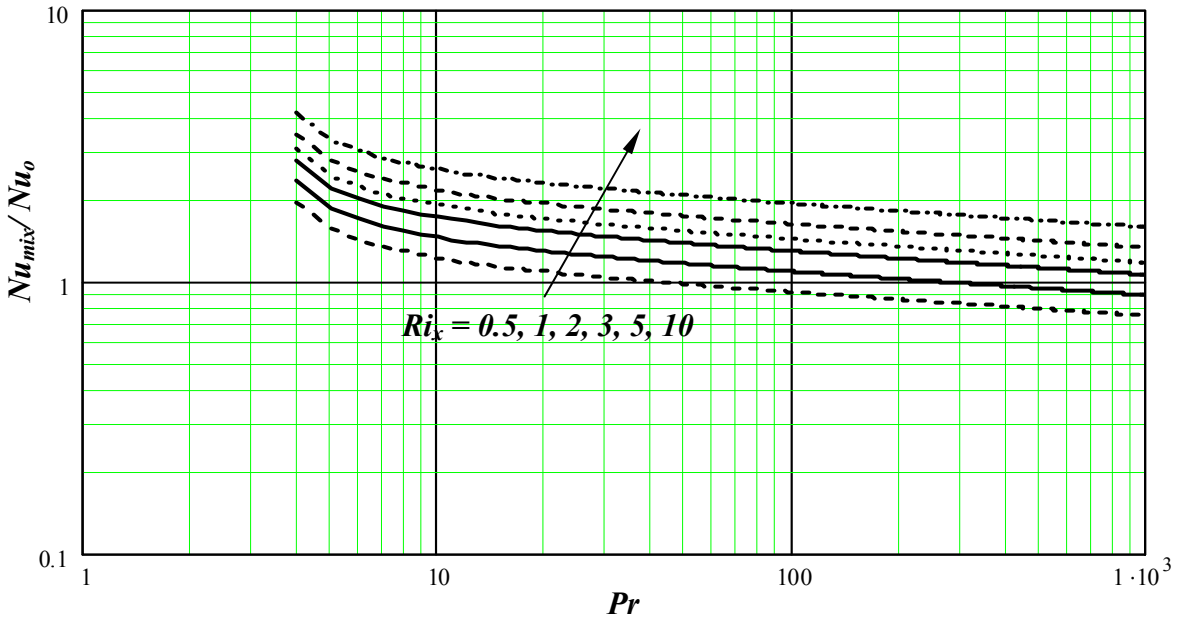

Fig. (4-46): Variation of (Nu_{mix}/Nu_o) with Richardson number of 0.5, 1, 2, 3, 5 and 10 inclination angle of 60˚ for Pr = 3.462 to 1000 eq. (3.90).

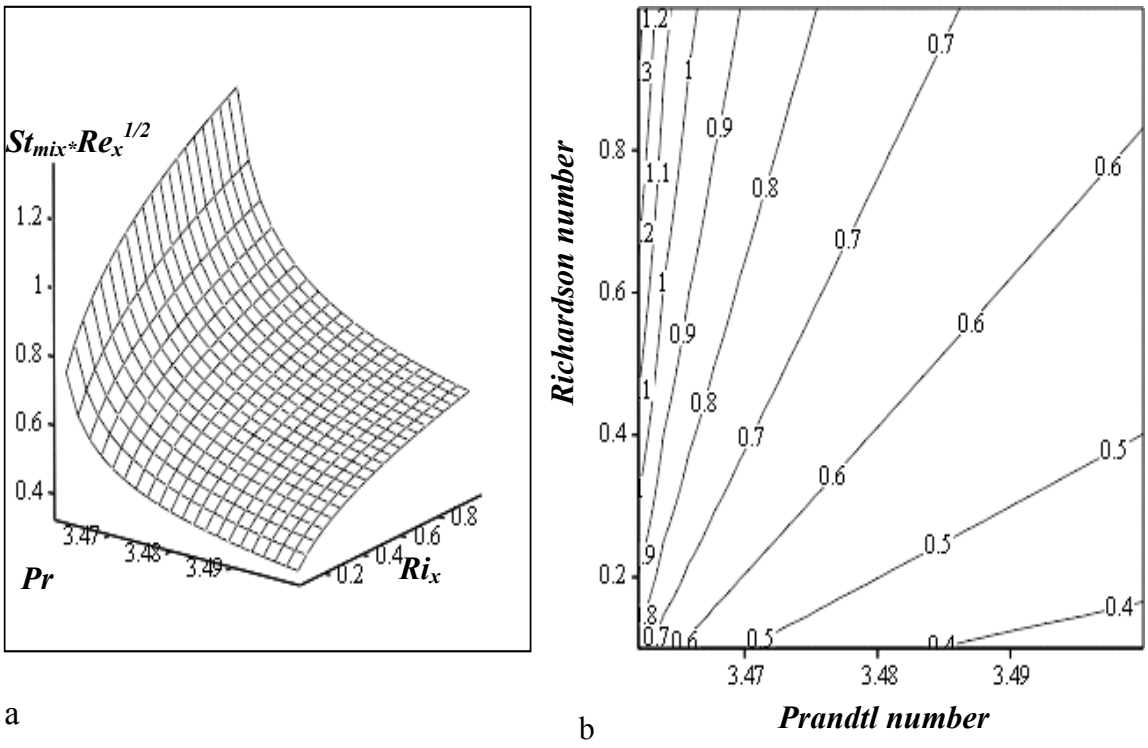

Fig. (4-47): Variation of ($St_{mix}*(Re_x)^{1/2}$) with Richardson number range of 0.1 to 1 and Prandtl number range of 3.462 to 3.5 for Φ = 60˚, eq. (3.92).

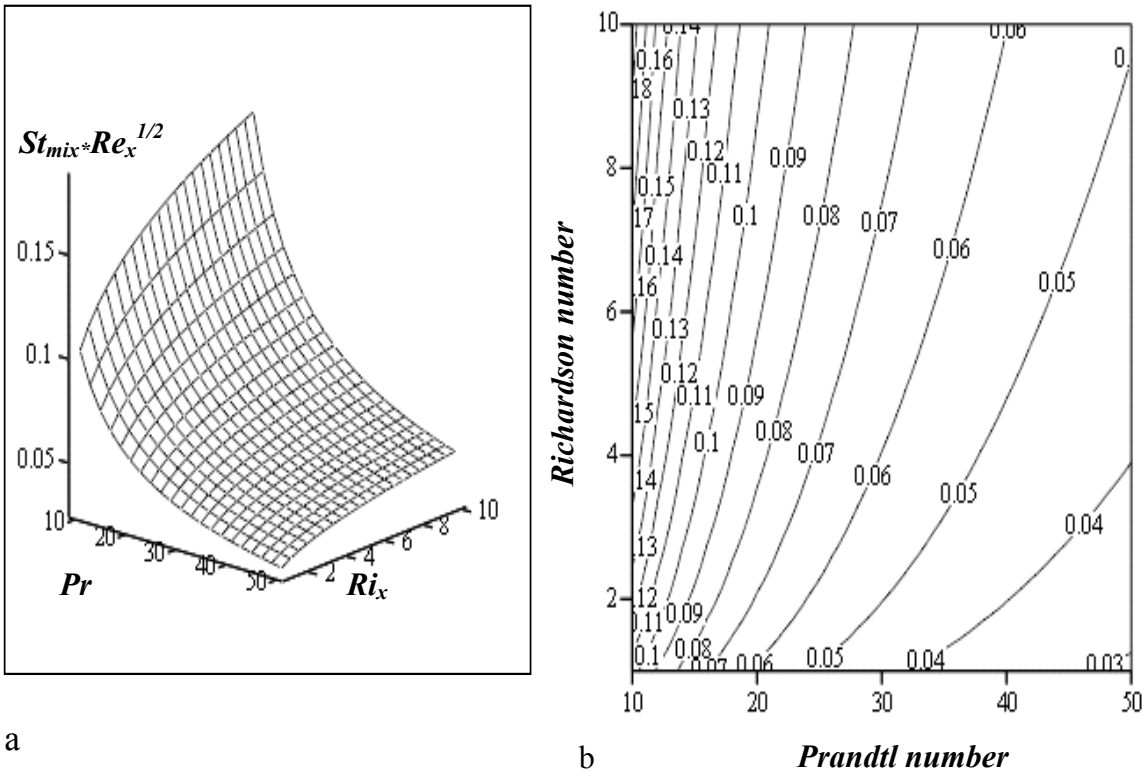

Fig. (4-48): Variation of ($St_{mix}*(Re_x)^{1/2}$) with Richardson number range of 1 to 10 and Prandtl number range of 10 to 50 for Φ = 60˚, eq. (3.92).

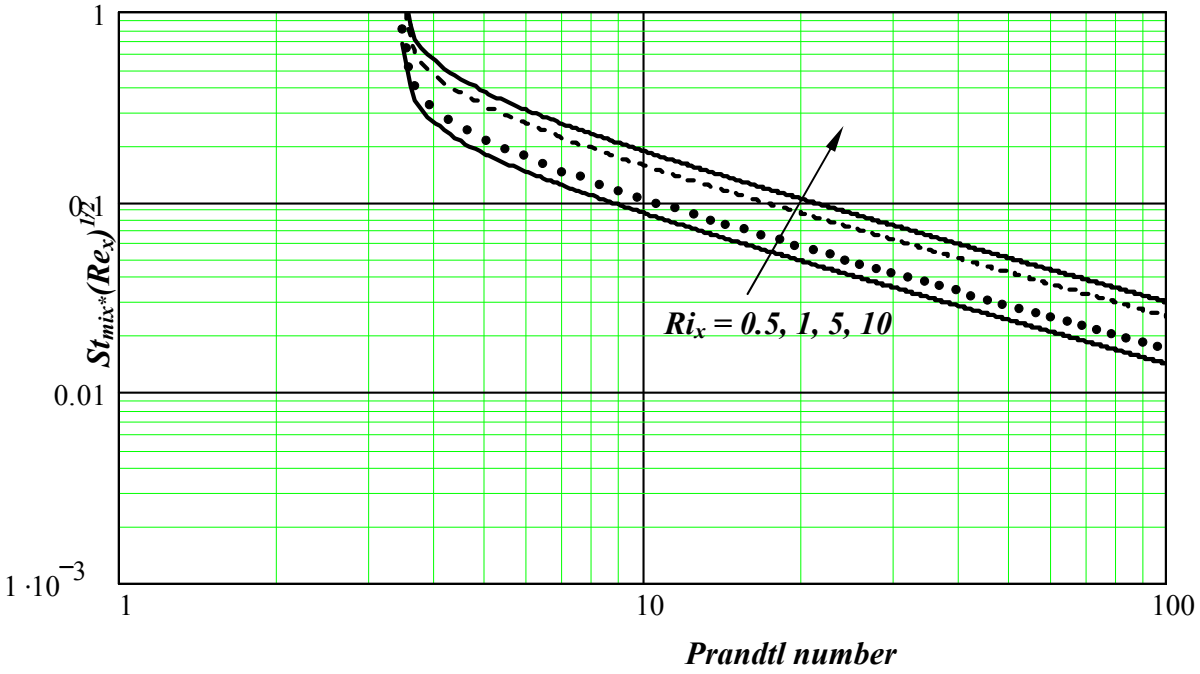

Fig. (4-49): Variation of $(St_{mix^*}(Re_x)^{1/2})$ with Richardson number of 0.5, 1, 5 and 10 and Prandtl number range of 3.462 to 1000 for $\Phi = 60^\circ$, eq. (3.92).

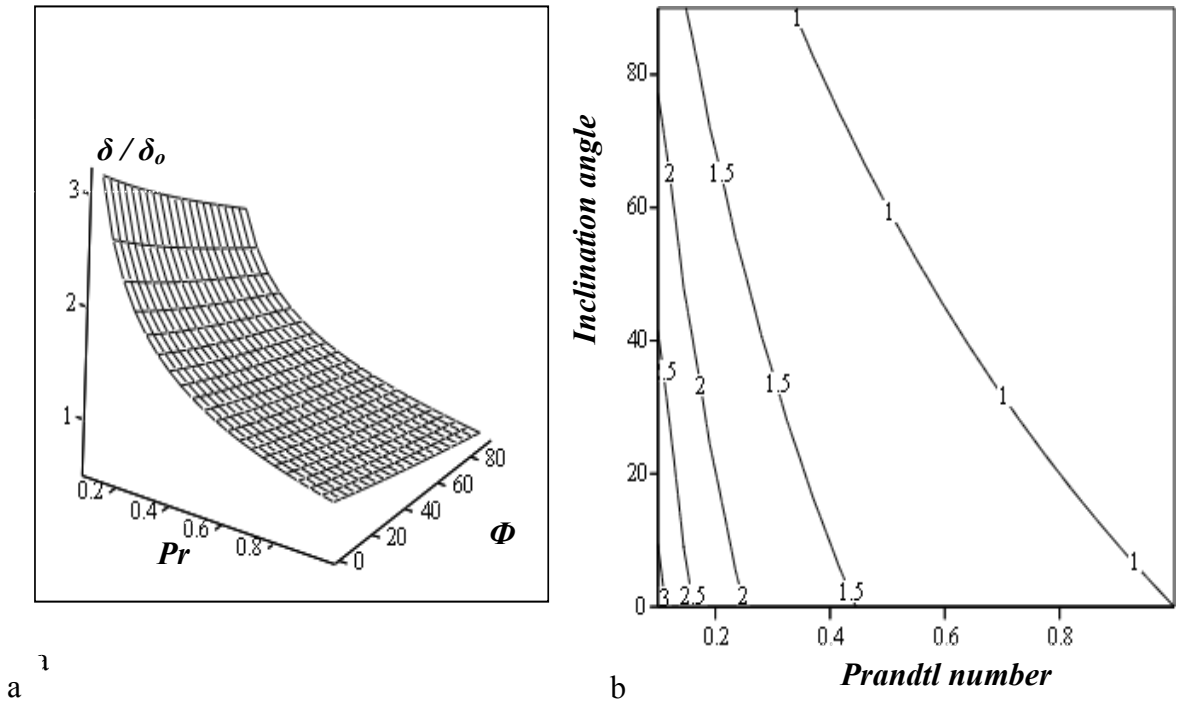

Fig. (4-50): Variation of boundary layer thickness ratio (δ / δ_o) with Prandtl number range of 0.1 to 1 and Inclination angle range of 0° to 90°, by eq. (3.101).

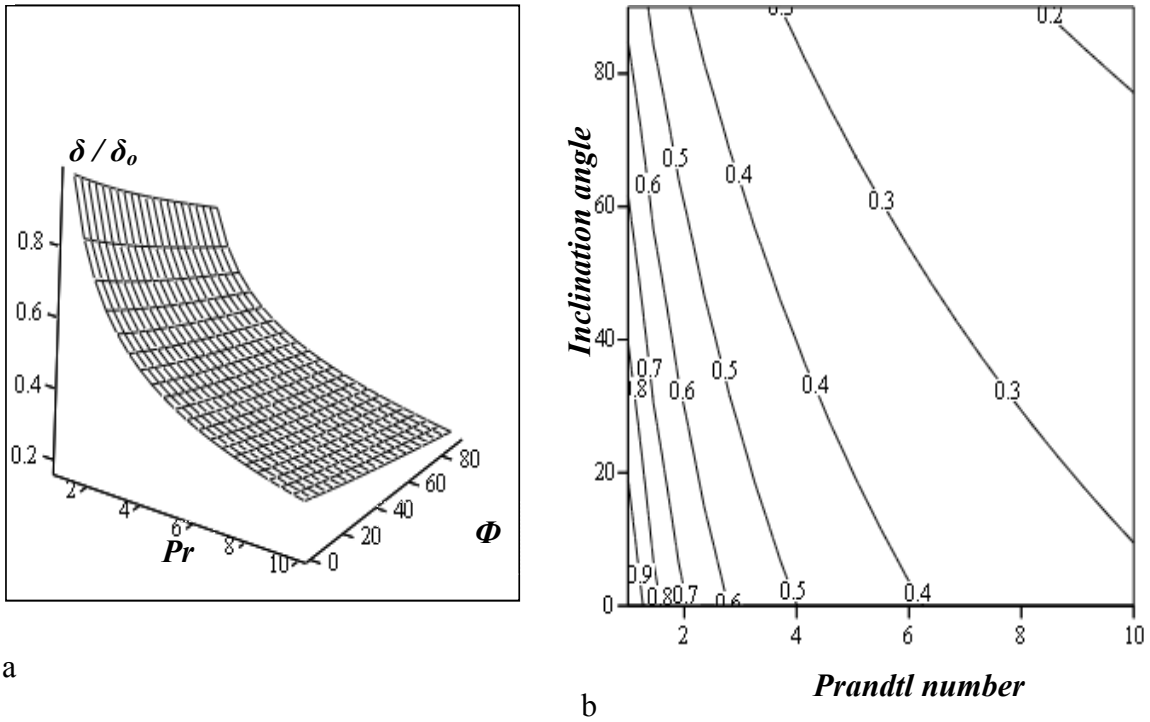

a b

Fig. (4-51): Variation of boundary layer thickness ratio (δ / δ_o) with Prandtl number range of 1 to 10 and Inclination angle range of 0˚ to 90˚, by eq. (3.101).

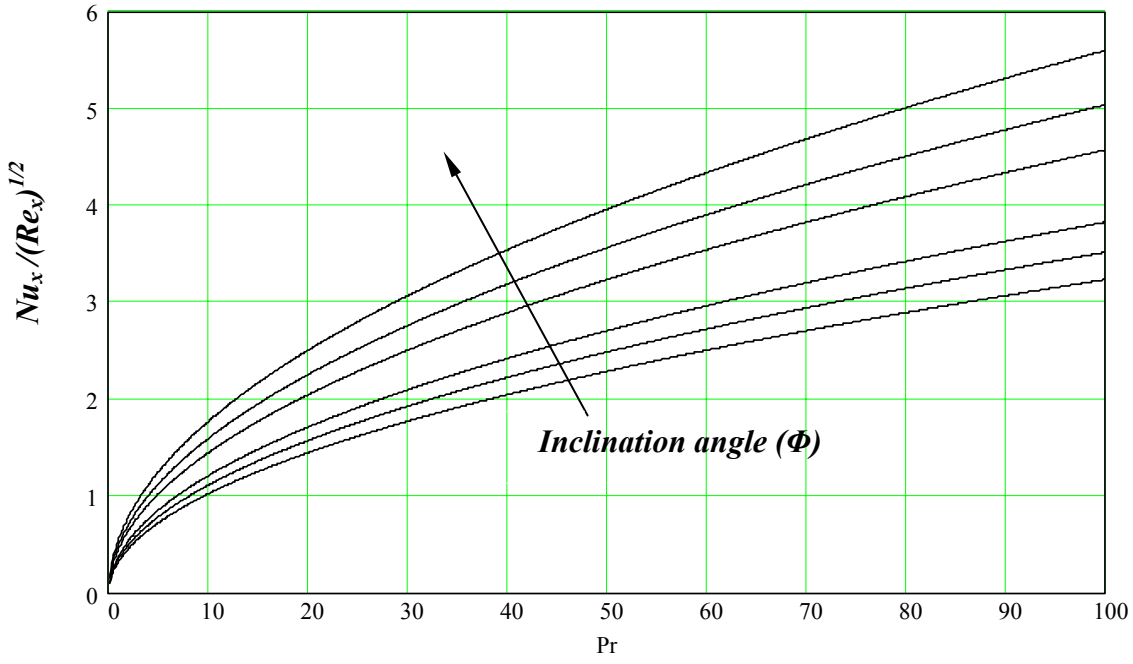

Fig. (4-52): Variation of $(Nu_x/(Re_x)^{1/2})$ with Prandtl number range of 0 to 100 and inclination angle of 0˚, 15˚, 30˚ ,60˚,75˚and 90˚ for $Ri_x = 0$, by eq. (3.102).

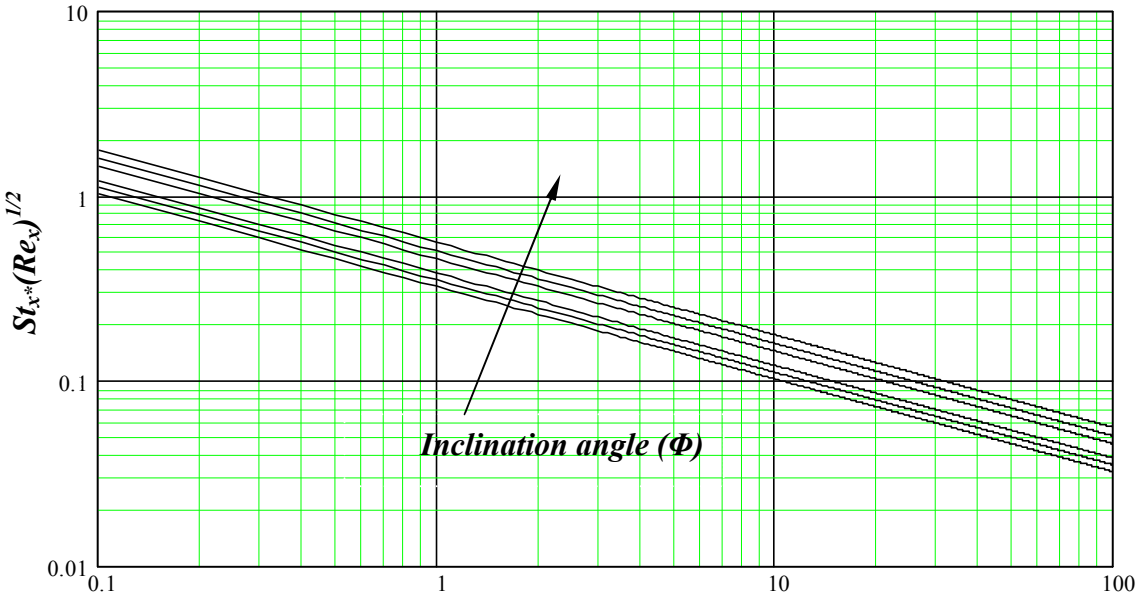

Fig. (4-53): Variation of $(St_{x^*}(Re_x)^{1/2})$ with Prandtl number range of 0 to 100 and inclination angle of 0˚, 15˚, 30˚ ,60˚,75˚and 90˚ for Ri_x = 0, by eq. (3.105).

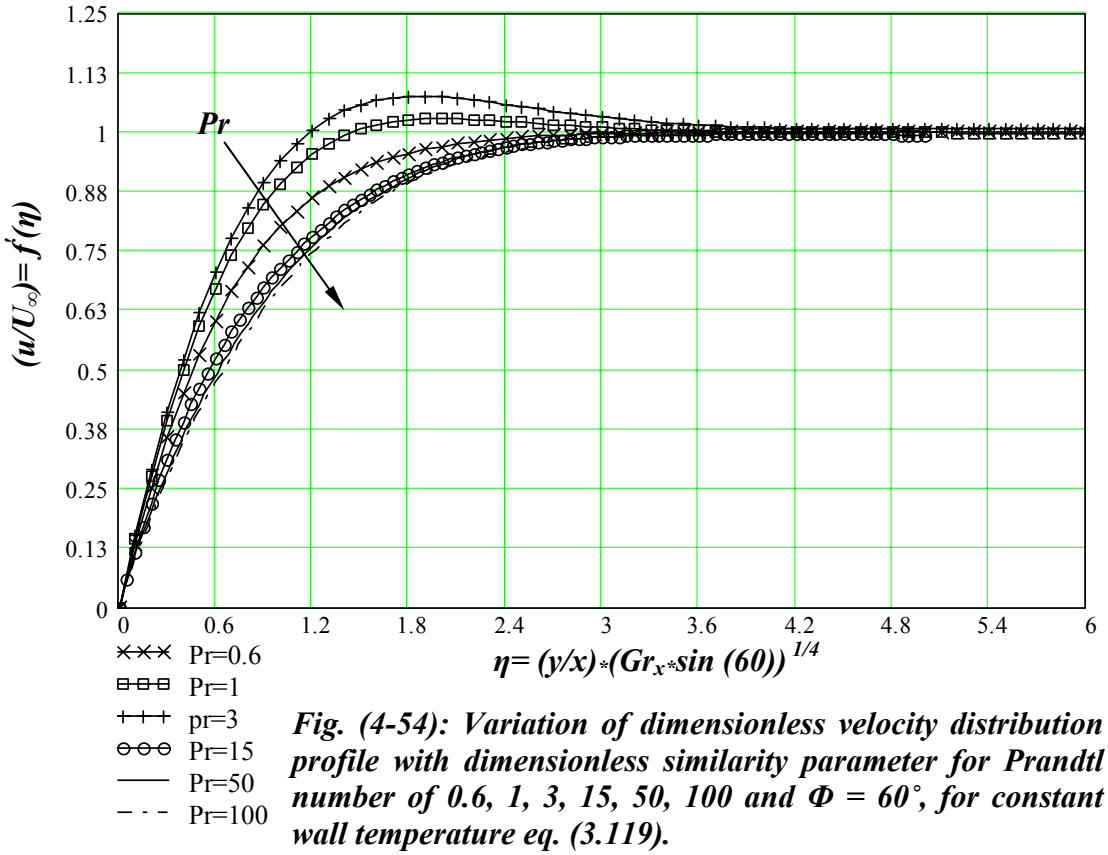

Fig. (4-54): Variation of dimensionless velocity distribution profile with dimensionless similarity parameter for Prandtl number of 0.6, 1, 3, 15, 50, 100 and Φ = 60˚, for constant wall temperature eq. (3.119).

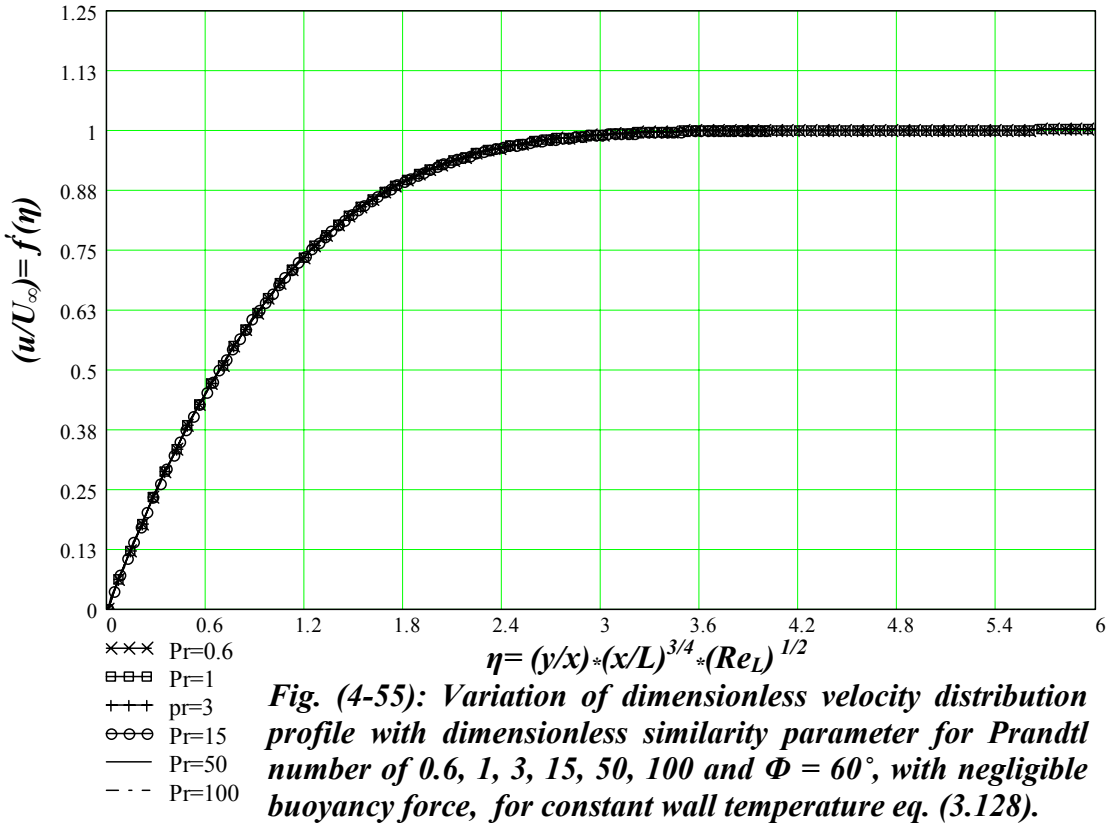

Fig. (4-55): Variation of dimensionless velocity distribution profile with dimensionless similarity parameter for Prandtl number of 0.6, 1, 3, 15, 50, 100 and Φ = 60°, with negligible buoyancy force, for constant wall temperature eq. (3.128).

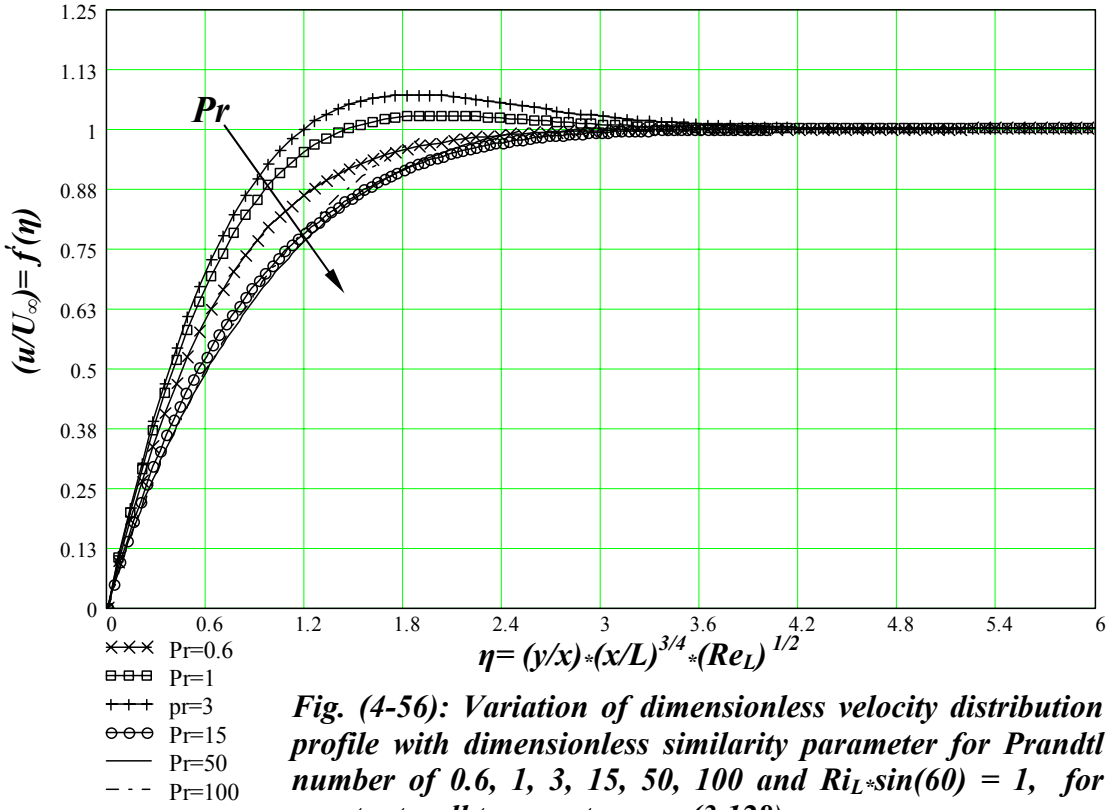

Fig. (4-56): Variation of dimensionless velocity distribution profile with dimensionless similarity parameter for Prandtl number of 0.6, 1, 3, 15, 50, 100 and Ri_L*sin(60) = 1, for constant wall temperature eq. (3.128).

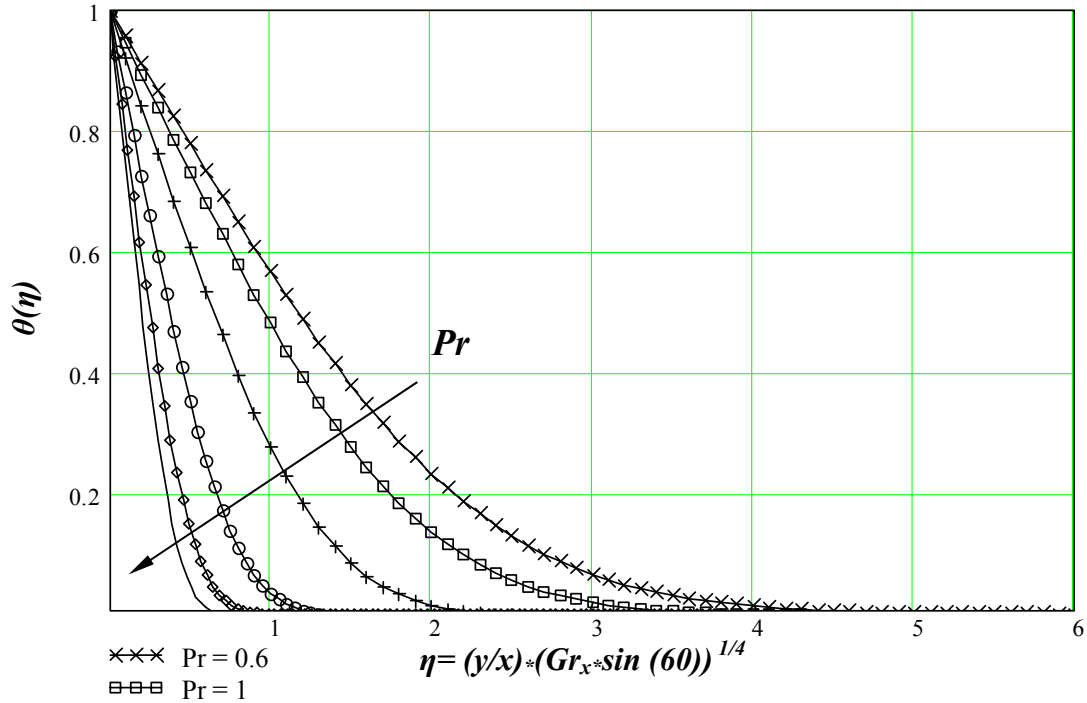

Fig. (4-57): Variation of dimensionless temperature distribution profile with dimensionless similarity parameter for Prandtl number of 0.6, 1, 3, 15, 50, 100 and Φ = 60°, for constant wall temperature eq. (3.120).

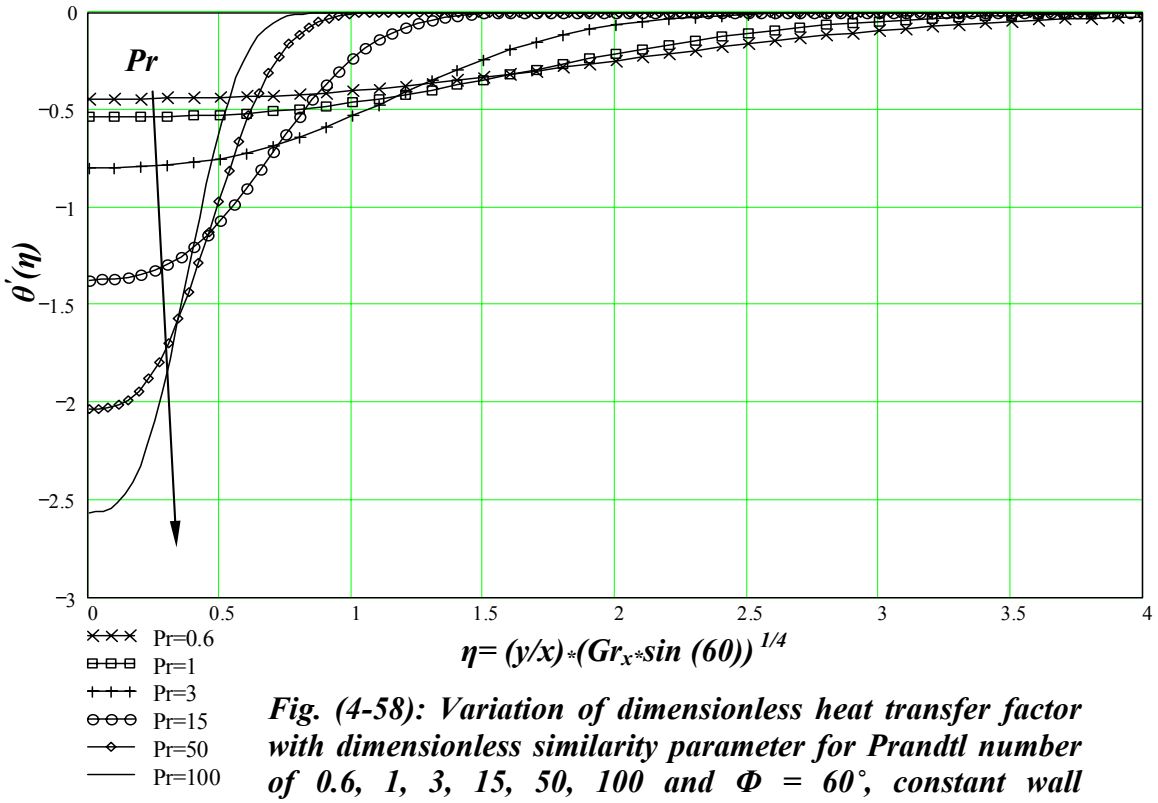

Fig. (4-58): Variation of dimensionless heat transfer factor with dimensionless similarity parameter for Prandtl number of 0.6, 1, 3, 15, 50, 100 and Φ = 60°, constant wall temperature eq. (3.120).

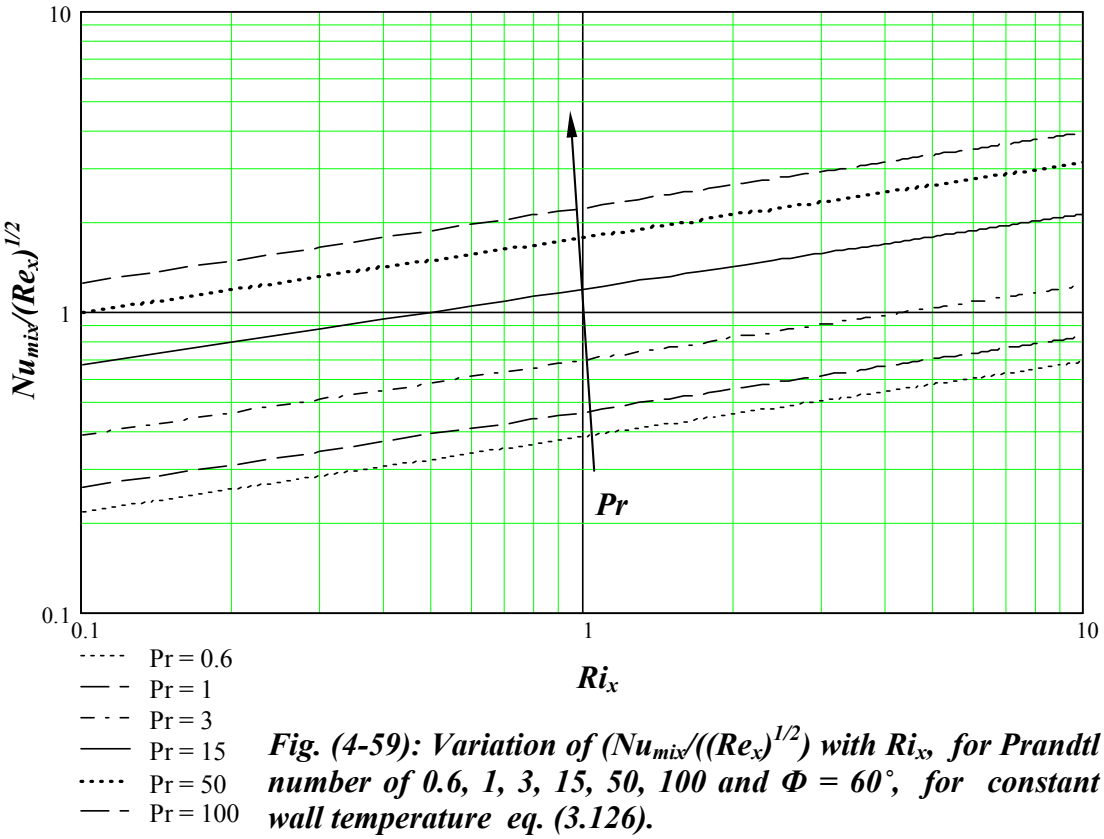

Fig. (4-59): Variation of $(Nu_{mix}/((Re_x)^{1/2})$ with Ri_x, for Prandtl number of 0.6, 1, 3, 15, 50, 100 and $\Phi = 60^{\circ}$, for constant wall temperature eq. (3.126).

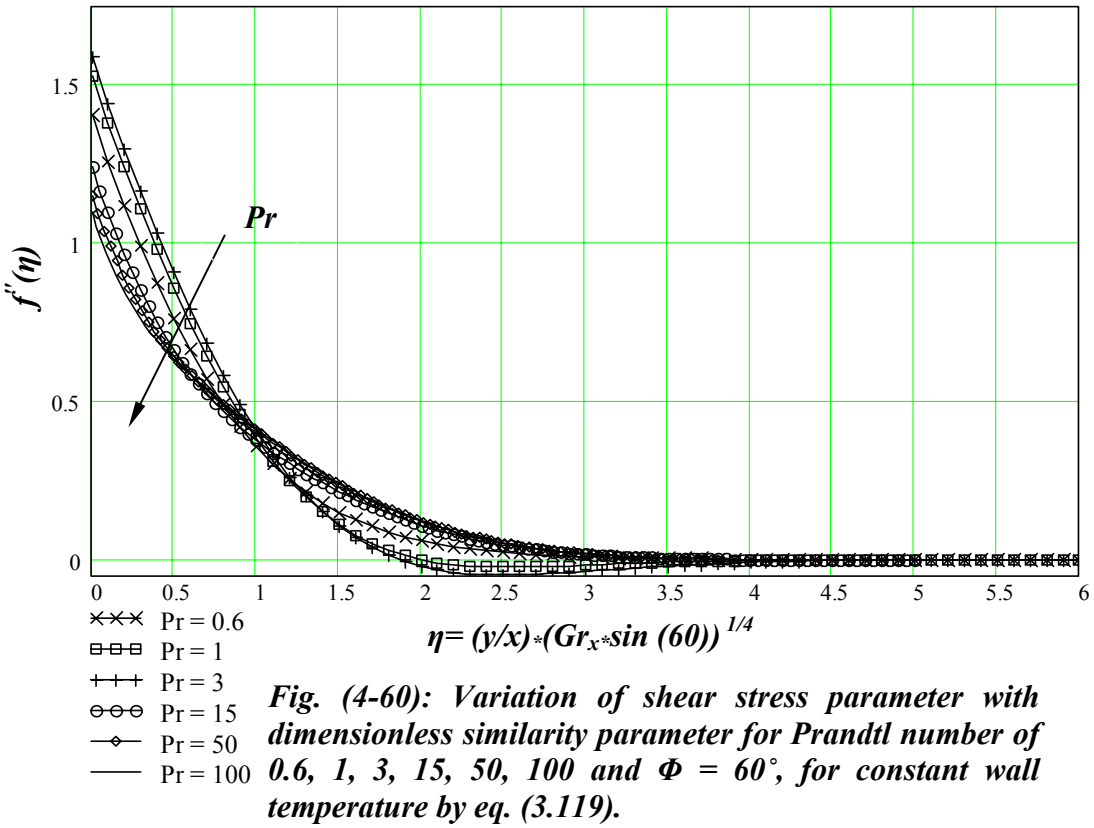

Fig. (4-60): Variation of shear stress parameter with dimensionless similarity parameter for Prandtl number of 0.6, 1, 3, 15, 50, 100 and $\Phi = 60^{\circ}$, for constant wall temperature by eq. (3.119).

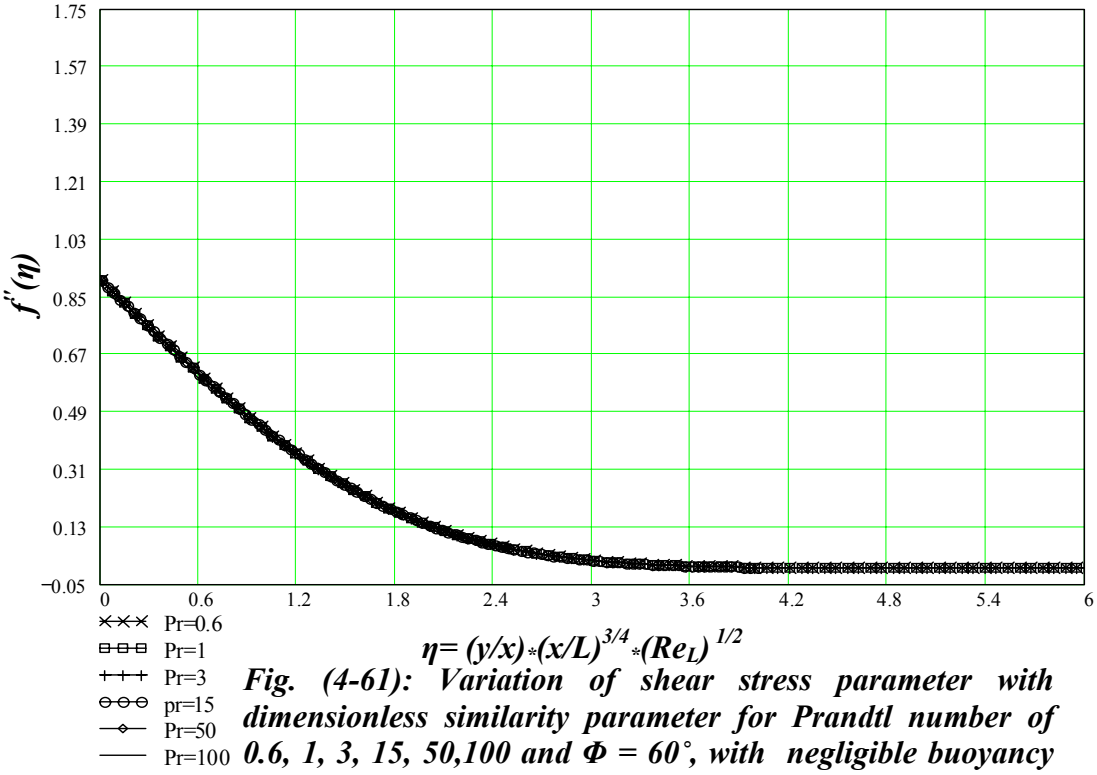

Fig. (4-61): Variation of shear stress parameter with dimensionless similarity parameter for Prandtl number of 0.6, 1, 3, 15, 50,100 and Φ = 60˚, with negligible buoyancy force, for constant wall temperature by eq. (3.128).

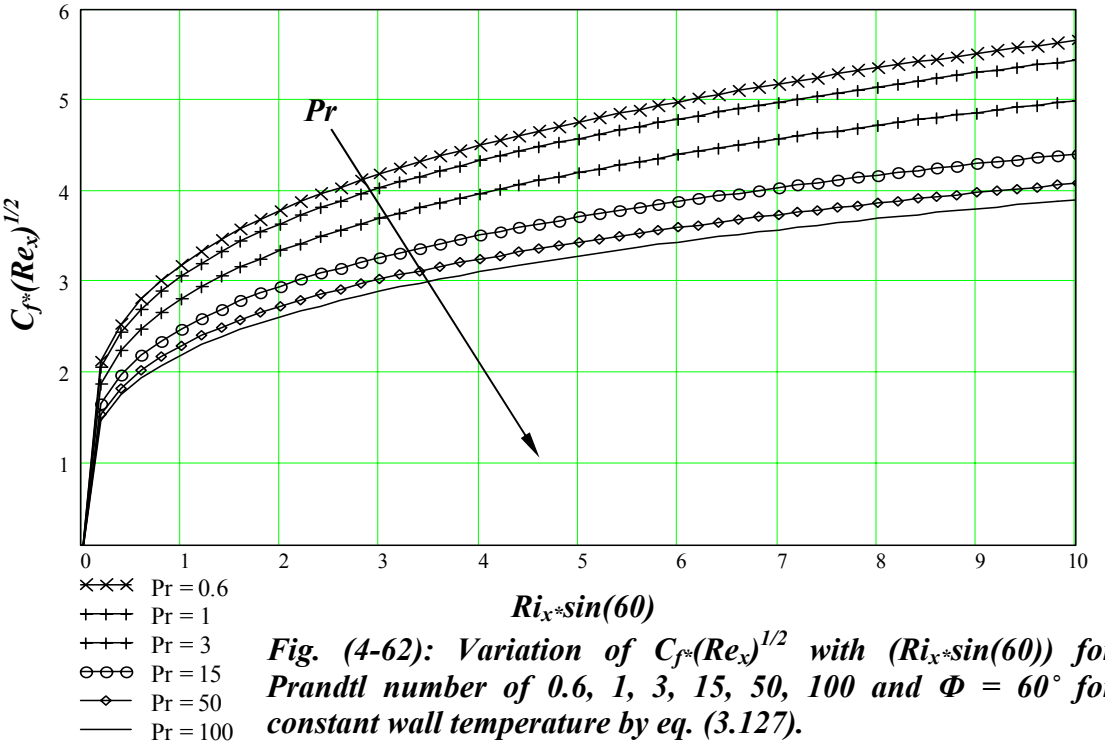

Fig. (4-62): Variation of $C_f*(Re_x)^{1/2}$ with $(Ri_x*\sin(60))$ for Prandtl number of 0.6, 1, 3, 15, 50, 100 and Φ = 60˚ for constant wall temperature by eq. (3.127).

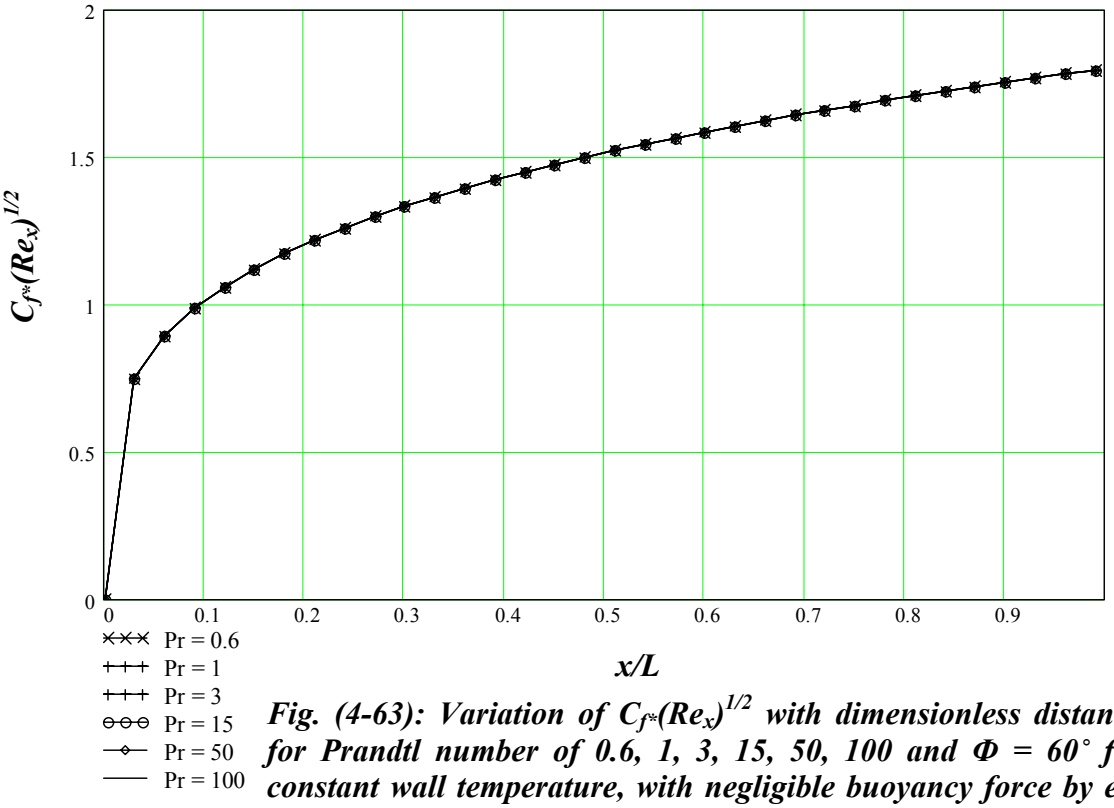

Fig. (4-63): Variation of $C_{f*}(Re_x)^{1/2}$ with dimensionless distance for Prandtl number of 0.6, 1, 3, 15, 50, 100 and Φ = 60° for constant wall temperature, with negligible buoyancy force by eq. (3.130).

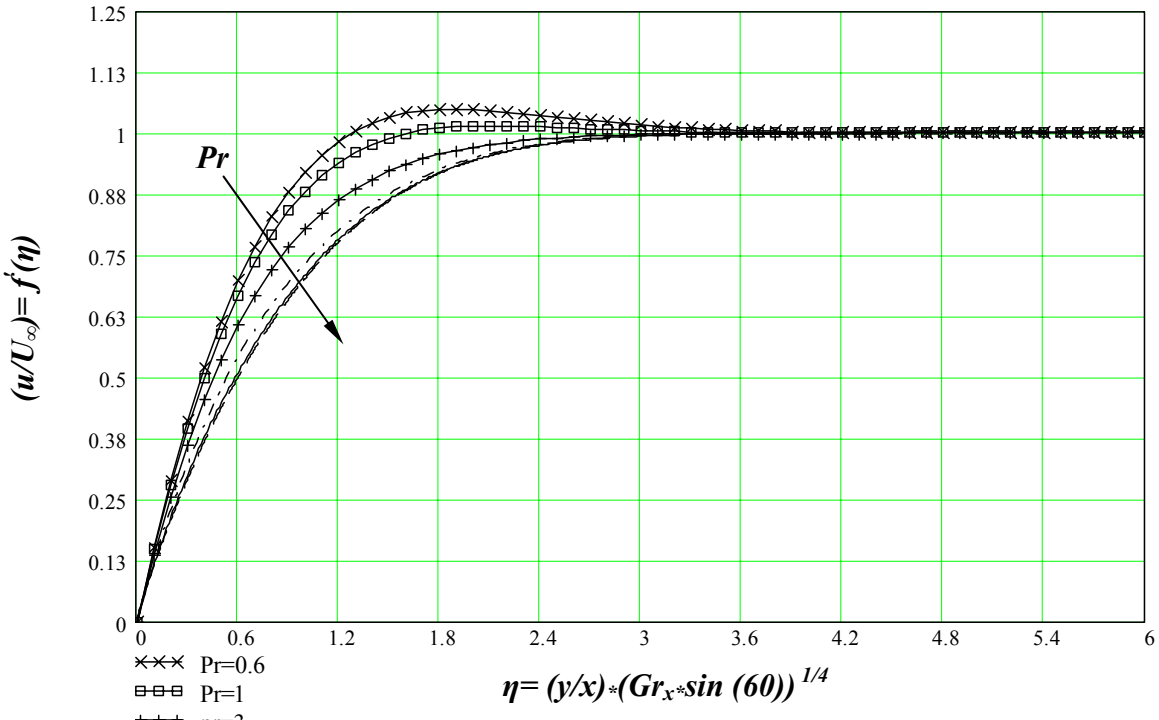

Fig. (4-64): Variation of dimensionless velocity distribution profile with dimensionless similarity parameter for Prandtl number of 0.6, 1, 3, 15, 50, 100 and Φ = 60°, for constant heat flux eq. (3.139).

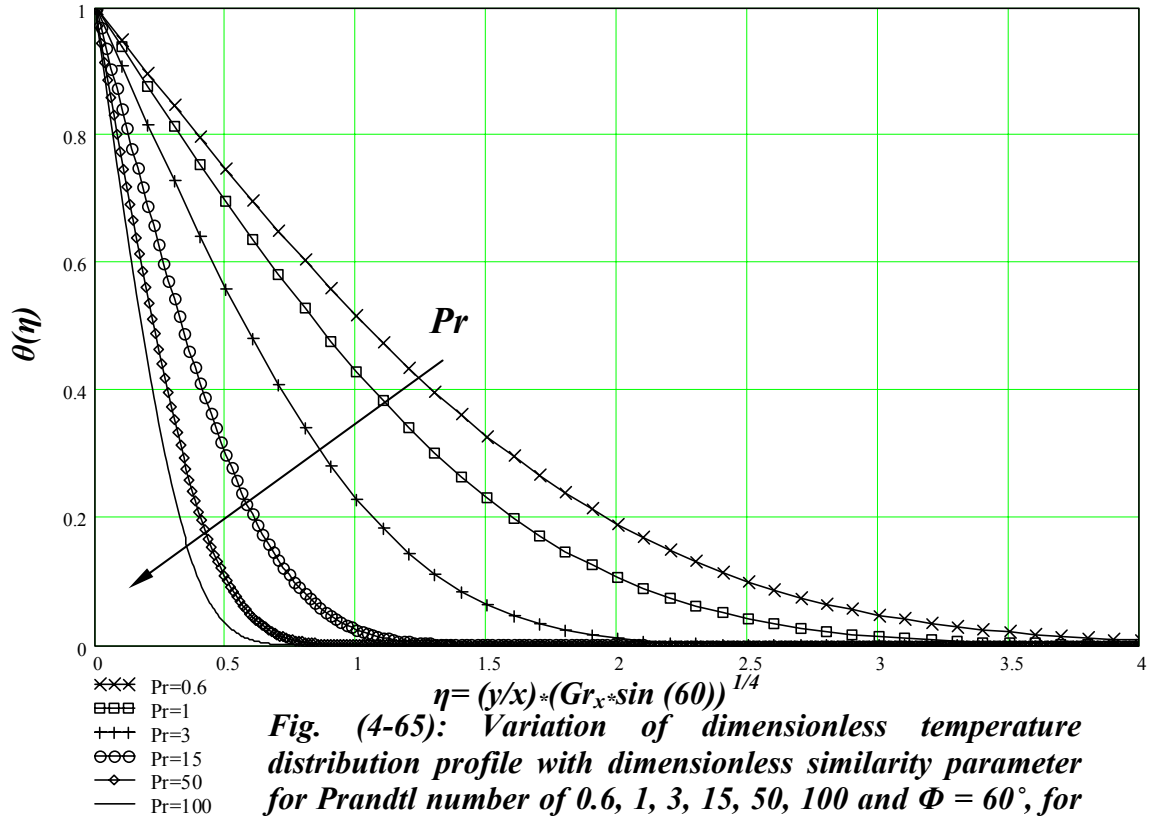

Fig. (4-65): Variation of dimensionless temperature distribution profile with dimensionless similarity parameter for Prandtl number of 0.6, 1, 3, 15, 50, 100 and Φ = 60˚, for constant heat flux eq. (3.140).

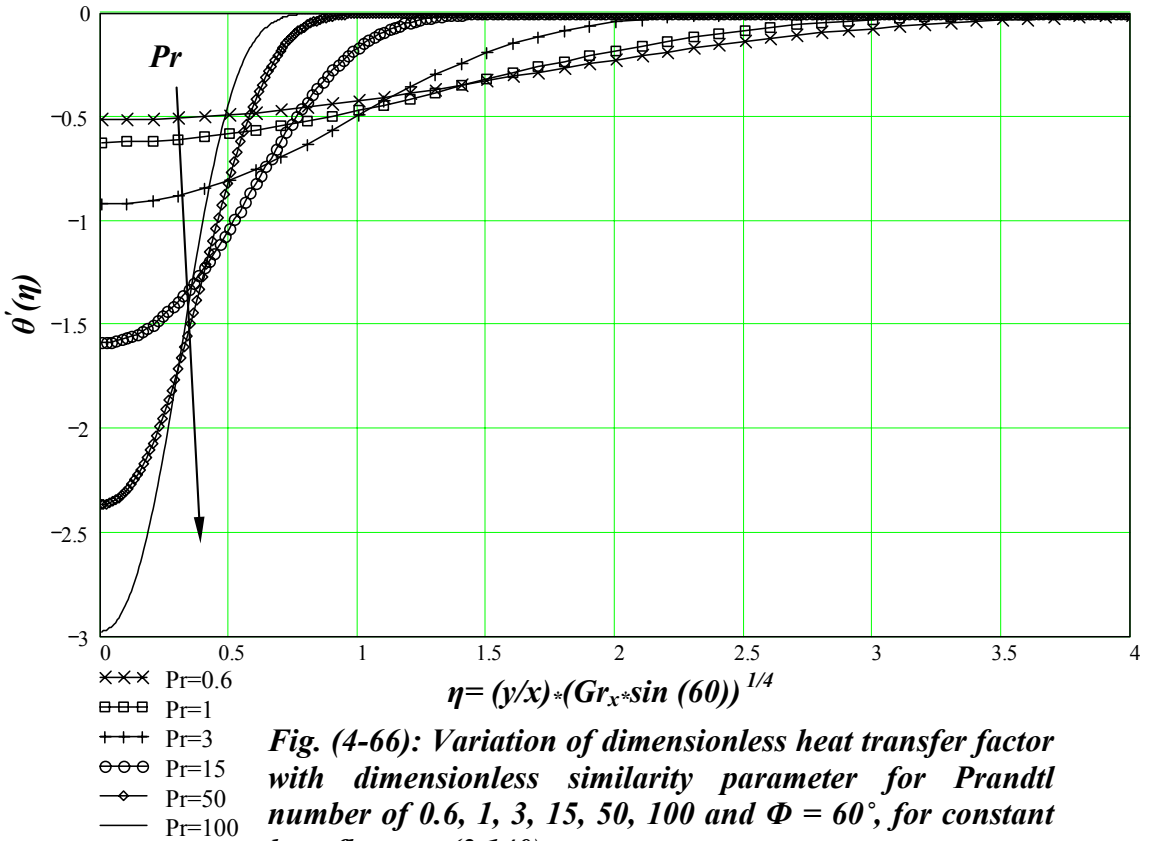

Fig. (4-66): Variation of dimensionless heat transfer factor with dimensionless similarity parameter for Prandtl number of 0.6, 1, 3, 15, 50, 100 and Φ = 60˚, for constant heat flux eq. (3.140).

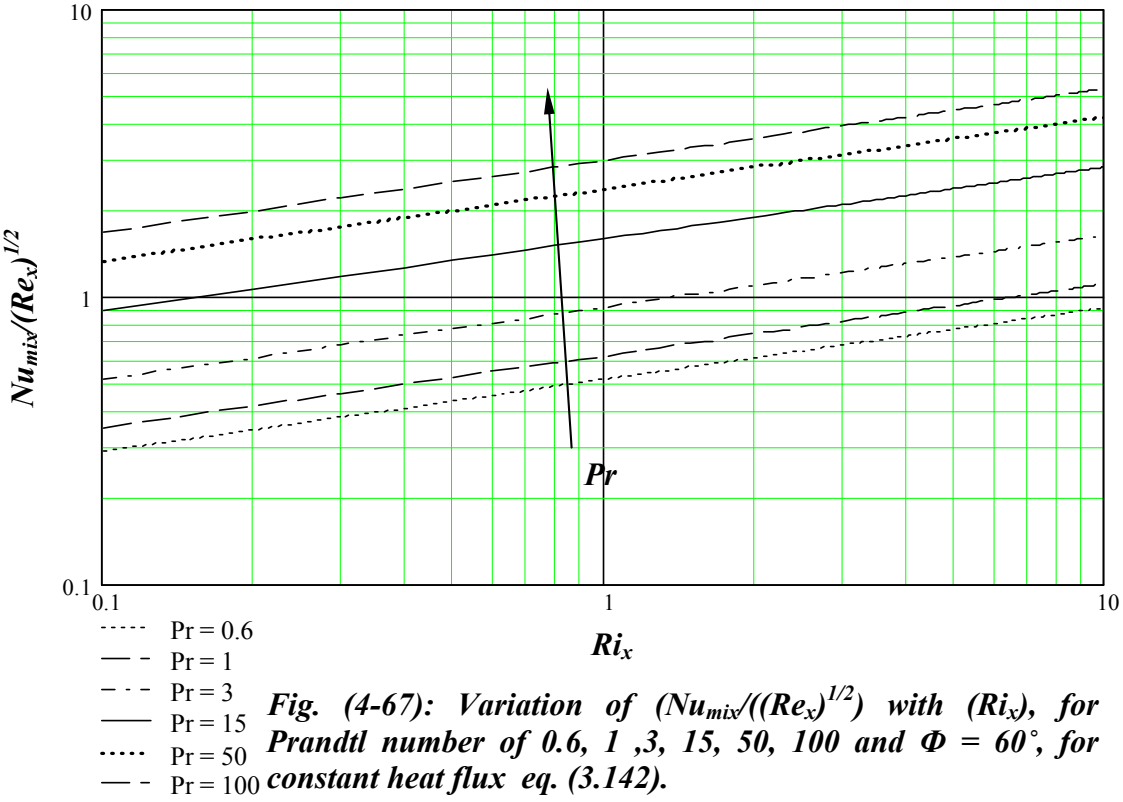

Fig. (4-67): Variation of $(Nu_{mix}/((Re_x)^{1/2})$ with (Ri_x), for Prandtl number of 0.6, 1 ,3, 15, 50, 100 and Φ = 60˚, for constant heat flux eq. (3.142).

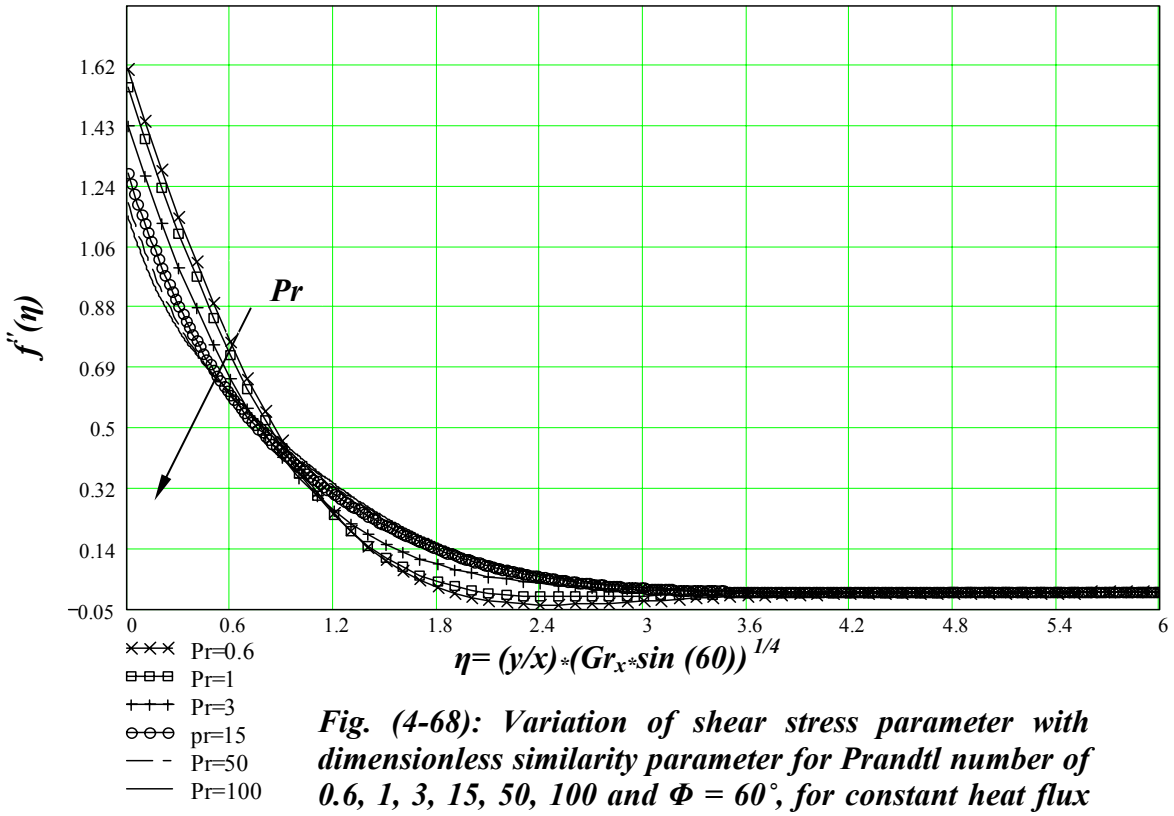

Fig. (4-68): Variation of shear stress parameter with dimensionless similarity parameter for Prandtl number of 0.6, 1, 3, 15, 50, 100 and Φ = 60˚, for constant heat flux by eq. (3.139).

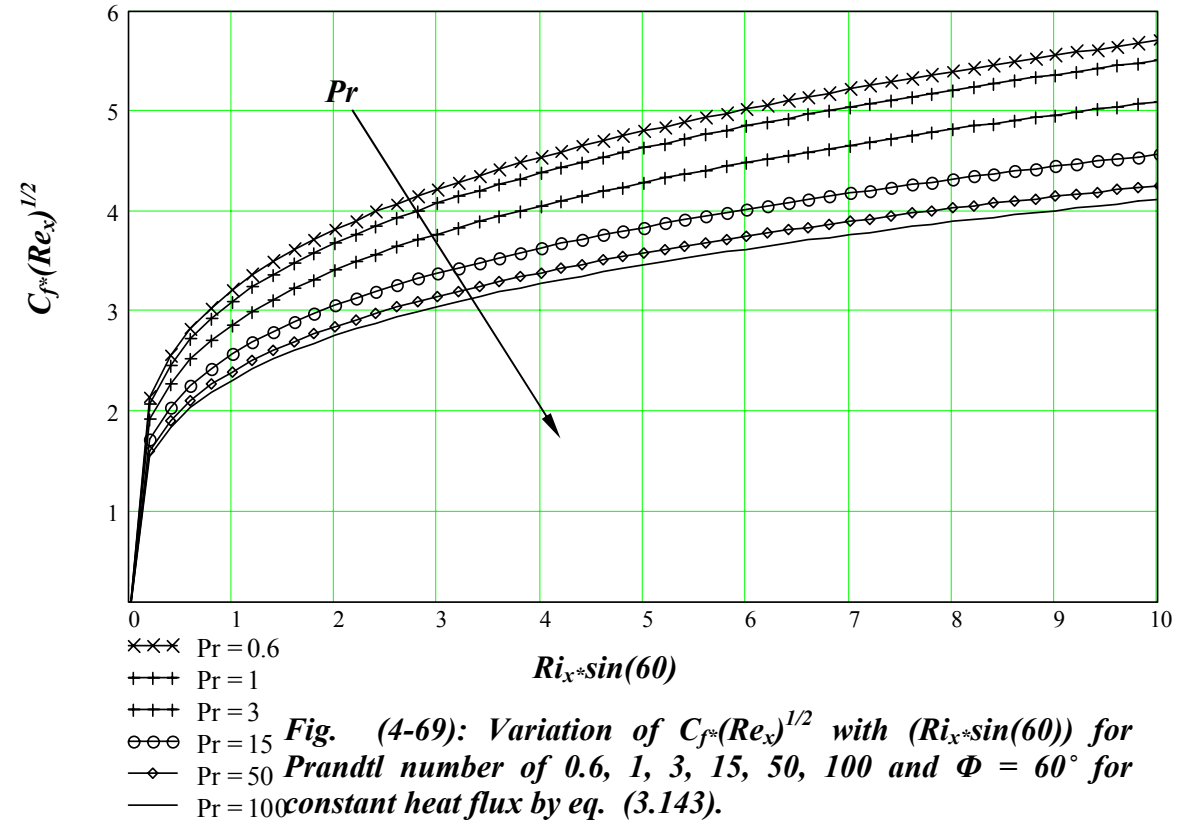

Fig. (4-69): Variation of $C_{f^*}(Re_x)^{1/2}$ with (Ri_x*sin(60)) for Prandtl number of 0.6, 1, 3, 15, 50, 100 and Φ = 60° for constant heat flux by eq. (3.143).

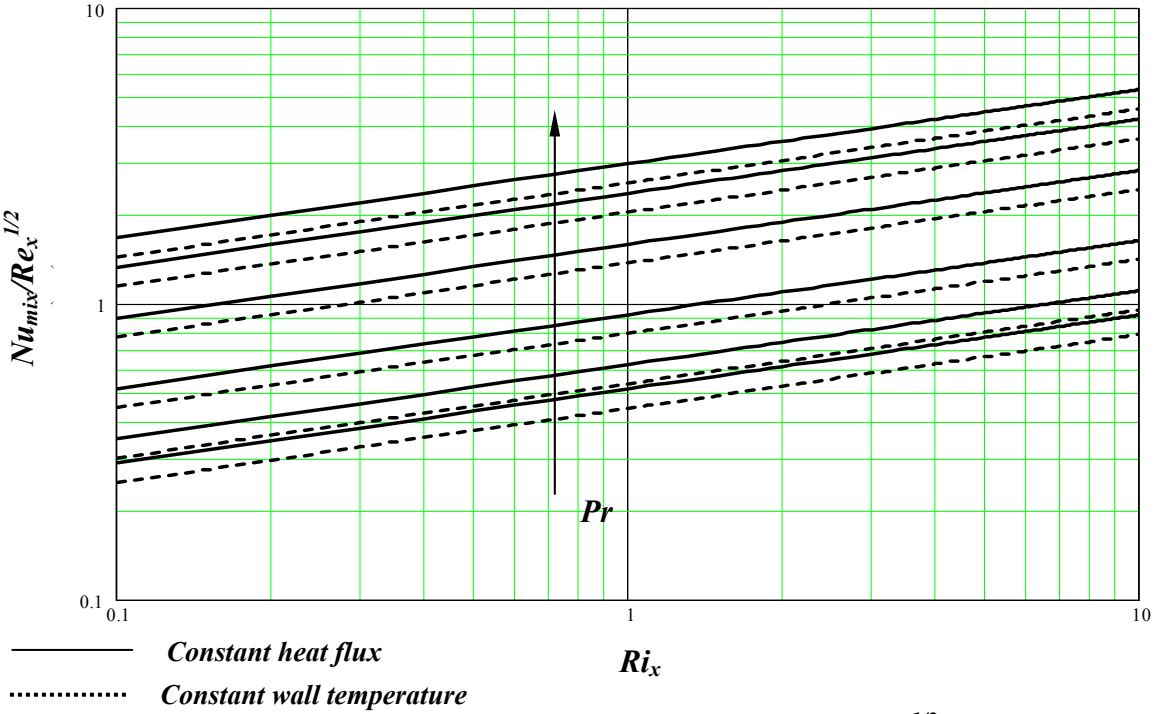

Fig. (4-70): Comparison of the variation of ($Nu_{mix}/(Re_x)^{1/2}$) with (Ri_x), for Prandtl number of 0.6, 1, 3, 15, 50, 100 and Φ = 60°, for constant heat flux and constant wall temperature.

CHAPTER FIVE

CONCLUSIONS AND

RECOMMENDATIONS

5-1 Conclusions:

The present theoretical investigation shows the significant effect of combined free and forced convection on the variation of Nusselt number, temperature profile, velocity profile and shear stresses along heated inclined flat plate. The following observations have been made on the bases of the calculations of the present study.

1. For given Reynolds number and wall temperature the buoyancy effects is negligible at the leading edge of the plate.
2. At low Reynolds number, the Nusselt number increases with surface temperature downstream due to the increases of buoyancy effects.
3. At high Reynolds number, there is no effect for increasing wall temperature on the Nusselt number downstream due to the dominate force convection on the heat transfer process (the buoyancy is very week at this region).
4. For the same Reynolds number and buoyancy force term (Richardson number), Nusselt number increases with the increases of the inclination angle due to the increases of buoyancy force term component.
5. The temperature profile along the plate shows a steep profile near the heated surface with thermal boundary layer thickness decreases with the increases of buoyancy force term component.
6. The velocity profile along the plate shows a steep profile far of the plate with acceleration of growth of hydrodynamic boundary layer thickness with increases of buoyancy force term component.
7. Increases of shear stress due to the increases of coefficient of friction with increases of buoyancy force term component.

5-2 Recommendation for the future works:

According to the extension of this work, the following recommendation are suggested:

1. The inclined flat plate in case of constant heat flux and constant wall temperature can be studied taking into consideration unsteady state cases.
2. Different array of inclined flat plates as is it a group of fins can be studied.
3. Study the thermal flow over inclined flat plate by using suction or magnetic field.
4. Steady and unsteady flow over cooled inclined flat plate (opposing flow) can be studied.

REFERENCES

[1] Kumari, M. and Nath, G., "Development of Mixed Convection Flow over a Vertical Plate due to an Impulsive Motion" Arch Math 49: 977-990, (2001).

[2] Satish Kumar and Masayoshi Shimo, "Numerical Analysis of Mixed Convection over An Isothermal vertical Plate" Int. J. Me 605 Convection of Heat and Mass Transfer, (2003).

[3] Incropera, F.P. and De Witt, "Introduction to Heat Transfer" John Wiley & Sons, New York, NY, (1990).

[4] Schlichting, H., "Boundary-layer theory" McGraw-Hill, Germany, (1979).

[5] Holman, J.P., "Heat Transfer" McGraw-Hill, (1985).

[6] Arpaci, Vedat S. and Larsen, Poul S., "Convection Heat Transfer", (1984).

[7] Powell, h., "Forced convection and free convection equations" http:/www. Process associates. Com/process, (2003).

[8] Ecert, E. R. and Robert, M. "Analysis of Heat and Mass Transfer", (1972).

[9] James G. Kandosen, Hoyt, C. Adel, F. Sarofim and Phillip., "Heat and mass transfer" Mc Graw-Hill companies, Inc-(1999)

[10] Incropera, F.P. and De Witt, "Introduction to Heat Transfer" Mc Graw-Hill, (2002).

[11] Robert W., "Numerical Marching Techniques for Fluid Flow with Heat Transfer" NASA, U.S.A, (1973).

[12] Manning, K.S. and Qureshi Z.H., "Transport Correlations for Laminar Aiding Mixed Convection over a Vertical Isothermal Surface"
J. Heat Transfer, vol. 116/777 (1994).

[13] Schneider, W. and Wasel, M.G., "Breakdown of the Boundary-Layer Approximation for Mixed Convection above Horizontal Plate" Int.J. Heat and Mass Transfer, Vol.28, No.12, pp 2307-2313, (1985).

[14] Tasawwur Hussain and Noor Afzal, "Mixed Convection Boundary Layer Flow on a Horizontal Plate in a Uniform Stream" J. Heat Mass Transfer. Vol. 31, No.12, pp 2505-2516, (1988).

[15] Appukuttan, A. Shyy, W. Sheplok, M. and Cattafesta, L., "Mixed convection induced by MEMS-Based thermal sheer stress sensor" Int.J. Heat transfer, part A,43: 283-305, (2003).

[16] Manca, O. Nardini, S. Khanfer K., "Effect of heated wall position mixed convection in a channel with an open cavity" Int. Numerical heat transfer, part A, 43: 259-282, (2003).

[17] Khalil Khanafer, Kambiz V. and Marilyn L., " Mixed convection heat transfer in two-dimensional open-ended enclosures" International Journal of Heat and Mass Transfer, vol. 45, 5171–5190, (2002).

[18] Chamkha, A.J. Takhar, H.S. Nath, G., "Mixed Convection Flow over a Vertical Plate with Localized Heating, Cooling, Magnetic Field and Injections" Int. Heat Fluid 37:139-146, (2004).

[19] Ali, M. and Al-Yousef F., "Laminar Mixed Convection from continuously moving vertical surface with suction or injection" Int. J. Heat and Mass Transfer vol.33No.4, pp 1432-1181 (1998).

[20] Salim, A. Hossain, M.A. and Rees, D. A. S., "The effect of surface mass transfer on mixed convection flow past a heated vertical flat permeable plate with thermophoresis" Int. J. Thermal Science vol.42 973-982, (2003).

[21] Idiri, M. and Souidi, F., "Higher order term boundary layer effect in an opposed mixed convection problem" Int. J. Science and engineering. Volume 27.number 2c. (2002).

[22] Herbert Steinruck, "mixed convection flow along vertical flat plate" Int. J. Fluid dynamic research , 32. 1-13, (2003).

[23] Ramos, R. Pérez J. S. and Figueira, E., "Mixed convection" Int. J. Num. Meth. fluids chapter II.5, (1997).

[24] Ping Cheng, "Combined Free and Forced Convection Flow about Inclined Surface in Porous Media" Int. J. Heat and Mass Transfer, Vol.20, pp 807-814 (1977).

[25] Rogerio Ramos and Guerrero, "An Integral Transform Application to Mixed Convection in Laminar Flow between Inclined Parallel Plates" Int. International Conference on Computational Heat and Mass Transfer, (2001).

[26] Bahlaoui, A. Raji A. and Hasnaoui, M., "combined mixed convection and radiation in a channel discretely heated from below" Int. J. Heat and Mass Transfer 28: 1857-1854 (1999).

[27] Yang H. Q. and Yang K.T., "mixed convection from heated inclined plate in a channel with application to CVD" Int. J. heat mass transfer. Vol 32. No. 9, pp 1681-1695, (1989).

[28] Kumari, M. Takher H.S. and Nath G., "mixed convection flow over a vertical wedge with magnetic field embedded in porous medium" Int. J. heat mass transfer. Vol 37, pp 139-146,(2001).

APPENDICES

Appendix (A.1): The Program (M) for the similarity solution with 60° Inclination angle and constant wall temperature:

$$g := \begin{pmatrix} 1.528723 \\ -0.537936 \end{pmatrix} \qquad Pr := 1$$

$x1 := 0 \quad x2 := 7$ Interval endpoints.

$$Dh(x,H) := \begin{bmatrix} H_1 \\ H_2 \\ \frac{-3}{4}\cdot H_0 \cdot H_2 - \frac{1}{2}\cdot\left[1 - (H_1)^2\right] - H_3 \\ H_4 \\ \frac{-3}{4}\cdot H_0 \cdot H_4 \cdot Pr \end{bmatrix}$$ Derivative function.

$$load2(x,V) := \begin{pmatrix} 0 \\ 0 \\ V_0 \\ 1 \\ V_1 \end{pmatrix}$$

$$score2(x,V) := \begin{pmatrix} V_1 - 1 \\ V_3 - 0 \end{pmatrix}$$

$ic2 := sbval(g, x1, x2, Dh, load2, score2)$

$$ic2 = \begin{pmatrix} 1.528724 \\ -0.537936 \end{pmatrix}$$

$$IC := \begin{pmatrix} 0 \\ 0 \\ ic2_0 \\ 1 \\ ic2_1 \end{pmatrix}$$

N := 30

S := rkfixed(IC , x1 , 10 , N , Dh)

$\eta := S^{\langle 0 \rangle}$ f := $S^{\langle 1 \rangle}$ f' := $S^{\langle 2 \rangle}$ f'' := $S^{\langle 3 \rangle}$ $\theta := S^{\langle 4 \rangle}$ $\theta' := S^{\langle 5 \rangle}$

S =

	0	1	2	3	4	5
0	0	0	0	1.528724	1	-0.537936
1	0.333333	0.076047	0.429817	1.062235	0.821005	-0.534457
2	0.666667	0.27083	0.716924	0.67537	0.645795	-0.512826
3	1	0.541492	0.890281	0.380997	0.482244	-0.463893
4	1.333333	0.855332	0.981209	0.179848	0.339396	-0.389837
5	1.666667	1.189882	1.019092	0.059874	0.223921	-0.301985
6	2	1.531611	1.027717	0.000529	0.137989	-0.214929
7	2.333333	1.873714	1.023534	-0.020572	0.079236	-0.140439
8	2.666667	2.213676	1.016035	-0.022083	0.042338	-0.084286
9	3	2.551223	1.009505	-0.016404	0.02104	-0.046504
10	3.333333	2.886937	1.005116	-0.01001	0.009733	-0.023613
11	3.666667	3.221516	1.00262	-0.005275	0.004206	-0.011048
12	4	3.555489	1.001383	-0.002435	0.001716	-0.00477
13	4.333333	3.889179	1.000849	-0.000966	0.000682	-0.001905
14	4.666667	4.222757	1.000657	-0.000292	0.000284	-0.000705
15	5	4.556299	1.000615	-0.000013	0.000143	-0.000243
16	5.333333	4.889839	1.000633	0.000094	0.000096	-0.000079
17	5.666667	5.223389	1.000672	0.000133	0.000081	-0.000024
18	6	5.556954	1.000719	0.000147	0.000077	-0.000007
19	6.333333	5.890536	1.000769	0.000154	0.000076	-0.000002
20	6.666667	6.224134	1.000821	0.000158	0.000076	-0.000001
21	7	6.55775	1.000874	0.000161	0.000076	-0
22	7.333333	6.891384	1.000929	0.000164	0.000076	-0
23	7.666667	7.225036	1.000984	0.000166	0.000075	-0
24	8	7.558706	1.001039	0.000169	0.000075	-0
25	8.333333	7.892395	1.001096	0.000171	0.000075	-0
26	8.666667	8.226104	1.001154	0.000174	0.000075	-0
27	9	8.559831	1.001212	0.000176	0.000075	-0
28	9.333333	8.893578	1.001271	0.000178	0.000075	-0
29	9.666667	9.227345	1.001331	0.000181	0.000075	-0
30	10	9.561132	1.001391	0.000183	0.000075	-0

Appendix (A.2): The Program (N) for the similarity solution with 60° Inclination angle and constant wall temperature:

$$g := \begin{pmatrix} 0.899717 \\ -0.477575 \end{pmatrix} \qquad Pr := 1 \qquad Ris := 0$$

$x1 := 0 \quad x2 := 7$ Interval endpoints. Ris =Ri.sin(ϕ)

$$Dh(x,H) := \begin{bmatrix} H_1 \\ H_2 \\ \frac{-3}{4}\cdot H_0\cdot H_2 - \frac{1}{2}\cdot\left[1-(H_1)^2\right] - Ris\cdot H_3 \\ H_4 \\ \frac{-3}{4}\cdot H_0\cdot H_4\cdot Pr \end{bmatrix}$$ Derivative function.

$$load2(x,V) := \begin{pmatrix} 0 \\ 0 \\ V_0 \\ 1 \\ V_1 \end{pmatrix}$$

$$score2(x,V) := \begin{pmatrix} V_1 - 1 \\ V_3 - 0 \end{pmatrix}$$

$ic2 := sbval(g, x1, x2, Dh, load2, score2)$

$$ic2 = \begin{pmatrix} 0.899717 \\ -0.477572 \end{pmatrix}$$

$$IC := \begin{pmatrix} 0 \\ 0 \\ ic2_0 \\ 1 \\ ic2_1 \end{pmatrix}$$

$N := 30$

$S := rkfixed(IC, x1, 10, N, Dh)$

$\eta := S^{\langle 0 \rangle}$ $f := S^{\langle 1 \rangle}$ $f' := S^{\langle 2 \rangle}$ $f'' := S^{\langle 3 \rangle}$ $\theta := S^{\langle 4 \rangle}$ $\theta' := S^{\langle 5 \rangle}$

$S =$

	0	1	2	3	4	5
0	0	0	0	0.899717	1	-0.477572
1	0.333333	0.046933	0.272223	0.734309	0.840975	-0.475681
2	0.666667	0.175518	0.490344	0.576337	0.684067	-0.463346
3	1	0.368268	0.658026	0.432774	0.53407	-0.433411
4	1.333333	0.609284	0.781065	0.309298	0.397343	-0.383895
5	1.666667	0.884877	0.866807	0.209362	0.279916	-0.31869
6	2	1.183949	0.92329	0.133639	0.185713	-0.246172
7	2.333333	1.498065	0.958322	0.080148	0.115534	-0.176104
8	2.666667	1.821244	0.97871	0.045033	0.067169	-0.116331
9	3	2.149542	0.989817	0.023658	0.036404	-0.070848
10	3.333333	2.480543	0.99547	0.01161	0.018365	-0.039752
11	3.666667	2.812878	0.998157	0.005326	0.00862	-0.020548
12	4	3.145828	0.999353	0.002295	0.003769	-0.009791
13	4.333333	3.479044	0.999854	0.000942	0.001544	-0.004305
14	4.666667	3.812369	1.000057	0.000383	0.000602	-0.00175
15	5	4.145738	1.000142	0.000169	0.000234	-0.000659
16	5.333333	4.479126	1.000182	0.000093	0.0001	-0.000231
17	5.666667	4.812525	1.000208	0.000069	0.000055	-0.000076
18	6	5.145931	1.00023	0.000062	0.000041	-0.000023
19	6.333333	5.479345	1.00025	0.000061	0.000037	-0.000007
20	6.666667	5.812765	1.00027	0.000061	0.000036	-0.000002
21	7	6.146192	1.000291	0.000062	0.000036	-0.000001
22	7.333333	6.479625	1.000312	0.000064	0.000036	-0
23	7.666667	6.813066	1.000333	0.000065	0.000036	-0
24	8	7.146514	1.000355	0.000066	0.000036	-0
25	8.333333	7.47997	1.000377	0.000067	0.000036	-0
26	8.666667	7.813433	1.0004	0.000068	0.000036	-0
27	9	8.146903	1.000422	0.000069	0.000036	-0
28	9.333333	8.480381	1.000445	0.00007	0.000036	-0
29	9.666667	8.813866	1.000469	0.00007	0.000036	-0
30	10	9.14736	1.000492	0.000071	0.000036	-0

Appendix (A.3): The Program (L) for the similarity solution with 60° Inclination angle and Heat flux:

$$g := \begin{pmatrix} 1.548008 \\ -0.6231234 \end{pmatrix} \qquad Pr := 1$$

$x1 := 0 \quad x2 := 6$ Interval endpoints.

$$Dh(x,H) := \begin{bmatrix} H_1 \\ H_2 \\ \frac{-4}{5}\cdot H_0\cdot H_2 + \frac{-3}{5}\cdot\left[1-(H_1)^2\right] - H_3 \\ H_4 \\ -\left[\left(\frac{4}{5}\cdot H_0\cdot H_4\right) + \frac{-1}{5}\cdot H_1\cdot H_3\right]\cdot Pr \end{bmatrix}$$ Derivative function.

$$load2(x,V) := \begin{pmatrix} 0 \\ 0 \\ V_0 \\ 1 \\ V_1 \end{pmatrix}$$

$$score2(x,V) := \begin{pmatrix} V_1 - 1 \\ V_3 - 0 \end{pmatrix}$$

$ic2 := sbval(g, x1, x2, Dh, load2, score2)$

$$ic2 = \begin{pmatrix} 1.548008 \\ -0.623123 \end{pmatrix}$$

$$IC := \begin{pmatrix} 0 \\ 0 \\ ic2_0 \\ 1 \\ ic2_1 \end{pmatrix}$$

N := 30

S := rkfixed(IC , x1 , 10 , N , Dh)

$\eta := S^{\langle 0 \rangle}$ f := $S^{\langle 1 \rangle}$ f' := $S^{\langle 2 \rangle}$ f'' := $S^{\langle 3 \rangle}$ $\theta := S^{\langle 4 \rangle}$ $\theta' := S^{\langle 5 \rangle}$

S =

	0	1	2	3	4	5
0	0	0	0	1.548008	1	-0.623123
1	0.333333	0.076568	0.431375	1.054648	0.794249	-0.605629
2	0.666667	0.27118	0.713635	0.656554	0.600178	-0.553341
3	1	0.539701	0.880768	0.364323	0.4287	-0.471531
4	1.333333	0.849602	0.967523	0.172171	0.287807	-0.372246
5	1.666667	1.179351	1.004461	0.06168	0.180771	-0.270981
6	2	1.516438	1.014825	0.008548	0.105857	-0.181416
7	2.333333	1.854744	1.013766	-0.010431	0.057652	-0.111554
8	2.666667	2.192005	1.009557	-0.012844	0.02916	-0.062977
9	3	2.527866	1.005743	-0.009463	0.013698	-0.032643
10	3.333333	2.862665	1.003258	-0.00548	0.005993	-0.015542
11	3.666667	3.196839	1.001942	-0.002621	0.002467	-0.006803
12	4	3.530708	1.001371	-0.000986	0.000984	-0.002741
13	4.333333	3.864461	1.001195	-0.000183	0.000411	-0.001017
14	4.666667	4.19819	1.001203	0.000169	0.000207	-0.000347
15	5	4.531937	1.001288	0.000313	0.000141	-0.000108
16	5.333333	4.865718	1.001404	0.000371	0.000122	-0.000029
17	5.666667	5.199541	1.001533	0.000399	0.000118	-0.000004
18	6	5.533408	1.001669	0.000416	0.000118	0.000003
19	6.333333	5.867321	1.00181	0.000429	0.000119	0.000004
20	6.666667	6.201282	1.001955	0.000442	0.000121	0.000005
21	7	6.535292	1.002105	0.000453	0.000123	0.000005
22	7.333333	6.869352	1.002258	0.000465	0.000124	0.000005
23	7.666667	7.203464	1.002415	0.000476	0.000126	0.000004
24	8	7.537629	1.002575	0.000487	0.000127	0.000004
25	8.333333	7.871847	1.002739	0.000497	0.000129	0.000004
26	8.666667	8.206122	1.002906	0.000507	0.00013	0.000004
27	9	8.540452	1.003077	0.000518	0.000131	0.000004
28	9.333333	8.87484	1.003251	0.000527	0.000133	0.000004
29	9.666667	9.209287	1.003429	0.000537	0.000134	0.000004
30	10	9.543793	1.00361	0.000547	0.000135	0.000004

Appendix (B): Previous Study's Equations:

B.1: Equations of the problem of mixed convection over vertical flat plate which solved by **Manning and Qureshi,** [12].

$F_f = 0.339 \cdot \Pr^{\frac{1}{3}} \cdot \left(0.1 \cdot \Pr^{\frac{-3}{4}} + 1 \right)^{\frac{-2}{9}}$ Heat transfer factor for forced convection.

$Fn = 0.503 \cdot \Pr^{\frac{1}{4}} \cdot \left(0.670 \cdot \Pr^{\frac{-9}{16}} + 1 \right)^{\frac{-4}{9}}$ Heat transfer factor for natural convection.

Thus for mixed convection correlation Nusselt number defined as:

$$\frac{Nu_{mix}}{\sqrt{\mathrm{Re}_x}} = \left({F_f}^n + \left(F_n \cdot {Ri_x}^{\frac{1}{4}} \right)^n \right)^{\frac{1}{n}} \qquad \text{.....(B.1)}$$

Where: $n = 3.5 \cdot \Pr^{0.075}$

ألخلاصه

مسألة الحمل الحراري المركب الحر والقسري فوق صفيحه مستوية مائلة لها تطبيقات كثيرة في ألأجزاء الميكانيكية، ألأجهزة ألإلكترونيه ألمبرده بواسطة المراوح الصغيرة و المبادلات الحرارية المعرضة لمائع ذو سرعة بطيئة، تعتبر طريقتي تكامل المتغيرات المحدد لطول ألصفيحه وطريقة الحل بالتشابه (الحل المضبوط) من الطرق الشائعة لحل مسائل من هذا النوع.

الهدف من هذه الدراسة هو دراسة تأثير كل من قوة الطفو وزاوية الميلان لجريان طباقي منتظم ثنائي البعد فوق صفيحة مستوية مسخنه ومائلة لحالتي ثبوت درجة حرارة سطح ألصفيحه وثبوت معدل التدفق الحراري منها على تغير رقم ناسلت (Nu_x) ألموقعي للصفيحة وكذلك على المعادلات اللابعديه لتوزيع درجة الحرارة وتوزيع السرعة و على الخواص الهيدروديناميكية بوجود الحمل الحراري المركب الحر والقسري .

أجريت التحليلات النظرية بطريقتي الحل التحليلي و العددي لدراسة انتقال الحرارة ألموقعي بطريقة الحمل المركب للمائع المنتظم السرعة المستقر ذو الخواص الفيزيائية ألمتمثله برقم براندتل (Pr) بمدى من 0 إلى 100 فوق صفيحه مستوية اعتبرت بأنها متجانسة الخواص، مائلة ومسخنه. وبحالتي درجة حرارة سطح ثابتة حيث تم استخدام الحل التحليلي بطريقتي تكامل المتغيرات المحدد لطول ألصفيحة ومعدل تدفق حراري ثابت حيث تم استخدام الحل العددي بطريقة الحل بالتشابه (الحل المضبوط) بإعداد برامج حاسوبي مساعد بواسطة (MathCAD 2001).

النتائج توضح تغير سمك الطبقه الحديه المتآخمه ورقم ناسلت (Nu_x) وأجهادات القص مع تغير قوة الطفو وزاوية الميلان و الخواص الفيزيائية ألمتمثله برقم براندتل (Pr). حيث أظهرت النتائج أن رقم ناسلت (Nu_x) ألموقعي يزداد بثبوت رقم(Re_x) بمعدل من $0.3*Re_x^{1/2}$ إلى $6*Re_x^{1/2}$ ، ورقم (St_x) بمعدل من $0.3/Re_x^{1/2}$ إلى $6/Re_x^{1/2}$ بزيادة كل من (Ri_x) بمعدل من 0 إلى 10 وزاوية الميلان بمعدل من 0^o إلى 90^o في حين يقل سمك الطبقه الحديه المتآخمه.

وزارة التعليم العالي والبحث العلمي
جامعة بابل / كلية الهند سه

الحمل الحراري المركب الحر والقسري فوق صفيحه مستويه مائله

أطروحة مقدمة

إلى

قسم الهندسة الميكانيكية

كلية الهندسة / جامعة بابل

كجزء من متطلبات نيل شهادة

(الماجستير علوم)

في

الهندسة الميكانيكية

(هندسة قدرة)

من قبل المهندس

فؤاد عبد الأمير خلف

(بكالوريوس)

(1999)

1427هـ 2006 م